Effective Thermal Conductivity of Composite Fluidic Thermal Interface Materials

by

Paul Karayacoubian

A thesis
presented to the University of Waterloo
in fulfilment of the
thesis requirement for the degree of
Master of Applied Science
in
Mechanical Engineering

Waterloo, Ontario, Canada, 2006

I hereby declare that I am the sole author of this thesis. This is a true copy of the thesis, including any required final versions, as accepted by my examiners.

I understand that my thesis may be made electronically available to the public.

Paul Karayacoubian

Abstract

Thermally enhanced greases made of dispersions of small conductive particles suspended in fluidic polymers can offer significant advantages when used as a thermal interface material (TIM) in microelectronics cooling applications. A fundamental problem which remains to be addressed is how to predict the effective thermal conductivity of these materials, an important parameter in establishing the bulk resistance to heat flow through the TIM.

The following study presents the application of two simple theorems for establishing bounds on the effective thermal conductivity of such inhomogeneous media. These theorems are applied to the development of models which are the geometric means of the upper and lower bounds for effective thermal conductivity of base fluids into which are suspended particles of various geometries.

Numerical work indicates that the models show generally good agreement for the various geometric dispersions, in particular for particles with low to moderate aspect ratios. The numerical results approach the lower bound as the conductivity ratio is increased. An important observation is that orienting the particles in the direction of heat flow leads to substantial enhancment in the thermal conductivity of the base fluid. Clustering leads to a small enhancement in effective thermal conductivity beyond that which is predicted for systems composed of regular arrays of particles. Although significant enhancement is possible if the clusters are large, in reality, clustering to the extent that solid agglomerates span large distances is unlikely since such clusters would settle out of the fluid.

In addition, experimental work available in the literature indicates that the agreement between the selected experimental data and the geometric mean of the upper and lower bounds for a sphere in a unit cell are in excellent agreement, even for particles which are irregular in shape.

Acknowledgements

Some students in England once worked out how much their favourite author Rudyard Kipling earned per word and asked him to send them his favourite one, the small sum of money enclosed in the envelope. He wrote back "Thanks."

There are many people to whom I am indebted for their assistance with this work. I would first like to thank my supervisor Professor J. R. Culham for the freedom he gave me in pursuing my research, for his careful editing of my thesis, and for his support throughout the culmination of this work, as well as the Centre for Microelectronics Assembly and Packaging (CMAP) for its financial support. I also wish to express thanks to Professor Emeritus M. M. Yovanovich for his pellucid intellectual clarity and for his guidance and encouragement during the course of this investigation, Dr. Pete Teertstra, Professor Gauthier, and Shahla Aliakbari for help with the experimental program which was later set aside, and Majid Bahrami, with whom I shared many valuable discussions, my first conference paper, and pleasant times in the lab. I am also grateful to my office mate Josh Gibbins and to all the other graduate students who helped make this a rewarding experience. Finally, I wish to thank my family and friends for their moral support these past couple years.

And if the old man climbed out of the cart and stretched himself (things were gathering pace now) and looked where the pump had been that the soldiers had blown up so that nothing should be left standing, and complained, saying, "What are we going to do about water?", he, Michael K, would produce a teaspoon from his pocket, a teaspoon and a long roll of string. He would clear the rubble from the mouth of the shaft, he would bend the handle of the teaspoon in a loop and tie the string to it, he would lower it down the shaft deep into the earth, and when he brought it up, there would be water in the bowl of the spoon; and in that way, he would say, one can live.

– J. M. Coetzee, Life and Times of Michael K

Contents

List of Figures

xi

List of Tables

Nomenclature

A cross-sectional area, $[m^2]$; lattice spacing along $x-$axis, $[m]$

a minor axis of particle along $x-$axis, $[m]$;

         contact spot diameter, $[m]$

B lattice spacing along $y-$axis, $[m]$

b minor axis of particle along $y-$axis, $[m]$;

         diameter of finite isotropic cylindrical tube, $[m]$

BLT bond-line thickness, $[m]$

C lattice spacing along $z-$axis, $[m]$

c major axis of particle along $z-$axis, $[m]$

h height of cylinder relative to lattice spacing, $[m]$

I integral

K $\equiv 1 - 1/\kappa$

k thermal conductivity, $[W/mK]$

L distance between boundaries, $[m]$

M number of terms in multipole expansion

n local normal; number of numerical and analytical values

Q total heat flow rate, $[W]$

q heat flux $\equiv Q/A$, $[W/m^2]$

R thermal resistance $\equiv \Delta T/Q$, $[K/W]$

RMS root mean square deviation

T temperature, $[K]$

t thickness of finite isotropic cylindrical tube, $[m]$

V volume, $[m^3]$

x numerical/analytical value

Subscripts

$1, 2$	regions of the cell
c	contact; coating
e	effective
f	fluid (continuous surrounding medium)
H, L	high, low
lb, ub	lower bound, upper bound
s	solid (particle, discontinuous phase); spreading; source
t	tube
tot	total

Greek Symbols

α	aspect ratio of cylinder $\equiv h/\epsilon$
ϵ	radius of particle relative to lattice spacing
κ	conductivity ratio $\equiv k_s/k_f$
ϕ	volume fraction $\equiv V_s/(V_s + V_f)$
ψ	sphericity $\equiv A_{sphere}/A_s$
τ	thickness of particle coating, $[m]$

Chapter 1

Introduction

When two real conforming solid surfaces are brought into contact, a finite temperature drop exists at the interface between the contacting solids. This temperature drop can be appreciable and is attributed to what is known as thermal contact resistance, R_c. The existence of thermal contact resistance is due principally to surface roughness effects[1]. A real mechanical joint in air, for example, consists of numerous discrete microcontacts distributed over the apparent contact area with air gaps appearing wherever there is absence of solid-to-solid contact (Figure 1.1).

Thermal contact resistance between interfaces comprises a significant portion of the total thermal resistance in microelectronics applications. As a result, much work has been done to identify ways of minimizing R_c. This is typically achieved by introducing interstitial materials which can displace the air entrained in the gaps formed between the contacting surfaces with a highly conductive substance: examples include thin metallic foils, powders, wire screens, epoxies, and coatings. Greases which completely fill these gaps can significantly reduce the contact resistance despite

---

[1]Some researchers have also noted the effect of extra phonon scattering produced by an acoustic mismatch between two contacting materials of different conductivities. This effect is more prominent at low temperatures, however [1], [2].
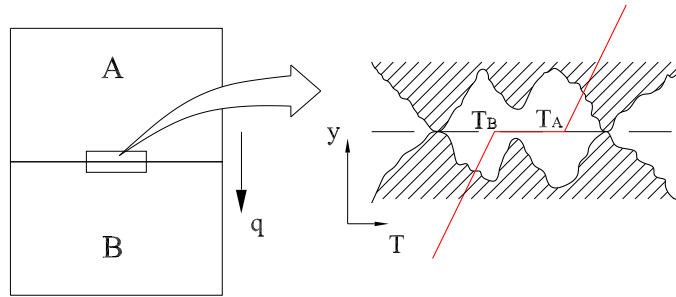
Figure 1.1: Temperature drop due to finite thermal contact resistance

the relatively lower thermal conductivity of a fluid with respect to that of a solid $(k_f/k_s \sim 10^{-3})$ [3].

Thermally enhanced greases made of dispersions of small conductive particles suspended in fluidic polymers are the latest thermal interface materials (TIMs) being investigated for use in microelectronics cooling applications. The base fluid is typically ethylene glycol or a silicone oil; typical materials used for the conductive dispersed phase include aluminum, copper, and silver as well as their oxides which inevitably form (except in the case of silver) in most practical applications.

The total thermal resistance between interfaces with thermally enhanced greases has two components: (1) the contact resistance between the solid and the TIM at both interfaces, R_{c1} and R_{c2}, and (2) the bulk resistance of the material, which displaces the two surfaces, R_b (Figure 1.2). The total thermal resistance is given by [4]

$$R = R_{c1} + R_{c2} + \frac{BLT}{k_e} \tag{1.1}$$

where BLT is the bond-line thickness and k_e is the effective thermal conductivity of the inhomogeneous mixture. Equation (1.1) applies specifically to one-dimensional heat flow through samples of constant cross-section since the area terms have been cancelled. Each parameter in Equation (1.1) requires further modeling. The present work is a study of the effective conductivity, k_e, which is in general a function of (a) the thermal conductivities of the two phases, (b) the volume concentrations of the two phases, and (c) the microstructure of the inhomogeneous media.

2
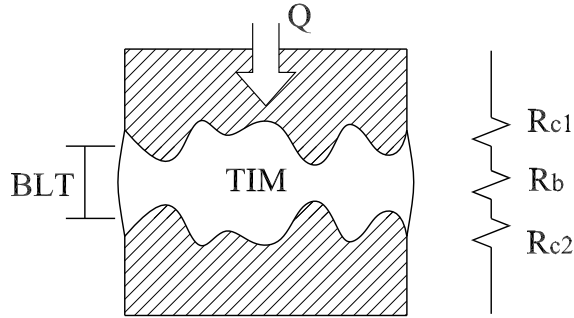
Figure 1.2: Thermally enhanced grease

1.1   Problem Statement

Consider a temperature gradient imposed across a slab of thickness L into which are dispersed many small particles of a material with different thermal properties. The particles are fully wetted by the surrounding medium. The imposed temperature gradient causes heat to flow from one side to the other. If the material in the slab is stationary and the heat flow is assumed one-dimensional, the effective thermal conductivity is obtained from Fourier's law and is given by

$$q = \frac{Q}{A} = k_e \frac{\Delta T}{L} \quad \Rightarrow \quad k_e = \frac{q}{\Delta T/L} \tag{1.2}$$

where $\Delta T/L$ is the negative effective temperature gradient across the slab. Using these effective quantities, the mixture of the continuous phase and particles is represented as an effective homogeneous medium.

If, as in the above problem, the temperature gradient is specified, the effective thermal conductivity depends only on the heat flux. The heat flux can be measured experimentally and is in general a function of the thermal conductivities of the constituents of the inhomogeneous medium as well as of the microstructure. The purpose of the present work is to develop analytical and numerical models for the effective thermal conductivity of various geometric dispersions. Effects such as particle volume fraction, alignment, distribution, and clustering of the particles in the continuous phase as well as thin coatings on the effective thermal conductivity are studied.

1.2 Overview

Existing models for the effective thermal conductivity of inhomogeneous media are reviewed in Chapter 2. The steady heat conduction problem is posed generally and shown to be governed by a set of equations which are formally identical to those governing a wide range of problems in physics and engineering. A vast body of literature from multiple disciplines is thus available for review. Rather than assessing the usefulness of a model based on the agreement between its predictions and experimental data, the development of some of the models is emphasized so that their limitations can be fully appreciated. The models and general approaches to this problem have been ordered roughly chronologically.

The set of partial differential equations with boundary conditions governing the thermal problem is presented in Chapter 3. A simple cubic lattice structure is assumed and a characteristic cell is identified. Although well-posed, there is no simple analytical solution available for the general case of the coupled heat conduction equations for particles of arbitrary geometry subject to the given boundary conditions. Numerical work is required to determine the temperature fields in the particle and the surrounding medium.

It is possible, however, to obtain upper and lower bounds on the effective conductivity of the cell. These bounds, which are in many instances quite useful since they give a narrow range of possible values of effective thermal conductivity, are developed and described in Chapter 4 for various geometric dispersions.

Numerical solutions of the effective thermal conductivity of the specific cases studied in the previous chapter are performed using the finite element analysis technique in Chapter 5. Effects such as alignment and distribution of the highly conductive phase in the medium and thin coatings (of either highly conductive or highly resistive material) are discussed. In addition, the effect of clustering which has been cited as a possible source of disagreement between experimental data and theory is discussed.

Experimental data of the effective thermal conductivity for inhomogeneous media were selected from the literature. The data are required to establish that the assumptions made in the present work are valid for the class of materials which are of interest in microelectronics cooling applications.

The final chapter summarizes the important findings of the present study and includes recommendations for future work.

Chapter 2

Literature Review

Many theoretical models for effective thermal conductivity of heterogeneous media have been developed. Given the large number of distinct equations presented in the literature, it is not possible to analyze or even identify all in any single investigation. Fortunately, it is possible to individuate distinct approaches used by various researchers and, when possible, describe representative models which proceed from these grounds.

The formal equations governing steady heat conduction for constant thermal conductivity posed generally can be written as

$$\mathbf{q} = -k \, \nabla T \qquad \nabla \cdot \mathbf{q} = 0 \qquad \nabla \times \nabla T = 0 \tag{2.1}$$

where $\mathbf{q}$ is the heat flux, k is the thermal conductivity, and ∇T is the temperature gradient. Equation (2.1) is mathematically identical to the basic equations governing a wide range of problems in physics and engineering including elasticity, dielectrics, magnetism, species diffusion, and flow in porous media [5], [6]. As a result, identical approaches have been used to treat all of these problems. These approaches include: (1) mathematical analysis of various arrays of regular particles, (2) effective medium theory, (3) percolation theory, (4) statistical methods in which bounds are established

based on information regarding the microstructure of the heterogeneous media, and
(5) numerical solutions of the steady state heat conduction equation for heterogeneous
media of specified microstructure.

Many of the models which have been developed to predict effective thermal con-
ductivity have been adapted from models developed to predict effective dielectric
strength and elastic constant. In fact, very few models developed to predict effective
thermal conductivity from thermal transport principles were identified in the liter-
ature. Care must be taken in adapting models originally developed to model other
properties, for although the problems are governed by formally identical equations,
there are instances where the analogies are inappropriate. Consider, for example,
effective viscosity of filled systems and effective elastic constant of air-filled metallic
foams. Whereas the viscosity of a solid filler and elastic constant of air are ill-defined
quantities, the thermal conductivities of both phases in heterogeneous media are al-
ways finite.

The distribution of two phases in the material, in particular the geometry and
orientation of the dispersed phase, has a significant influence on effective thermal
conductivity of heterogeneous media. Many of the theoretical models are valid only
for specific types of dispersions and distributions. In addition, there are models such
as effective medium theory which do not make the distinction between the dispersed
phase and the continuous phase, but rather allow for the formation of an internal
network in the structure.

Given only information regarding the volume fractions and thermal conductivities
of the two phases, it is possible to establish upper and lower bounds on effective
thermal conductivity. The upper bound is given when the two phases are arranged
parallel to the direction of heat flow and is most appropropriate for heterogeneous
media in which both phases are well-connected throughout:

$$k_e = k_s \phi_s + k_f \phi_f \qquad (2.2)$$

7

where k_e is effective thermal conductivity, k_s and k_f are thermal conductivities of the solid and fluid (more specifically, liquid) phases, and where ϕ_s and $\phi_f = 1 - \phi_s$ are volume fractions of the solid and fluid phases in the heterogeneous media. The lower bound treats the components as layers perpendicular to the direction of heat flow. This results in an insulating effect that is dominated by the phase with the lower conductivity, thus providing a lower bound on k_e given by series conduction through both phases:

$$\frac{1}{k_e} = \frac{\phi_s}{k_s} + \frac{\phi_f}{k_f} \tag{2.3}$$

The bounds provided by Equations (2.2) and (2.3) can be multiple orders of magnitude apart which can be problematic when trying to use the average to obtain an accurate estimate of effective thermal conductivity. In addition, Equation (2.2) describes a system in which the dispersed phase consists of long fibers with their axes oriented in the direction of heat flow and extending from one end of the medium to the other. Equation (2.3) is appropriate for systems in which the dispersed phase has settled. Neither model, therefore, reasonably describes a uniform and isotropic suspension of spheres in a continuous liquid phase. As a result, more sophisticated approaches which assume certain characteristics of the microstructure are necessary to model effective thermal conductivity of particulate-filled heterogeneous media.

2.1   Mathematical Analysis of Regular Arrays of Particles

Maxwell [7] derived an equation for effective electrical resistivity of a homogeneous material into which is dispersed many small spherical particles. He selected a characteristic cell and introduced an effective (equivalent homogeneous) medium surrounding this cell (Figure 2.1). Eucken [8] adapted this analysis to the problem of effective thermal conductivity of a heterogeneous medium. By imposing a uniform temperature
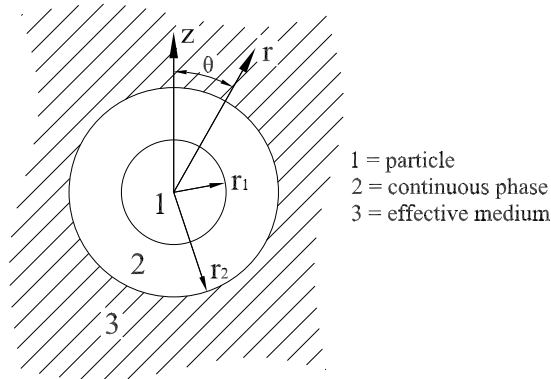
Figure 2.1: Cell geometry subject to Maxwell's analysis

gradient in the effective medium, the solution of the coupled azimuthally-independent steady heat conduction equations in the sphere, the continuous phase, and the effective medium subject to appropriate boundary conditions (Appendix A) gives the following relationship for effective thermal conductivity:

$$k_e = k_f \frac{2k_f + k_s - 2\phi_s(k_f - k_s)}{2k_f + k_s + \phi_s(k_f - k_s)} \tag{2.4}$$

By introducing the effective medium, Maxwell assumed that the particles are non-interacting. This assumption is valid for $\phi_s \leq 0.30$ which will be shown quantitatively in the following paragraphs.

Lord Rayleigh [9] improved the Maxwell equation by using the principle of multiple pole expansion to take into account the contribution of induced octopole moments on the field of the neighbourhood of the central particle. The effective thermal conductivity according to Rayleigh is given by [1]

$$k_e = k_f \frac{A - 2\phi_s - 0.525B\phi_s^{10/3}}{A + \phi_s - 0.525B\phi_s^{10/3}} \tag{2.5}$$

where

$$A = \frac{2 + k_s}{1 - k_s} \quad \text{and} \quad B = \frac{3 - 3k_s}{4 + 3k_s} \tag{2.6}$$

---

[1]Equation (2.5) includes a numerical correction made by I. Runge [10]

Like the Maxwell equation, Equation (2.5) is inaccurate when the spheres are close to touching and $k_s \gg k_f$.

By considering higher order terms in the series expression for the potential in the surrounding medium, Meredith and Tobias [11] later improved on the Rayleigh equation. The relationship derived by Meredith and Tobias is given by

$$k_e = k_f \frac{A - 2\phi_s + 0.409C\phi_s^{7/3} - 2.133B\phi_s^{10/3}}{A + \phi_s + 0.409C\phi_s^{7/3} - 0.906B\phi_s^{10/3}} \tag{2.7}$$

where

$$A = \frac{2 + k_s}{1 - k_s}, \quad B = \frac{3 - 3k_s}{4 + 3k_s}, \quad \text{and} \quad C = \frac{6 + 3k_s}{4 + 3k_s} \tag{2.8}$$

Experimental results confirm that Equation (2.7) does indeed give better agreement for cubic arrays of spheres than Equations (2.4) and (2.5), in particular when the spheres are close to touching and $k_s \gg k_f$.

In a critical work, McPhedran and McKenzie [12], [13] further extended the method devised by Rayleigh to calculate the conductivity of spheres arranged in simple cubic, body-centered cubic, and face-centered cubic lattices. Their extended theory is capable of including effects of multipoles of arbitrarily high order (i.e. infinitely many neighbouring particles) and yields excellent agreement with experimental measurements even when the spheres are close to touching and $k_s \gg k_f$. In addition, their model for the simple cubic lattice recovers the equations of Maxwell, Rayleigh, and Meredith and Tobias when the number of terms in the multipole expansion is equal to 1, 2, and 3, respectively (Figure 2.2). Because the form of the solution requires the evaluation of an infinite series, the authors solved for the parameters numerically and only presented the model for 4 terms in the multipole expansion ($M = 4$). This was shown to be sufficiently close to the solution for $M \to \infty$ for moderate volume fractions and conductivities. Because the equation for effective thermal conductivity with $M = 4$ is still quite cumbersome, the interested reader is directed to their work [12].
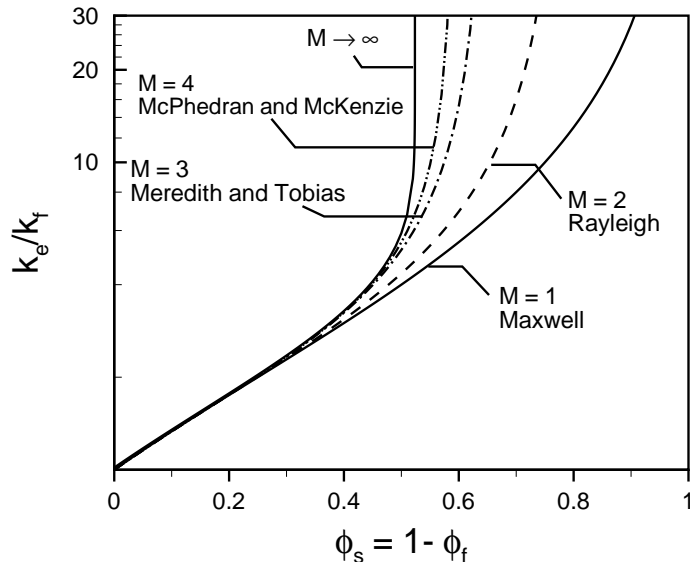
Figure 2.2: Effective conductivity models for various multipole expansions (M) in a simple cubic lattice structure $(k_s/k_f \to \infty)$

McPhedran and McKenzie also pointed out that no other existing theory gives the expected divergence at the critical volume fraction for a simple cubic lattice $(\phi_s = \pi/6)$ when the spheres are perfectly conducting $(k_s/k_f \to \infty)$. In addition, an asymptotic solution derived by Batchelor and O'Brien [14] was in fact asymptotically approached by their solution. In a separate work, McKenzie and McPhedran [13] derived similar relationships and obtained the expected singuarities for the effective conductivity of spheres in body-centered and face-centered cubic arrays.

Inaccuracy in the assumption of non-interacting particles can be assessed by comparison of the predictions of Maxwell with those of McPhedran and McKenzie. For $\phi_s = 0.30$, the predictions of Maxwell, Rayleigh, Meredith and Tobias, and McPhedran and McKenzie are all within 3% of each other, with the theory of Maxwell giving the lowest predictions. The simpler equation of Maxwell is thus appropriate for suspensions of spherical particles for which $\phi_s \leq 0.30$.

2.1.1   Extensions of the Maxwell Equation

Discrepancies occurring between measurements and the multiple pole theory of McPhe-
dran and McKenzie have typically been attributed to either a distribution of particle
shapes and orientations or to a variation with size of the dispersed phase. Given
the difficulty of working with the multiple pole theory, numerous researchers have
investigated the possible contributions of these effects within the framework of the
approximation of Maxwell. The Maxwell formulation has since been modified to in-
clude effects such as irregular particle geometry, boundary resistance at the interface
between the particle and the continuous phase, and thin coatings on the particle in
hope of obtaining better agreement with experimental data.

Hamilton and Crosser [15] extended the Maxwell theory to include effects due to
irregular particle geometries. They showed that the effective thermal conductivity
can be written as

$$k_e = k_f \frac{k_s + (n-1)k_f - (n-1)\phi_s(k_f - k_s)}{k_s + (n-1)k_f + \phi_s(k_f - k_s)} \tag{2.9}$$

where n depends upon both the shape of the dispersed particles and the ratio of
conductivities of the two phases. They then experimentally determined n to be of
the form

$$n = \frac{3}{\psi} \tag{2.10}$$

where $\psi \equiv A_{sphere}/A_s$ is the sphericity of the particle. Equation (2.9) recovers the
Maxwell equation for spherical inclusions ($n = 3$).

Alternatively, Verma et al. [16] suggested the use of a modified volume fraction
which accounts for the sphericity in the Maxwell equation to treat dispersions of
irregular geometries,

$$\phi_s' = \exp\left[-\psi(1 - \phi_s)\right] \tag{2.11}$$

where ψ is the sphericity. By replacing ϕ_s with ϕ_s' in Equation (2.4), it is seen that
the proposed modified volume fraction does not recover the Maxwell equation for

spherical inclusions ($\psi = 1$) nor does it recover the conductivity of the continuous phase if $\phi_s = 0$. Nevertheless, Verma et al. showed the modified volume fraction to give slightly better agreement for larger volume fractions. The form of Equation (2.11) was given justification on the basis of a random dispersion of particles in the formulation of effective thermal conductivity given by Cheng and Vachon [17].

Benveniste [18] considered the effective thermal conductivity of a particulate composite with thermal contact resistance at the interface. Using the same formulation as Maxwell but with a modified boundary condition accounting for finite contact conductance at the interface, the effective conductivity is given as

$$k_e = k_f \frac{k_f(1 - \phi_s) + \beta\left[2k_f + k_s - 2\phi_s(k_f - k_s)\right]}{k_f(2 + \phi_s) + \beta\left[2k_f + k_s + \phi_s(k_f - k_s)\right]} \tag{2.12}$$

where $\beta = hr/k_s$ and h is the contact conductance at the interface between the spherical particle of radius r and the continuous phase. In the limit of ideal thermal contact ($\beta \to \infty$), Equation (2.12) recovers the Maxwell equation.

In a study on syntactic foam insulation produced by hollow glass microspheres embedded in a plastic resin, Felske [19] extended Maxwell's model to treat *composite* spheres. The composite spheres were taken to have a homogeneous core surrounded by a homogeneous shell of a different material. Contact resistance at the interface between the continuous medium and the shell was accounted. The development is fully analytic and general so that it recovers both the Maxwell equation in the limit of ideal thermal contact and the Benveniste equation in the limit of the coating and particle having the same thermal conductivities.

2.2 Effective Medium Theory (EMT)

Effective medium theory (EMT) treats the contributions of each phase equally. Consider the microstructure depicted in Figure 2.3. There is no distinction to be drawn between the continuous and discontinuous phases in this case. To apply the theory of
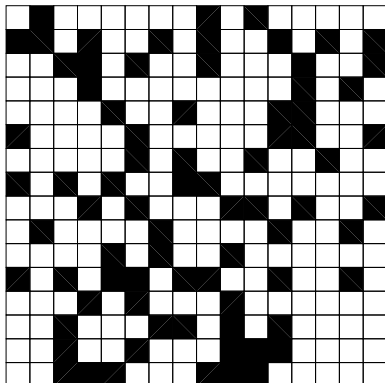
Figure 2.3: Random dispersion of two phases in which neither phase is continuous

Maxwell, the continuous and discontinuous phases must first be identified since Equation (2.4) is not symmetric. Systems in which there is the formation of an internal network in the structure are more accurately represented with EMT.

Like the equation of Maxwell, EMT is derived from the solution of the Laplace equation applied to a single sphere surrounded by a continuous medium, and subjected to a steady-state temperature gradient in the direction of the z-axis. Maxwell assumed that the local distortions to the temperature distributions around the dispersed spheres did not affect their neighbours. The essence of EMT, however, lies in the assumption that for a completely random distribution of components, the effect of local distortions to the temperature distribution caused by individual inclusions could be averaged such that over a sufficiently large volume (or ensemble) the temperature distribution within the material could be approximated by a material having a uniform temperature distribution and thermal conductivity k_e [20]. This requires that [2]

$$\phi_s \frac{k_s - k_e}{k_s + 2k_e} + \phi_f \frac{k_f - k_e}{k_f + 2k_e} = 0 \tag{2.13}$$

---

[2]Equation (2.13) can easily be extended to composites of any number of phases. In general, for n phases

$$\sum_{i=1}^{n} \phi_i \frac{k_i - k_e}{k_i + 2k_e} = 0$$

Rearranging Equation (2.13),

$$k_e = \frac{1}{4}\left(\gamma + \sqrt{\gamma^2 + 8k_s k_f}\right) \tag{2.14}$$

where

$$\gamma = (3\phi_s - 1)\,k_s + (3\phi_f - 1)\,k_f \tag{2.15}$$

Note that Equations (2.14) and (2.15) are symmetric.

The solution of Equation (2.14) has an interesting behaviour in the limit as k_f approaches 0. In this limit, we have

$$k_e = \begin{cases} 0 & \phi_s < 1/3 \\[2ex] k_s\left(\dfrac{3\phi_s - 1}{2}\right) & \phi_s \geq 1/3 \end{cases} \tag{2.16}$$

Note that $\phi_s = 1/3$ is the critical volume fraction below which $k_e = 0$. This critical volume fraction coincides with the so-called percolation threshold ϕ_c and physically corresponds to the volume fraction above which the conductive phase will likely form a well-connected path from one boundary to the other. This is a phenomena that has not been observed experimentally except in systems in which there is no continuous phase [21]. This will be discussed in more detail in Section 2.3.

2.2.1 Bruggeman Equation

Bruggeman [22] introduced another popular effective medium theory that is now widely known as the differential scheme or the Bruggeman equation. Bruggeman proceeds from the premise that the fields of neighbouring particles can be taken into account by adding the dispersed particles incrementally, taking the surrounding medium to be the existing composite at each stage.

Consider again an effective medium surrounding an ensemble in which a spherical particle is surrounded by the continuous medium in the same proportion as in the
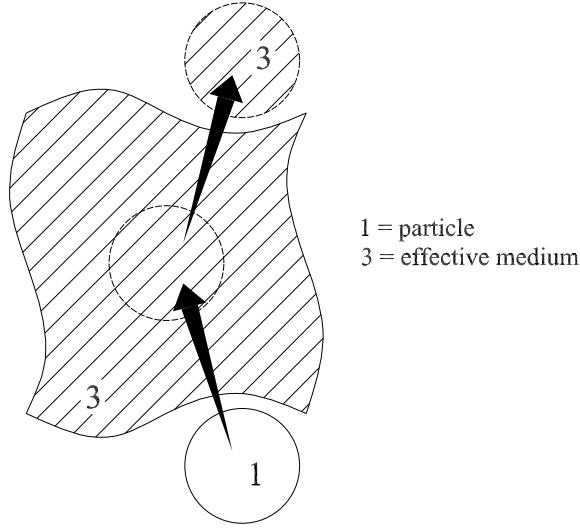
Figure 2.4: Cell geometry subject to Bruggeman's analysis – A differential volume of material with k_e is carved out and replaced with material of k_1

mixture as a whole. If the volume fraction of the composite is increased from ϕ_s to $\phi_s + d\phi_s$ by carving out of the ensemble a spherical cavity with conductivity k_e and inserting a large spherical particle with conductivity k_s (Figure 2.4), the medium surrounding these new inclusions can be treated as the same effective medium (i.e $k_e(\phi_s)$) without introducing much error.

The Bruggeman equation for the effective conductivity of the inhomogeneous medium is given by

$$\left(\frac{k_s - k_e}{k_s - k_f}\right)\left(\frac{k_f}{k_e}\right)^{1/3} = 1 - \phi_s \qquad (2.17)$$

Equation (2.17) is an implicit relationship and may be solved numerically for given values of k_s, k_f, and ϕ_s. Its predictions for k_e are always greater than those of the Maxwell equation.

The Bruggeman equation is most appropriate for composites containing spherical particles with a very wide size distribution. Ideally, the size distribution should be wide enough that any two spheres of comparable size are far from each other. Like the Maxwell equation, the Bruggeman equation may also be extended to include effects

16

such as boundary resistance, thin coatings, and irregular particle geometries.

2.3 Percolation Theory

Consider a large square lattice in which each site is either occupied with a probability p or empty with a probability $1 - p$ similar to the structure shown in Figure 2.3. An occupied site is assigned a conductivity k_s and an unoccupied site a conductivity k_f. The fundamental premise of percolation theory is contained in the idea of a sharp increase in the effective conductivity of the disordered media at a critical volume fraction known as the percolation threshold ϕ_c at which long-range connectivity of the system appears.

When $k_s \neq 0$, $k_f = 0$, and $\phi_s < \phi_c$, no macroscopic conducting pathway exists and the composite remains in the insulating phase. When $\phi_s \geq \phi_c$, however, the system becomes conducting as a cluster of bonds of conductivity k_s almost certainly forms a connected bridge between the two boundaries of the disordered media across which the potential is applied. In the vicinity of the transition volume fraction ϕ_c, one has [23]

$$
k_e \sim
\begin{cases}
0 & \phi_s \leq \phi_c \\[2ex]
k_s(\phi_s - \phi_c)^t & \phi_s > \phi_c
\end{cases}
\tag{2.18}
$$

where the symbol $\sim$ means *is asymptotically proportional to* as $\phi_s \rightarrow \phi_c$. The critical exponent t has a universal value of $t = 2.0$ in 3-D and $t = 1.3$ in 2-D problems.

Equation (2.18) may be compared with Equation (2.16) derived from effective medium theory which predicts $\phi_c = 1/3$, applicable to spheres. The existence of a critical percolation threshold for electrical conductivity has since been demonstrated for a wide variety of fillers, all at concentrations below the maximum packing fraction [24]. The percolation threshold in an actual granular aggregate is in general a function of the lattice structure of the phases, and ranges from $\phi_c \approx 0.2$ for a face-centered

cubic arrangement to $\phi_c \approx 0.7$ for a honeycomb arrangement and can be calculated exactly for certain simple lattices.

The original problem was posed by Broadbent and Hammersley [25] who obtained a simplified lattice percolation model for fluid flow in a porous medium. They were able to show rigorously that their model possessed a threshold. It has since been applied to many other related problems including thermal conduction in disordered media [26], continuing work on fluid flow in porous media [27], the spreading of forest fires [28] and disease in a population [29], and many others.

The critical point can be approached in different ways. For example, when $k_s \to \infty$ and $k_f \neq 0$, the effective conductivity diverges as ϕ_c is approached from below and is written as

$$
k_e \sim \begin{cases} k_f(\phi_c - \phi_s)^{-t} & \phi_s < \phi_c \\ \\ \infty & \phi_s \geq \phi_c \end{cases}
\tag{2.19}
$$

and when both k_s and $k_f \neq 0$ and $k_f/k_s \to 0$, one has

$$
k_e \sim k_s^{1-t} k_f^t \qquad \phi_s = \phi_c
\tag{2.20}
$$

Devpura et al. [26] applied percolation theory to the problem of determining the effective thermal conductivity of fluidic composite thermal interface materials. They simulated random resistor networks and solved a system of linear equations numerically using the transfer matrix approach [30]. In their model, they assumed all particles to be cubic and later applied a correction factor for the case of spherical particles. Because the system randomly assigns the values of the resistors (according to k_s, k_f, ϕ_s), several simulations were performed for each given set of conditions and the average was presented. The singular behaviour of the effective thermal conductivity of the disordered media near the percolation threshold was observed and this threshold was found to be a function of the sample thickness and particle size distribution. Devpura et al. defined the percolation threshold as the volume fraction

at which

$$\frac{dk_e}{d\phi_s} \approx k_s \qquad (2.21)$$

Their results agreed well with certain selected experimental data, particularly for $\phi_s \leq \phi_c$.

Because of the complexity of implementing percolation theory and the eventual necessity of numerical work, the method has not been very popular. In addition, it has been suggested that in most cases, the presence of a network of filler particles does not change the basic mechanism of thermal transport in composite systems [21]. According to Torquato [31], a thermal transport network develops only at the maximum packing fraction.

2.4   Statistical Analysis and Bounding Techniques

Most fluidic composites are complex systems consisting of many small particles dispersed randomly in a continuous phase. In most cases, the details of the microstructure are not completely known. This naturally leads one to attempt to establish a range of possible values the effective properties can take given such limited sample information. As Sen and Torquato [32] point out, bounds on the effective properties are useful since (a) they can be used to test the merits of a theory or a computer experiment, (b) they become progressively narrower as more details of the microstructure become known, and (c) one of the bounds is generally a good model for the effective properties for a wide range of volume fractions.

Early attempts to develop more accurate models began with statistically summing the perturbations around each dispersed particle to calculate the effective thermal conductivity of the heterogeneous media. In general, the effective thermal conductivity of a particle suspension can be expressed as a series expansion of the localized

average thermal conductivity determined by considering the localized heat transfer. This expansion is given as follows [31]:

$$\frac{k_e}{k_f} = 1 + \sum_{n=1}^{\infty} A_n \left(\frac{k_s - k_f}{k_f} \right)^n \tag{2.22}$$

where A_n describes the local field. The first three values of A_n for spherical particles in a macroscopically isotropic media are given by

$$\left. \begin{aligned} A_1 &= \phi_s \\ A_2 &= \frac{\phi_s \phi_f}{3} \\ A_3 &= \frac{\phi_s \phi_f}{3} \left(\phi_f + 2\phi_s \right) \end{aligned} \right\} \tag{2.23}$$

Using only these first three terms of the expansion, Equation (2.22) is only valid up to $k_s/k_f \leq 2$. Additional coefficients are needed to treat systems in which the relative conductivity of the dispersed solid phase greatly exceeds that of the continuous fluid phase. This cannot be readily accomplished, however, since more details of the microstructure are needed.

Another series expansion approach that accounts for a wider range of k_s/k_f is given as [33]

$$\frac{k_e}{k_f} = 1 + \sum_{n=1}^{\infty} B_n \phi_s^n \tag{2.24}$$

Values of B_n have been evaluated for various geometric dispersions. Unfortunately, Equation (2.24) is inappropriate at high volume fractions.

The more recent statistical investigations of effective transport properties have focused on establishing upper and lower bounds. The most simple such bounds can be established from the particle volume fraction and thermal conductivities of the constituents alone. In this case, the upper and lower bounds are given when the materials are arranged in parallel or series with respect to heat flow, Equations (2.2) and (2.3). More restrictive upper and lower bounds can be derived if it is further assumed that the heterogeneous medium is macroscopically isotropic. Hashin and

Shtrikman [34] showed through variational principles that in this case, the upper and lower bounds are given as follows:

$$k_e \leq k_s \frac{2k_s + k_f - 2\phi_f(k_s - k_f)}{2k_s + k_f + \phi_f(k_s - k_f)} \tag{2.25}$$

$$k_e \geq k_f \frac{2k_f + k_s - 2\phi_s(k_f - k_s)}{2k_f + k_s + \phi_s(k_f - k_s)} \tag{2.26}$$

Equations (2.25) and (2.26) are mathematically equivalent to the equation of Maxwell evaluated for (a) the solid being the discontinuous phase (lower bound) and (b) the solid being the continuous phase (upper bound) for a specified solid volume fraction, ϕ_s. Carson et al. [35] suggested using these solutions together with Equation (2.14) to define internal and external porosity regions.

The most well-known technique of bounding the effective properties of inhomogeneous media is the use of variational principles, namely the *energy minimization* principles. Minimum potential energy of the system gives an upper bound on k_e,

$$\langle \nabla T \rangle \cdot \widetilde{\mathbf{k_e}} \cdot \langle \nabla T \rangle \leq \langle \mathbf{E} \cdot k\mathbf{E} \rangle \tag{2.27}$$

where $\nabla \times \mathbf{E} = \mathbf{0}$ and $\langle \mathbf{E} \rangle = \langle \nabla T \rangle$. Any $\mathbf{E}$ satisfying these conditions gives an upper bound on the tensor of the effective conductivity, $\widetilde{\mathbf{k_e}}$. Minimum complementary energy of the system gives a lower bound on $\widetilde{\mathbf{k_e}}$,

$$\langle \mathbf{q} \rangle \cdot \widetilde{\mathbf{k_e}}^{-1} \cdot \langle \mathbf{q} \rangle \geq \langle \mathbf{J} \cdot k^{-1}\mathbf{J} \rangle \tag{2.28}$$

where $\nabla \cdot \mathbf{J} = 0$ and $\langle \mathbf{J} \rangle = \langle \mathbf{q} \rangle$, the angular brackets denoting an ensemble average[3]. It is helpful to think of $\mathbf{E}$ and $\mathbf{J}$ as trial vectors for the temperature gradient and heat flux, respectively; any $\mathbf{E}$ and $\mathbf{J}$ satisfying the above conditions give the upper and lower bounds on $\widetilde{\mathbf{k_e}}$ when applied to Equations (2.27) and (2.28), respectively. For

---

[3]An ensemble is a collection of a large number of systems which are identical in their macroscopic details but are different in their microscopic details [36]. Within a given ensemble, we are interested only in the average values of the flux and temperature gradient.

example, by taking the temperature gradient and heat flux vectors to be constants, Equations (2.2) and (2.3) are recovered.

Application of Equations (2.27) and (2.28) requires certain idealizations to be made. Many theoretical bounds have been derived for various dispersed phases [36]. The main problem with this approach is that, in order to be successful at constraining the effective thermal conductivity to a narrow range of possible values, more information about the microstructure is needed than is usually available.

2.5 Numerical Solutions

Schneider and Romilly [37] studied the effective thermal conductivity of long cylindrical fibers in a matrix. A finite element method was used to solve the two-dimensional Laplace equation in Cartesian co-ordinates with governing boundary conditions. A correlation of the numerical results was presented which provided agreement with a maximum error of correlation of 2.8%.

Yovanovich et al. [38] studied the effective thermal conductivity of a two-dimensional array of equally spaced square fibers. Using the finite difference technique, they found that the numerical results were in close agreement with the average of upper and lower bounds determined for a characteristic cell. The upper and lower bounds were determined using a procedure described by Elrod [39] in which the upper bound is determined when isotherms are arbitrarily specified and the lower bound is determined when parallel adiabats are specified. This method is described in more detail in Chapter 4.

Carson et al. [40] performed two-dimensional finite element simulations of randomly distributed cylinders oriented with their axes perpendicular to the direction of heat flow. They found that in addition to the component thermal conductivity ratio and volume fractions, the identification of continuous and dispersed phases and

the degree of contact between inclusions were both influential variables, whereas the individual size and shape of the inclusions had only minor effects on determining the effective thermal conductivity of the heterogeneous media, if any at all. They also concluded that "it is unrealistic to expect a model that is a function of the component thermal conductivities and volume fractions alone to provide accurate predictions for all porous materials."

Kumar and Murthy [50] developed a numerical technique using an unstructured finite-volume method for establishing the effective thermal conductivity of three dimensional suspensions of either randomly or regularly placed spheres and cylindrical rods. They used temperature-jump periodic conditions for the characteristic cell. In particular, they studied the effects of varying the surface area, aspect ratio, volume fraction, orientation and distribution of the discontinuous phase for various relative conductivity ratios. Kumar and Murthy concluded that the effects of randomly arranged spherical particles and clustering do not show a significant enhancement in the effective thermal conductivity of an inhomogeneous medium with respect to the enhancement of an ordered array of particles. Preferentially orienting particles in the direction of heat transfer and using high aspect ratio particles, however, provides significant enhancement in effective thermal conductivity and is a promising way of developing high thermal conductivity nanofluids.

2.6 Other Models

Lewis and Nielsen [42] modified the Halpin-Tsai equations for the effective relative shear modulus of a composite to bring it into closer agreement with the experimental data by taking into account the maximum packing fraction of the filler particles. The modified equations for two-phase systems are

$$\frac{k_e}{k_f} = \frac{1 + AB\phi_s}{1 - B\psi\phi_s} \tag{2.29}$$

where

$$B = \frac{\kappa - 1}{\kappa + A} \quad \text{and} \quad \psi = 1 + \phi_s \left(\frac{1 - \phi_m}{\phi_m^2} \right) \tag{2.30}$$

where ϕ_m is the maximum packing fraction of the randomly packed heterogeneous media, $\phi_m = 0.637$ for spheres, and $\kappa = k_s/k_f$ is the relative conductivity ratio of the two phases. The coefficient A depends upon the geometry and orientation of the dispersed phase. Nielsen [43] provides values of A and ϕ_m for a wide range of common geometric dispersions.

If the Maxwell equation is re-written in the following equivalent form,

$$\frac{k_e}{k_f} = \frac{1 + 2\phi_s\beta}{1 - \phi_s\beta} \tag{2.31}$$

where

$$\beta = \frac{\kappa - 1}{\kappa + 2} \tag{2.32}$$

it has a form similar to the Lewis-Nielsen equation, Equation (2.29). The major modification to be noted is the addition of a term which accounts for the maximum packing fraction. This produces a more significant enhancement in the effective thermal conductivity at higher volume fractions where the Maxwell equation tends to underpredict experimental data [21]. For volume fractions less than about 0.30, the predictions of the Maxwell equation and the Lewis-Nielsen equation for spheres are in good agreement. For larger volume fractions, however, the predictions between the two begin to diverge (Figure 2.5). This again provides quantitative justification for neglecting particle-particle interactions for $\phi_s \leq 0.30$. In the limit of $\kappa \to \infty$, Equation (2.29) gives the expected divergence as $\phi_s \to \phi_m$. It can thus be appreciated that for $\phi_s > 0.50$, not shown in Figure 2.5, the predictions of the Lewis-Nielsen equation will be significantly higher than those of the Maxwell equation.

In an experimental study of the effective conductivity of quartz sand packs surrounded by air, Woodside and Messmer [44] proposed an empirical relationship which
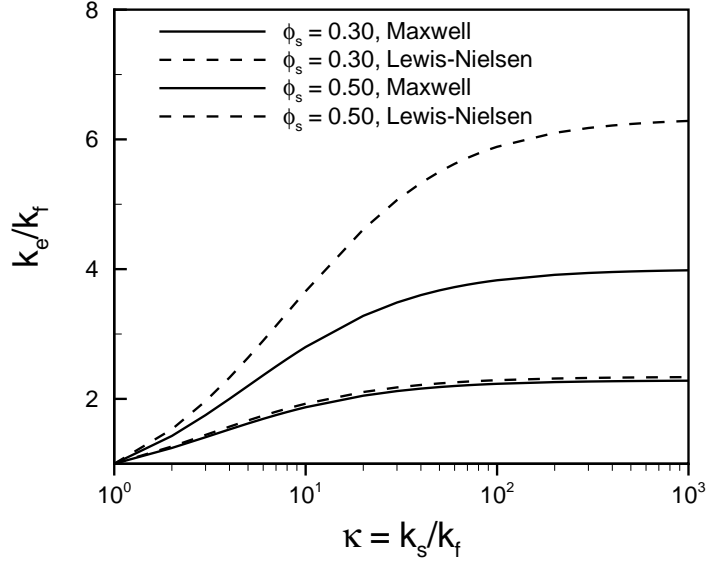
Figure 2.5: Comparison between the Maxwell and Lewis-Nielsen equations for $\phi_s = 0.30$ and $\phi_s = 0.50$

they called the modified geometric mean given as follows:

$$k_e = k_s{}^{\phi_s} k_f{}^{\phi_f} \tag{2.33}$$

Although Equation (2.33) has shown good agreement with selected experimental data for irregularly shaped particles, Parrot and Stuckes [45] have indicated that it is physically unsound and tends to overestimate k_e. Note that Equation (2.33) can be written as a weighted arithmetic mean of the logarithms of the conductivies of the two phases:

$$\log(k_e) = \phi_s \log(k_s) + \phi_f \log(k_f) \tag{2.34}$$

Agari and Uno [46] proposed an empirical relationship for predicting the effective thermal conductivity of generalized dispersions (including spheres, irregular particles, and fibers) based on logarithmic averaging of the thermal conductivities of the two phases, in a similar manner to Equation (2.34):

$$\log(k_e) = \phi C_2 \log(k_s) + (1 - \phi) \log(C_1 k_f) \tag{2.35}$$

25

where C_1 and C_2 are experimentally determined constants of order unity. In this expression, C_1 is attributed to the effect of the dispersed phase on the crystallinity of the continuous phase and C_2 is related to the ability of the dispersed phase to form a network (i.e. percolate). Although Equation (2.35) gives good agreement with experimental data in many instances, experimental work is presently required to establish accurate values of C_1 and C_2 for a given heterogeneous medium.

Cheng and Vachon [17] obtained a theoretical solution to Tsao's probabilistic model by assuming a parabolic distribution of the discontinuous phase in the continuous phase. By selecting a characteristic ensemble of the inhomogeneous medium, and rearranging infinitesimally thin slices of the ensemble in direction parallel to heat flow, they derived the following model for the effective thermal conductivity of the medium:

$$\frac{k_e}{k_f} = (1 - B) + \frac{\ln\left(\frac{\sqrt{1 + B(\kappa - 1)} + B/2\sqrt{C(\kappa - 1)}}{\sqrt{1 + B(\kappa - 1)} - B/2\sqrt{C(\kappa - 1)}}\right)}{\sqrt{C(\kappa - 1)[1 + B(\kappa - 1)]}} \tag{2.36}$$

where

$$B = \sqrt{\frac{3\phi_s}{2}} \quad \text{and} \quad C = \frac{4}{B} \tag{2.37}$$

and $\kappa = k_s/k_f$ as before. Note that Equation (2.36) diverges in the limit of $\kappa \to 1$.

2.7 The Limiting Enhancement

Many of the theoretical models for effective thermal conductivity exhibit some limiting enhancement as the relative conductivity of the particle becomes infinite with respect to the conductivity of the continuous phase. In addition, this limiting enhancement is typically reached once $\kappa \approx 100$ for moderate volume fractions as can be seen in Figure 2.5, for example. This means that physically, once $k_s/k_f \approx 100$, the temperature field inside the particle is practically uniform so that any further enhancement in the
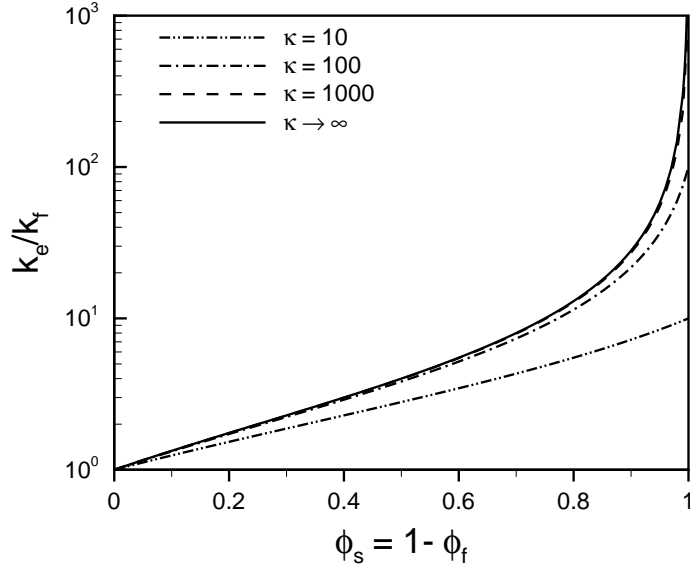
Figure 2.6: Limiting enhancement in effective conductivity

relative conductivity produces very little change in the temperature field inside the particle.

Taking the limit as $k_s/k_f \to \infty$ in the Maxwell equation yields the following:

$$\frac{k_e}{k_f} = \frac{1 + 2\phi_s}{1 - \phi_s} \qquad (2.38)$$

This enhancement in the conductivity of the matrix is reached within 3% once $\kappa = k_s/k_f \simeq 100$ for $\phi_s \approx 0.30$ (Figure 2.6). Since the relative conductivity of the dispersed phase in fluidic thermal interface materials is typically $k_s/k_f \sim 1000$, the assumption of an isothermal particle is thus justified for $\phi_s \leq 0.30$.

This limiting enhancement is also observed in other theoretical models. For example, taking the limit as $k_s/k_f \to \infty$ in the Bruggeman equation gives

$$\frac{k_e}{k_f} = \left(\frac{1}{1 - \phi_s}\right)^3 \qquad (2.39)$$

which, unlike Equation (2.17), is explicit. In addition, the limiting enhancement predicted by the Lewis-Nielsen equation gives

$$\frac{k_e}{k_f} = \frac{1 + A\phi_s}{1 - \psi\phi_s} \qquad (2.40)$$

27

where ψ is given by Equation (2.30) as before.

To enhance the conductivities of fluidic polymers, efforts should thus be directed towards investigating effects associated with various geometries, distribution, orientation, and boundary resistance at the interface between the solid and fluid phases.

2.8   Closing Remarks

The literature review reveals that there are many distinct equations used in the literature to predict effective thermal conductivity of two-phase heterogeneous media. Many equations are valid in the limiting cases of (a) dilute suspensions or (b) suspensions for which the relative conductivity of the dispersed phase is small with respect to the thermal conductivity of the continuous phase, but neither of these conditions are met in typical fluidic thermal interface materials used in microelectronics cooling applications. It remains to develop simple analytical equations with the potential of being extended to various geometries and including effects associated with distribution, orientation, and boundary resistance without treating the system with a modified volume fraction or assuming a dilute suspension.

Chapter 3

Problem Formulation

We consider the case for which the TIM is composed of a simple cubic lattice of identical solid particles of arbitrary geometry embedded in a continuous homogeneous fluid. Both the solid and the fluid phases are isotropic and have constant thermal conductivities k_s and k_f, respectively. Because the TIM is composed of many such particles, the effective conductivity of the system is relatively insensitive to the system boundary conditions so that a characteristic cell can be identified as the control volume subject to analysis without introducing much error (Figure 3.1). The boundary conditions of the cell are determined from symmetry. The four faces of the cell parallel to the direction of heat flow are adiabatic. The other two faces are isothermal with the upper surface being the hotter. Heat thus enters the control volume through the top boundary and exits through the bottom boundary.

Steady conduction through the cell according to Fourier's law is given by

$$Q = k_e A \frac{\Delta T}{L} \equiv \frac{\Delta T}{R} \tag{3.1}$$

where k_e is the effective thermal conductivity of the cell and therefore of the heterogeneous medium as well, A is the cross-sectional area, L is the distance between isothermal boundaries, $\Delta T = T_H - T_L$ is the temperature drop across the cell, and R
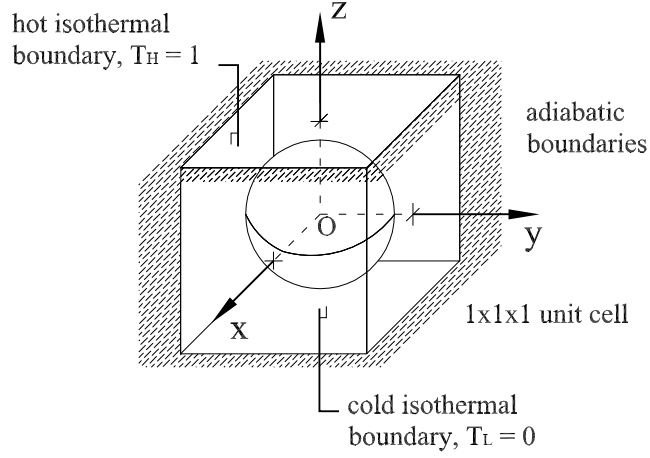
Figure 3.1: Characteristic (unit) cell

is the total thermal resistance of the cell. Upon rearranging Equation (3.1),

$$R = \frac{L}{k_e A} \tag{3.2}$$

If a unit cell is selected, the substitutions $L = 1\ m$ and $A = L^2 = 1\ m^2$ can be made in Equation (3.2), yielding

$$k_e = \frac{1}{R} \tag{3.3}$$

and if the substitution $\Delta T = 1\ K$ is made in Equation (3.1),

$$k_e \left[\frac{\text{W}}{\text{mK}} \right] = Q \left[\frac{\text{W} \cdot 1\text{m}}{1\text{K} \cdot 1\text{m}^2} \right] \tag{3.4}$$

The total thermal resistance, R, of the cell is given by the solution of the coupled 3-D Laplace equations for the solid and fluid phases which, for constant thermal conductivity, is written as

$$\nabla^2 T_i = \frac{\partial^2 T_i}{\partial x^2} + \frac{\partial^2 T_i}{\partial y^2} + \frac{\partial^2 T_i}{\partial z^2} = 0 \quad i = s, f \tag{3.5}$$

The boundary conditions on the four adiabatic boundaries are given by

$$\left(\frac{\partial T_f}{\partial x} \right) \bigg|_{x=\pm\frac{1}{2}} = 0 \tag{3.6}$$

$$\left(\frac{\partial T_f}{\partial y} \right) \bigg|_{y=\pm\frac{1}{2}} = 0 \tag{3.7}$$

The boundary conditions on the two isothermal boundaries are given by

$$T_f\left(x, y, \frac{1}{2}\right) = 1 \tag{3.8}$$

$$T_f\left(x, y, -\frac{1}{2}\right) = 0 \tag{3.9}$$

Perfect thermal contact between the particle and the surrounding medium is assumed. The boundary conditions at the interface are thus given by

$$T_s\left(x, y, z\right) = T_f\left(x, y, z\right) \tag{3.10}$$

$$k_s\left(\frac{\partial T_s}{\partial n}\right) = k_f\left(\frac{\partial T_f}{\partial n}\right) \tag{3.11}$$

where n is the local normal to the interface. In addition, the temperature at the centre of the particle must remain finite, so

$$T_s\left(0, 0, 0\right) \neq \infty \tag{3.12}$$

The total heat flow into or out of the cell can be obtained by applying Fourier's law across either of the isothermal boundaries,

$$Q = \int_{-\frac{1}{2}}^{\frac{1}{2}} \int_{-\frac{1}{2}}^{\frac{1}{2}} k_f\left(\frac{\partial T_f}{\partial z}\right)\Bigg|_{z=+\frac{1}{2}\ \text{or}-\frac{1}{2}} dxdy \tag{3.13}$$

Equation (3.13) also gives the effective conductivity of the unit cell and for constant thermal conductivity, at the upper boundary,

$$\frac{k_e}{k_f} = \int_{-\frac{1}{2}}^{\frac{1}{2}} \int_{-\frac{1}{2}}^{\frac{1}{2}} \left(\frac{\partial T_f}{\partial z}\right)\Bigg|_{z=\frac{1}{2}} dxdy \tag{3.14}$$

The above problem is well-posed but no simple analytical solution is available in general. Numerical work is required to determine the temperature fields in the particle and the surrounding medium.

It is possible, however, to obtain upper and lower bounds on the total heat transfer that can take place through the cell, and hence on the effective conductivity of the cell. These bounds, which are in many instances quite useful at constraining the solution of Equations (3.5) to (3.14) to a narrow range of possible values, are described in the next section.

Chapter 4

Model Development

The model development proceeds from the application of a theorem which is used to establish upper and lower bounds on the total heat transfer that can take place in heterogeneous media. Consider a temperature gradient imposed across a slab into which are dispersed many small particles of a material with different thermal properties. Elrod [39] presented two theorems for establishing bounds on the total heat transfer under such circumstances:

Theorem 1. If the thermal conductivity of the particles is increased or decreased with respect to the surrounding material, the heat flow from one surface to the other will also increase or decrease, respectively.

Theorem 2. The actual heat flow through the inhomogeneous media will be no less than that calculated when adiabats are arbitrarily specified and no more when isotherms are specified (Figure 4.1).

The second theorem can be deduced from the first by noting that nearly isothermal surfaces can be created within a conductive medium by adding thin layers of highly conductive material. If these layers have infinitesimal thickness and infinite conductivity, the specified surface is isothermal. According to Theorem 1, such changes can only tend to increase the total heat flow rate. In contrast, adiabatic surfaces can be
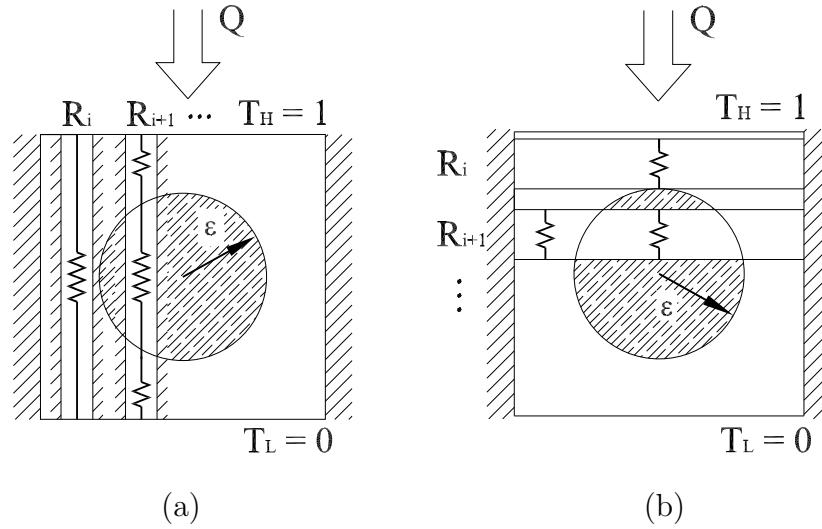
Figure 4.1: (a) Lower (parallel adiabats) and (b) upper (perpendicular isotherms) bounds

speficied by adding infinitesimally thin layers of perfect insualtion. This decreases the total heat flow through the medium.

Theorem 2 has been applied to establish bounds on the effective thermal conductivity of various geometric dispersions including a sphere, a cylinder oriented with its axis parallel to heat flow, a cylinder oriented with its axis perpendicular to heat flow, a rectangular prism, and an ellipsoid. Effects such as thin coatings of materials with different thermal properties and rectangular packing are taken into consideration.

4.1 Sphere in a Unit Cube

As an example of the application of Theorem 2, the TIM is assumed to be composed of a cubic array of uniform spheres in a surrounding medium. The details involved in the development of these bounds are presented for this case.

4.1.1 Lower Bound – Parallel Adiabats

When the adiabats are arranged in parallel as shown in Figure 4.1 (a), two regions within the cell can be identified: (1) the volume of material outside of a right circular cylinder enclosing the particle and (2) the volume of material inside this right circular cylinder. These two resistances are connected in parallel and are related to the total resistance of the cell as follows:

$$\frac{1}{R} = \frac{1}{R_1} + \frac{1}{R_2} = k_e \tag{4.1}$$

where $R_1 = [k_f(1 - \pi\epsilon^2)]^{-1}$ is the resistance of the medium inside region 1, surrounding a right circular cylinder enclosing the particle and R_2 is the resistance of the material inside the cylinder. The volume enclosed by the region inside the cylinder is symmetric so that only one quarter must be considered (Figure 4.2). A differential ring has two resistances in series and has a total resistance

$$dR_2 = dR_{2s} + dR_{2f}$$

$$\text{or} \quad \frac{1}{dR_2} = \frac{1}{dR_{2s} + dR_{2f}} \tag{4.2}$$

where dR_{2s} and dR_{2f} are the differential resistances of the solid and fluid phases in the ring. The differential resistance of the particle can be written from Fourier's law and the equation of a circle as

$$dR_{2s} = \frac{z}{k_s dA} = \frac{\sqrt{\epsilon^2 - x^2}}{k_s \pi x dx} \tag{4.3}$$

where ϵ is the radius of the particle and x is the radius of the ring. Likewise, the resistance of the part of the ring that is composed of the surrounding medium can be written as

$$dR_{2f} = \frac{0.5 - z}{k_f dA} = \frac{0.5 - \sqrt{\epsilon^2 - x^2}}{k_f \pi x dx} \tag{4.4}$$

Upon combining Equations (4.2) to (4.4) and integrating,

$$\frac{1}{R_2} = k_f \pi \int_0^\epsilon \frac{x dx}{0.5 - K\sqrt{\epsilon^2 - x^2}} = k_f \pi I_{lb} \tag{4.5}$$
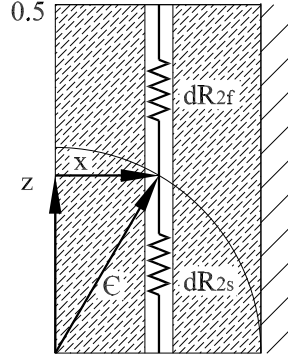
Figure 4.2: R_2, Thermal resistance of material inside right circular cylinder enclosing particle

where

$$K \equiv 1 - \frac{1}{\kappa}, \quad \kappa \equiv \frac{k_s}{k_f}, \quad \text{and} \quad I_{lb} \equiv \int_0^\epsilon \frac{x dx}{0.5 - K\sqrt{\epsilon^2 - x^2}} \tag{4.6}$$

The closed form relation for the integral I_{lb} is given by

$$I_{lb} = \frac{1}{2K^2} \ln \left(\frac{1}{1 - 2K\epsilon} \right) - \frac{\epsilon}{K} \tag{4.7}$$

The lower bound on the effective conductivity (non-dimensionalized with the conductivity of the surrounding medium) of the cell is thus given by

$$\left(\frac{k_e}{k_f} \right)_{lb} = 1 - \pi\epsilon^2 + \pi I_{lb} \tag{4.8}$$

4.1.2   Upper Bound – Perpendicular Isotherms

When the isotherms are arranged in series as shown in Figure 4.1 (b), two different regions in the unit cell can be identified: (1) the volume of material above and below a rectangular prism enclosing the particle and (2) the volume of material inside this rectangular prism. These two resistances are connected in series and are related to the total resistance of the cell as follows:

$$R = 2R_1 + R_2 = \frac{1}{k_e} \tag{4.9}$$

35

where $R_1 = (0.5 - \epsilon)/k_f$ is now the resistance of the medium above and below the rectangular prism enclosing the particle. Again, we consider one quarter (half of the upper half) of the resistance of the region shaded as R_2 (Figure 4.3). A differential ring now has two resistances in parallel and has a total resistance

$$\frac{1}{dR_2} = \frac{1}{dR_{2s}} + \frac{1}{dR_{2f}} \tag{4.10}$$

The differential resistance of the particle can be written as

$$dR_{2s} = \frac{dz}{k_s \left(\dfrac{\pi x^2}{2} \right)} = \frac{2dz}{k_s \pi (\epsilon^2 - z^2)} \tag{4.11}$$

and that of the part of the ring composed of the surrounding medium can be written as

$$dR_{2f} = \frac{dz}{k_f \left(0.5 - \dfrac{\pi x^2}{2} \right)} = \frac{2dz}{k_f (1 - \pi(\epsilon^2 - z^2))} \tag{4.12}$$

Upon combining Equations (4.10) to (4.12) and integrating,

$$R_2 = \frac{2}{k_f} \int_0^\epsilon \frac{dz}{1 + \pi(\kappa - 1)(\epsilon^2 - z^2)} = \frac{2I_{ub}}{k_f} \tag{4.13}$$

where

$$I_{ub} \equiv \int_0^\epsilon \frac{dz}{1 + \pi(\kappa - 1)(\epsilon^2 - z^2)} \tag{4.14}$$

again has an analytical solution which is given by

$$I_{ub} = \frac{\tanh^{-1}\left[\epsilon \sqrt{\dfrac{\pi(\kappa - 1)}{\pi(\kappa - 1)\epsilon^2 + 1}} \right]}{\sqrt{\pi(\kappa - 1)[1 + \pi(\kappa - 1)\epsilon^2]}} \tag{4.15}$$

and $\kappa = k_s/k_f$ as before.

The upper bound on the effective conductivity (non-dimensionalized with the conductivity of the surrounding medium) of the cell is thus given by

$$\left(\frac{k_e}{k_f} \right)_{ub} = [1 - 2\epsilon + 2I_{ub}]^{-1} \tag{4.16}$$

36
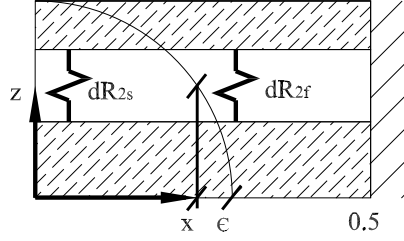
Figure 4.3: R_2, Thermal resistance of material inside rectangular prism enclosing particle

4.2 Other Geometries

Applying the same procedure described in Section 4.1, upper and lower bounds have been derived for (1) a cylinder oriented with its axis parallel to heat flow, (2) a cylinder oriented with its axis perpendicular to heat flow, (3) a rectangular prism, and (4) an ellipsoid in a unit cell (Figure 4.4).

4.2.1 Cylinder With Axis Parallel to Heat Flow

A finite circular cylinder oriented with its axis parallel to the direction of heat flow in a unit cell has the following lower and upper bounds on effective thermal conductivity:

$$\left(\frac{k_e}{k_f}\right)_{lb} = 1 - \pi\epsilon^2 + \frac{\pi\epsilon^2}{1 - 2Kh}$$

$$\left(\frac{k_e}{k_f}\right)_{ub} = \left(1 - 2h + \frac{2h}{1 + (\kappa - 1)\pi\epsilon^2}\right)^{-1}$$

(4.17)

where ϵ is the radius of the cylinder, $0 \leq \epsilon \leq 0.5$, and $2h$ is its height, $0 \leq 2h \leq 1$; and where κ and K are defined in Equation (4.6).

4.2.2 Cylinder With Axis Perpendicular to Heat Flow

A finite circular cylinder oriented with its axis oriented perpendicular to the direction of heat flow in a unit cell has the following lower and upper bounds on effective thermal

37
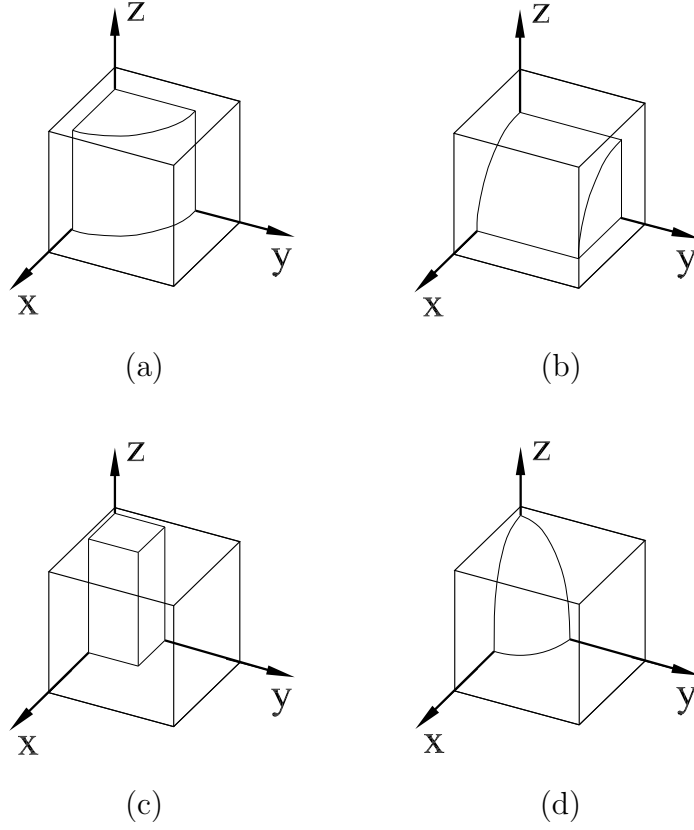
Figure 4.4: Upper and lower bounds presented for (a) cylinder with axis parallel to heat flow, (b) cylinder with axis perpendicular to heat flow, (c) rectangular prism, and (d) ellipsoid in a unit cell ($1/8^{\text{th}}$ cell shown). Heat flow is along the $z-$axis.

conductivity:

$$\left(\frac{k_e}{k_f}\right)_{lb} = 1 - 4\epsilon h - 2hI_{lb}$$

$$\left(\frac{k_e}{k_f}\right)_{ub} = (1 - 2\epsilon + I_{ub})^{-1}$$

(4.18)

where

$$I_{lb} = \frac{\pi}{2K} + \frac{\tan^{-1}\left(\frac{f(K\epsilon)}{0.5 - K\epsilon}\right)}{Kf(K\epsilon)}$$

(4.19)

and

$$I_{ub} = \frac{\pi}{2h\,(\kappa - 1)} - \frac{\tan^{-1}\left[\dfrac{f\,(4h\epsilon(\kappa - 1))}{0.5 + 2h\epsilon(\kappa - 1))}\right]}{h\,(\kappa - 1)\,f(4h\epsilon(\kappa - 1))} \tag{4.20}$$

in which $f(x) = \sqrt{0.5^2 - x^2}$ and where ϵ is the radius of the cylinder, $0 \le \epsilon \le 0.5$, and $2h$ is its height, $0 \le 2h \le 1$; κ and K are defined in Equation (4.6).

4.2.3 Rectangular Prism

A rectangular prism in a unit cell has the following lower and upper bounds on effective thermal conductivity:

$$\left(\frac{k_e}{k_f}\right)_{lb} = 1 - 4ab + \frac{4ab}{1 - 2Kc}$$

$$\left(\frac{k_e}{k_f}\right)_{ub} = \left(1 - 2c + \frac{2c}{1 + 4(\kappa - 1)ab}\right)^{-1} \tag{4.21}$$

where $2a$, $2b$, and $2c$ are the dimensions of the prism in the $x-$, $y-$, and $z-$axes, respectively. The direction of heat flow is along the $z-$axis. The dimensions $2a$ and $2b$ are interchangeable as expected. The terms κ and K are defined in Equation (4.6).

4.2.4 Ellipsoid

An ellipsoid in a unit cell has the following lower and upper bounds on effective thermal conductivity:

$$\left(\frac{k_e}{k_f}\right)_{lb} = 1 - \pi ab \left(1 + \frac{1}{Kc}\right) + 2I_{lb}$$

$$\left(\frac{k_e}{k_f}\right)_{ub} = (1 - 2c + 2I_{ub})^{-1} \tag{4.22}$$

where

$$I_{lb} = \int_0^b \tan^{-1}\left(\frac{\sqrt{0.5^2 - \alpha^2\beta^2}}{0.5 - \alpha\,\beta}\right) \frac{dy}{\alpha\sqrt{0.5^2 - \alpha^2\beta^2}} \tag{4.23}$$

in which

$$\alpha \equiv \frac{Kc}{a} \quad \text{and} \quad \beta \equiv a\sqrt{1 - \frac{y^2}{b^2}} \tag{4.24}$$

and

$$I_{ub} = \frac{c \ \tanh^{-1}\left[\sqrt{\frac{\pi ab(\kappa - 1)}{\pi ab(\kappa - 1) + 1}}\right]}{\sqrt{\pi ab(\kappa - 1)[1 + \pi ab(\kappa - 1)]}} \tag{4.25}$$

and where $2a$, $2b$, and $2c$ are the dimensions of the prism in the $x-$, $y-$, and $z-$axes, respectively. The direction of heat flow is along the $z-$axis. The dimensions $2a$ and $2b$ are interchangeable as expected. The terms κ and K are defined in Equation (4.6). The integral of Equation (4.23) must be evaluated numerically.

4.3 Thin Coatings

Upper and lower bounds have also been derived for the various geometries where the thermal properties of the surrounding shell are not necessarily equivalent to those of the particle itself. Forcing this thickness, τ, equal to 0, the relative conductivity of the coating, κ_c, equal to 1, and the dimensions of the rectangular cell, A, B, and C, equal to 0.5 recovers the previous relationships. A sphere in a unit cell with a coating of a material with thermal properties not necessarily equal to those of the sphere has the following lower and upper bounds on effective thermal conductivity:

$$\left(\frac{k_e}{k_f}\right)_{lb} = 1 - \frac{\pi(\epsilon + \tau)^2}{4AB} + \frac{\pi C}{2AB}(I_{lb,1} + I_{lb,2})$$

$$\left(\frac{k_e}{k_f}\right)_{ub} = \left[1 - \frac{(\epsilon + \tau)}{C} + \frac{4AB}{C}(I_{ub,1} + I_{ub,2})\right]^{-1} \tag{4.26}$$

where

$$I_{lb,1} = \int_0^\epsilon \frac{x dx}{C - K_c\sqrt{(\epsilon+\tau)^2 - x^2} - \left(\dfrac{1}{\kappa_c} - \dfrac{1}{\kappa}\right)\sqrt{\epsilon^2 - x^2}}$$

(4.27)

$$I_{lb,2} = \int_\epsilon^{\epsilon+\tau} \frac{x dx}{C - K_c\sqrt{(\epsilon+\tau)^2 - x^2}}$$

and

$$I_{ub,1} = \int_0^\epsilon \frac{dz}{4AB + (\kappa_c - 1)\pi[(\epsilon+\tau)^2 - z^2] + (\kappa - \kappa_c)\pi(\epsilon^2 - z^2)}$$

(4.28)

$$I_{ub,2} = \int_\epsilon^{\epsilon+\tau} \frac{dz}{4AB + (\kappa_c - 1)\pi[(\epsilon+\tau)^2 - z^2]}$$

where ϵ is the radius of the pure sphere and τ is the thickness of the coating; and κ and K are defined in Equation (4.6) and

$$\kappa_c \equiv k_c/k_f \qquad \text{and} \qquad K_c \equiv 1 - 1/\kappa_c$$

(4.29)

in which k_c is the thermal conductivity of the coating.

The upper and lower bounds have been derived for various other geometries with thin coatings. These results are presented in Appendix B.

Chapter 5

Numerical Solution Using the Finite Element Method

The numerical solution of the Laplace equation subject to appropriate boundary conditions was performed using the finite element method (FEM). The entire solution methodology was developed using the commercially available software FEMLAB (COMSOL Inc., USA) which can be run either as a programmable toolbox for the development of finite element solutions on MATLAB (The Mathworks Inc., USA) or as a simple graphical user interface-based integrated environment for solution of partial differential equations (PDEs) using the finite element method. The latter of these was adequate given the level of complexity of the problem formulation in the present work.

Details concerning the implementation of the finite element method to solve PDEs are available in standard textbooks, e.g. [47]. The goal of the present work was to employ a generalized technique that is widely available and can be implemented relatively easily to validate the proposed analytical models. Consequently, in this section, only the details of the procedure required to formulate the problem, the types of elements used, and mesh refinement and error control are discussed. The formulation

of the problem, specifically the statement of the problem in the generalized PDE form (see Chapter 3) and subsequent recasting in the weak form, are crucial steps in achieving a successful numerical solution.

5.1   Non-Dimensionalization and Weak Form of the Laplace Equation

The Laplace equation and boundary conditions governing the heat conduction problem can be non-dimensionalized by scaling the temperature as follows,

$$\Theta \equiv \frac{T - T_L}{T_H - T_L} \tag{5.1}$$

where Θ is the non-dimensional temperature scale, T is the local temperature, and T_H and T_L are the temperatures of the top and bottom faces of the cell, respectively. The non-dimensional Laplace equation is thus given by

$$\nabla^2 \Theta_j = 0 \qquad j = s, f \tag{5.2}$$

which is again valid inside the solid particle and inside the continuous fluidic phase.

Equation (5.2) represents a general PDE formulation of the type

$$\nabla \cdot \mathbf{\Gamma} = F \tag{5.3}$$

where $\mathbf{\Gamma} = \nabla \Theta_j$ and $F = 0$. Equation (5.3) is an example of a strong form of the PDE formulation. To implement a finite element solution, Equation (5.3) must be written in its weak form[1] which for the present problem is an expression of the non-dimensional Laplace equation as an equality of integrals. Multiplying both sides of

---

[1]So-called because a solution of the temperature field satisfying the weak formulation is also a solution of Equation (5.2) only if the solution is sufficiently smooth.

Equation (5.3) by an arbitrary test function[2] v and integrating over the volume, V, of the domain, we get

$$\int_V v \nabla \cdot \mathbf{\Gamma} dV = \int_V v F dV = 0 \qquad (5.4)$$

The divergence theorem can be applied to the above result to give

$$\int_V v \nabla \cdot \mathbf{\Gamma} dV = \int_A v \mathbf{\Gamma} \cdot \hat{\mathbf{n}} dA - \int_V \mathbf{\Gamma} \cdot \nabla v dV = 0 \qquad (5.5)$$

Now, we use the generalized Neumann boundary condition which is written as

$$-\mathbf{\Gamma} \cdot \hat{\mathbf{n}} = G \qquad (5.6)$$

Combining Equations (5.5) and (5.6) gives

$$\int_A v G dA + \int_V \mathbf{\Gamma} \cdot \nabla v dV = 0 \qquad (5.7)$$

Together with the Dirichlet boundary condition, stated as

$$\mathbf{R} = \mathbf{0} \qquad (5.8)$$

where $\mathbf{R}$ represents a vector of Dirichlet boundary conditions, this is the weak form of the Laplace equation.

5.2   Numerical Solution Procedure

This section describes the procedure used to approximate the solution of Equation (5.7) subject to Equation (5.8). The computational domain was first discretized into tetrahedrons, and Langrangian elements of second order (quadratic) were used. This implies that there exist ten nodes on each tetrahedral element – four at the vertices and one at the midpoint of each edge. For each of these nodes, there is a degree

---

[2]When discretizing a geometry into finite elements, the temperature field becomes piecewise smooth. As a result, it is not clear what it means to take its second derivative in Equation (5.2). A solution is to test the equation for the temperature field against suitable functions, v, of that class.

of freedom, U_i, and a basis function, ϕ_i. The degree of freedom is the value of the non-dimensional temperature at a node point, the set of which is called the finite element space. The basis functions are piecewise continuous functions (in this case, quadratic polynomials) on the intervals between adjacent nodes such that $\phi_i = 1$ at node i and $\phi_i = 0$ at all other nodes. The temperature for an element is thus given in terms of the basis functions and degrees of freedom as

$$T = \sum_i U_i \phi_i \tag{5.9}$$

The weak form of the Laplace equation was discretized by assuming the test function v to be the shape function ϕ_i in each element.

The boundaries of the geometry are partitioned into triangular boundary elements. Since the boundary of the dispersed particle is in general curved (a sphere, for example) the meshed surface is only an approximation to the original curved boundary. The mesh was generated to ensure that the domain error was small at the curved boundary thus yielding smaller elements near this boundary. The solution of the final assembled matrix was achieved using the conjugate gradient method. The conjugate gradient method is an iterative method and is applied to sparse systems which are too large to be handled efficiently by direct methods such as Gaussian elimination. The effective thermal conductivity was obtained from the average of the integrated normal heat flux over the top face and bottom faces of the cell. This process of obtaining a solution from which effective thermal conductivity is determined was repeated with a finer mesh until a global convergence criterion was attained, namely until

$$\left| \frac{\left(\dfrac{k_e}{k_f}\right)_{i+1} - \left(\dfrac{k_e}{k_f}\right)_{i}}{\left(\dfrac{k_e}{k_f}\right)_{i+1}} \right| \leq 0.005 \tag{5.10}$$

where i is iteration i and $i+1$ is iteration $i+1$ to ensure two-decimal place accuracy was typically achieved.

45

5.3 Validation of Finite Element Method of FEMLAB

A numerical solution for the total heat flow in a finite isotropic cylindrical tube with temperature-specified boundary conditions (Figure 5.1) was performed in FEMLAB. This is a problem for which there is an analytical solution. The exercise was necessary to establish confidence in the finite element technique of FEMLAB prior to studying the problem of effective thermal conductivity of inhomogeneous materials.

For steady conduction, the total thermal resistance of finite isotropic cylindrical tubes is given by

$$R_{tot} = \frac{\overline{T}_s - \overline{T}_{z=t}}{Q} = R_s + R_{1d} \tag{5.11}$$

where $\overline{T}_s$ is the mean source temperature, $\overline{T}_{z=t}$ is the mean temperature of the surface at $z = t$, and Q is the total heat flow; and where R_s and R_{1d} are the spreading and one-dimensional (or material) resistances, respectively.

The dimensionless spreading resistance for isotropic finite disks with negligible thermal resistance at the lower interface, $z = t$ (i.e. Bi $= hb/k \to \infty$) is given by the following solution [48]:

$$4kaR_s = \frac{8}{\pi\epsilon} \sum_{n=1}^{\infty} \frac{J_1(\delta_n\epsilon) \ \sin(\delta_n\epsilon)}{\delta_n^3 J_0^2(\delta_n)} \tanh(\delta_n\tau) \tag{5.12}$$

where $\epsilon = a/b$, $\tau = t/b$. J_0 and J_1 are Bessel functions of the first kind of order zero and one, respectively, with dimensionless eigenvalues δ_n.

The one-dimensional resistance of the region inside the finite disk is given by

$$R_{1d} = \frac{\overline{T}_{z=0} - \overline{T}_{z=t}}{Q} = \frac{t}{kA_t} \tag{5.13}$$

In the present problem, the temperature of the source and sink were taken as $T_1 = 1$ and $T_2 = 0$, respectively. The total heat flow rate is therefore given by

$$Q = \frac{1}{R_{tot}} \tag{5.14}$$
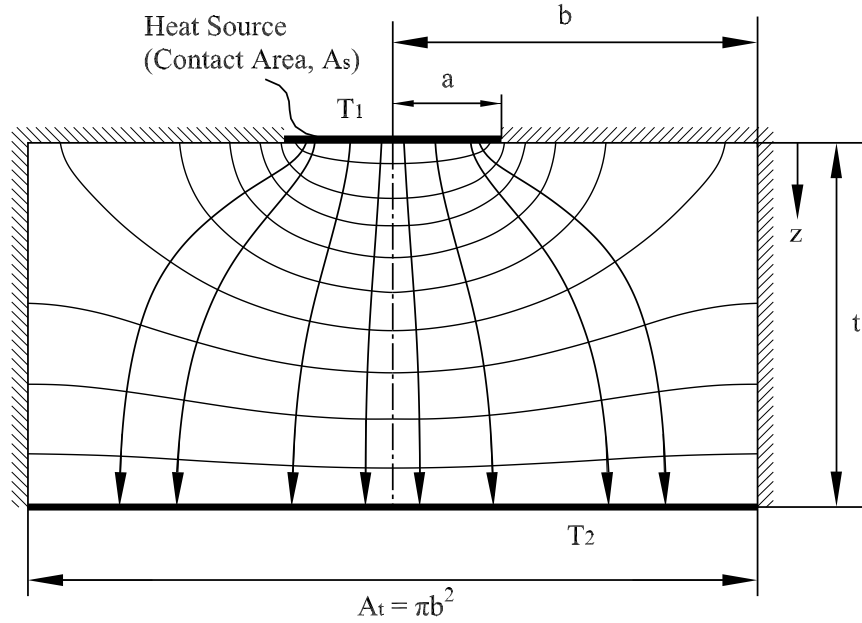
Figure 5.1: A finite isotropic cylindrical tube with isothermal source of area A_s and sink of area A_t

In addition, the height and radius of the tube were $t = 0.5\ m$ and $b = 1\ m$ with a source of radius $a = 0.2\ m$, and the material was specified as $k = 1\ W/mK$. The one-dimensional resistance is thus

$$R_{1d} = \frac{t}{kA_t} = \frac{1}{2\pi} \tag{5.15}$$

The spreading resistance must be programmed and solved numerically. The series in Equation (5.12) was implemented in Maple (Waterloo Maple Inc., Canada). The series converges quickly so that three-decimal place accuracy is achieved with only 300 terms. The total heat flow rate calculated from the analytical solution is $Q = 0.961\ W$.

A two-dimensional axially symmetric computational domain was identified for the present problem and studied using the finite element technique of FEMLAB. A very fine mesh was used at the boundaries, in particular in the vicinity of $(r \to a, z = 0)$ to resolve the very high flux. The computational domain was discretized into a triangular

47

mesh[3] and approximately 100K Langrangian elements of second order were used. The total heat flows integrated over the source and over the lower surface of the tube were $Q_1 = 0.956\ W$ and $Q_2 = 0.960\ W$, respectively. As a note, although $Q_1 = Q_2$ in theory, it is more appropriate to use the total heat flow rate integrated over the lower surface in the present problem. This is because there is likely some computational truncation error in multiplying very high values of heat flux by very finely resolved areas in the vicinity of the boundary of the source.

The numerical solution for the total heat flow in a finite isotropic cylindrical tube with temperature-specified boundary conditions is in very good agreement with the available analytical solution: $Q = 0.960\ W$ in comparison with $Q = 0.961\ W$, respectively. The reliability of the finite element technique of FEMLAB is thus sufficient for a numerical study of the effective conductivity of inhomogeneous media.

5.4   Numerical Results and Discussion

Numerical simulations were performed for various cases in which the geometry, volume fraction, and relative conductivity ratio κ of the dispersed phase were varied. First, the numerical results of effective thermal conductivity of a sphere in a unit cube are compared with the predictions of the model. Second, the aspect ratio and orientation of the particles are studied. As a result, a generalized condition can be identified for which effective thermal conductivities of various geometries are approximately equal for specified volume fraction, ϕ, and relative conductivity, κ. Third, the effects of a thin oxide and ordered liquid layering around the particle are studied. Finally, the effect of clustering (or agglomeration) of particles in the domain is investigated for a suspension of spheres. A large number of numerical data were produced as a result and are included in Appendix C.

---

[3]Ideally, the computational domain would be resolved in oblate spheroidal co-ordinates.
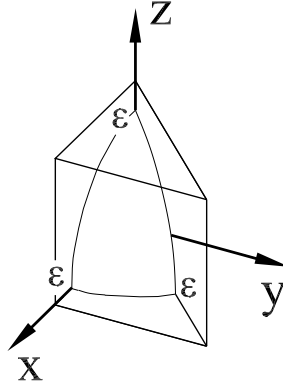
Figure 5.2: Computational domain for a sphere in a unit cell. Heat flow is along the $z-$axis.

5.4.1 Sphere in a Unit Cell

Consider first the case of a simple cubic lattice of identical solid spheres embedded in a homogeneous fluid. The conductivity of the sphere is specified by giving its ratio, κ, to that of the conductivity of the fluid. Likewise, the sphere radius is specified by its ratio, ϵ, to that of the lattice spacing. The volume fraction of the spherical inclusions is thus

$$\phi = \frac{V_s}{V_{cell}} = \frac{4}{3}\pi\epsilon^3 \qquad (5.16)$$

The above problem was studied numerically for volume fractions of 0.10, 0.20, 0.30, 0.40, and 0.45 and relative conductivities of 10, 100, and 1000. Symmetry in the Laplace equation, geometry, and boundary conditions reduces the computational domain to $1/16^{\text{th}}$ of the unit cell (Figure 5.2). Approximately 50000 tetrahedral elements were used in each simulation and numerical results were established to within two-decimal place accuracy from further refinement of the mesh.

The numerical work confirms that the upper and lower bounds for a sphere in a unit cell presented in Chapter 4 are indeed valid (Figures 5.3 to 5.5). The geometric mean of the upper and lower bounds gives good agreement with the numerical results. The RMS error and maximum % difference between the two are expressed as

49
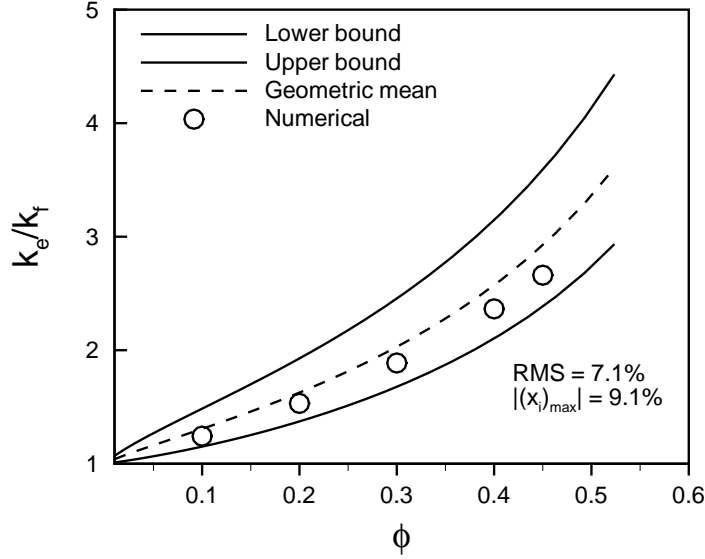
Figure 5.3: Numerical results versus upper and lower bounds for sphere, $\kappa = 10$

percentages and are shown in each of the figures. These are defined as follows:

$$\text{RMS} \equiv \sqrt{\frac{\sum_{i=1}^{n} x_i^2}{n}} \tag{5.17}$$

where

$$x_i \equiv \left| \frac{(k_e/k_f)_{model} - (k_e/k_f)_{numerical}}{(k_e/k_f)_{model}} \right| \tag{5.18}$$

and n is the number of points, in this case, 5. The maximum % difference, $(x_i)_{max}$, occurs at $\phi = 0.45$ for all three simulations. The RMS values for $\kappa = 10$, 100, and 1000 are 7.1%, 27.1%, and 34.5%, respectively. The maximum % difference for $\kappa = 10$, 100, and 1000 are 9.1%, 37.5%, and 49.4%, respectively. Both the RMS and the maximum % difference are largest when $\kappa = 1000$. This behaviour is expected since the % difference, as defined by x_i, asymptotically tends to zero as the conductivity ratio tends to unity when the volume fraction tends to zero (i.e. $x_i \to 0$ when $\kappa \to 1$ and when $\phi \to 0$).
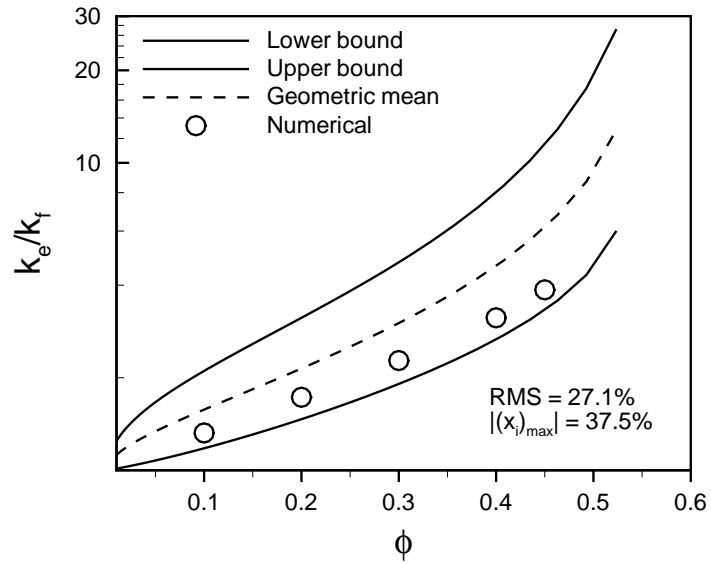
Figure 5.4: Numerical results versus upper and lower bounds for sphere, $\kappa = 100$
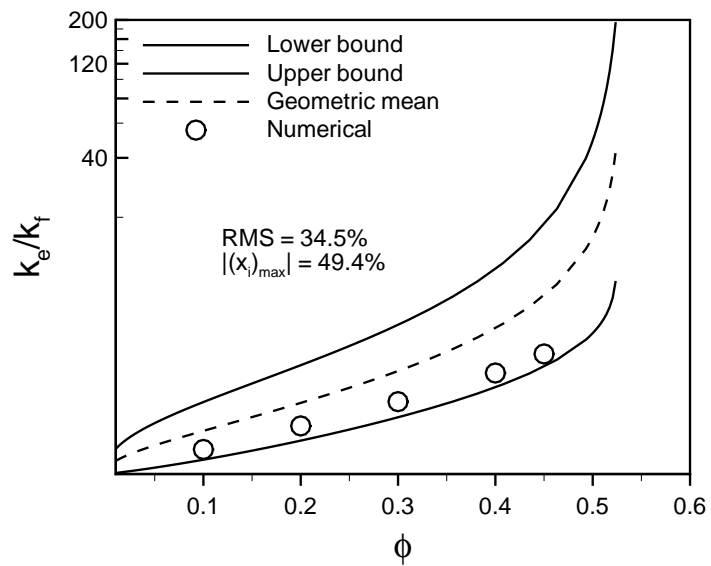
Figure 5.5: Numerical results versus upper and lower bounds for sphere, $\kappa = 1000$
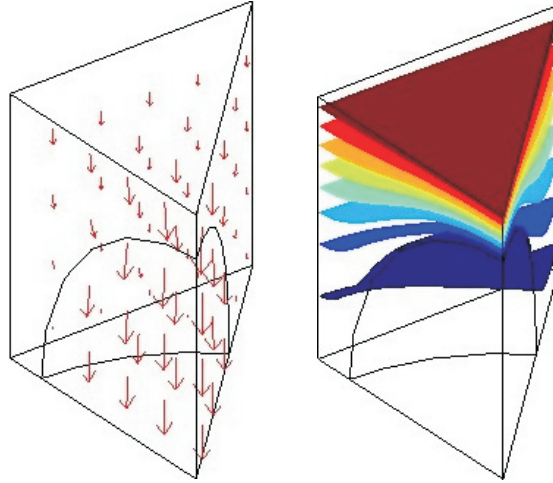
Figure 5.6: (a) Flux lines and (b) isotherms for $1/16^{\text{th}}$ cell, $\phi = 0.30$ and $\kappa = 100$

The model developed consistently overpredicts the numerical results for the three cases studied. This suggests that the 3-D temperature field inside the cell more closely resembles that for a system in which adiabats are assumed parallel to the direction of heat flow. Isotherms and lines of flux from the numerical results for $\kappa = 100$ and $\phi = 0.30$ are included in Figure 5.6. It is clear from this figure that the adiabats are neither parallel to the direction of heat flow nor are the isotherms perpendicular to it; and, in fact, if they were, both bounds would be mathematically equivalent and an analytical solution would be available.

The previous numerical results exhibit the limiting enhancement discussed in Chapter 2 (Figure 5.7). As the relative particle conductivity is increased from $\kappa = 10$ to $\kappa = 100$, there is significant improvement in effective thermal conducitivity, particularly at high volume fractions. The same is not true, however, as the relative particle conductivity is increased from $\kappa = 100$ to $\kappa = 1000$. In this instance, the enhancements in thermal conductivity are nearly identical. The particle is essentially isothermal if $\kappa > 100$, so any changes produced in the temperature field within the cell as a result of increasing κ beyond ~ 100 are relatively small when the volume fraction is less than about 0.4. A limiting enhancement in effective thermal conduc-
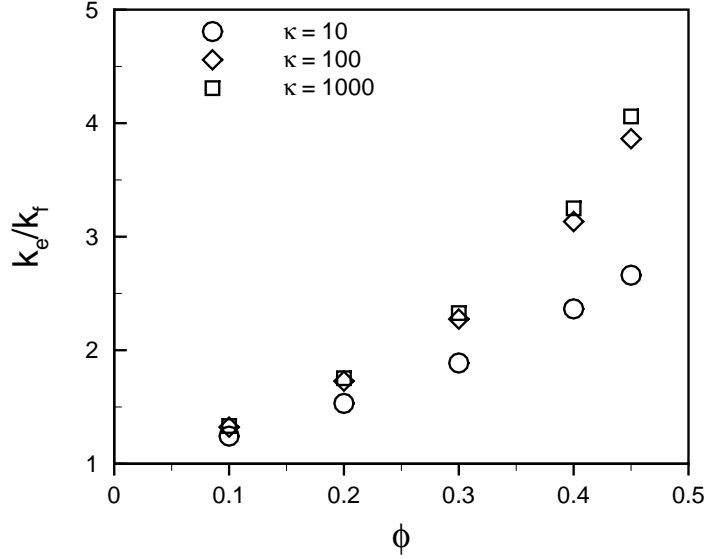
Figure 5.7: Numerical results for sphere in unit cell for $\kappa = 10$, $\kappa = 100$, and $\kappa = 1000$

tivity has been reached. In taking the limits as $\kappa \to \infty$ of the upper and lower bounds for effective thermal conductivity of a sphere in a unit cube (Chapter 4),

$$\lim_{\kappa \to \infty} \left(\frac{k_e}{k_f} \right)_{ub} = (1 - 2\epsilon)^{-1} \tag{5.19}$$

$$\lim_{\kappa \to \infty} \left(\frac{k_e}{k_f} \right)_{lb} = 1 - \pi\epsilon^2 + \pi \left[\frac{1}{2} \ln \left(\frac{1}{1 - 2\epsilon} \right) - \epsilon \right] \tag{5.20}$$

The limiting enhancement is given by the geometric mean of Equations (5.19) and (5.20). For $\phi = 0.30$, the relative particle conductivity must be increased by an order of magnitude (from $\kappa = 100$ to 1000) for a further enhancement of just 10% in effective thermal conductivity of the medium. Also, effective thermal conductivity for $\kappa = 100$ is within approximately 12% of its maximum possible enhancement ($\kappa \to \infty$) (Figure 5.8). The present model, derived from the upper and lower bounds, thus also exhibits the limiting enhancement in effective thermal conductivity observed from the numerical results. In addition, for the case of perfectly conducting spheres, the model gives the correct divergence of effective thermal conductivity as the spheres touch (i.e. as $\kappa \to \infty$ and $\phi \to \pi/6$, $k_e/k_f \to \infty$).

53
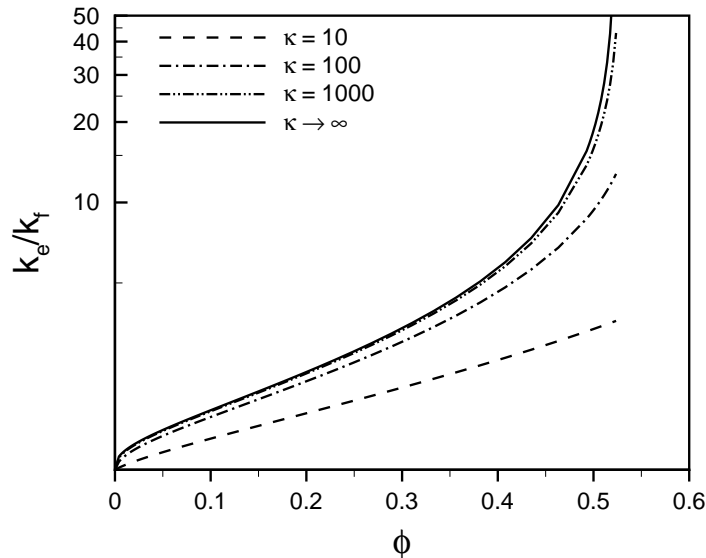
Figure 5.8: Limiting enhancement for $\kappa \to \infty$

The numerical results in Figure 5.5 ($\kappa = 1000$) are compared with the predictions of Maxwell [7], McPhedran and McKenzie ($M = 4$) [12], and Lewis and Nielsen [42], as well as with the predictions of the lower bound (Figure 5.9). The agreement between the numerical data and the model of McPhedran and McKenzie is excellent for $\phi \leq 0.45$ and also with the Maxwell equation for $\phi \leq 0.30$. Both the predictions of McPhedran and McKenzie and Maxwell consistently underpredict the results; however, this is expected since neither model accounts for the interactions of an infinite number of neighbouring particles which is the case studied. In addition, it is noted that the equation developed by Maxwell and the one developed by McPhedran and McKenzie fall below the lower bound at $\phi \approx 0.44$ and $\phi \approx 0.50$, respectively. These models are therefore inadequate for volume fractions exceeding these values when $\kappa = 1000$. In contrast , the Lewis-Nielsen equation consistently overpredicts the numerical results and never falls below the lower bound. It predicts effective thermal conductivities intermediate to the lower bound and the geometric mean of the bounds and essentially recovers the lower bound at the critical volume fraction, $\phi \approx 0.524$.
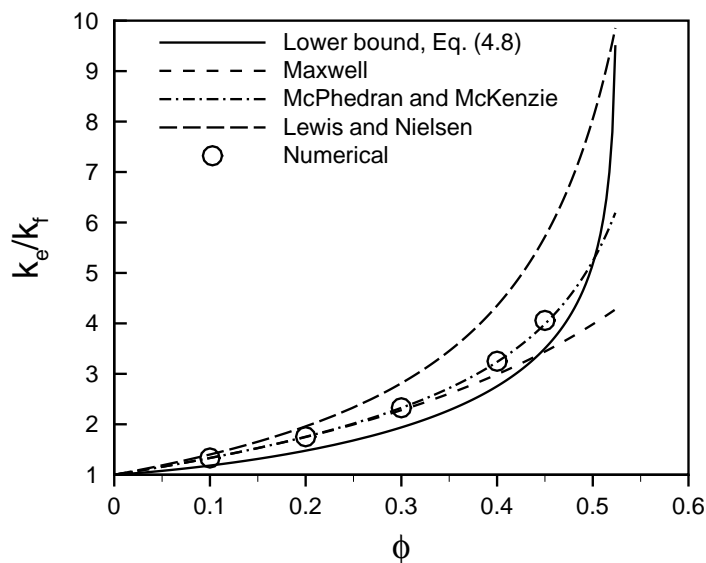
Figure 5.9: Numerical results with predictions of Maxwell [7], McPhedran and McKenzie [12], and Lewis and Nielsen [42]

5.4.2 Is Volume Fraction a Representative Non-dimensional Parameter for Various Geometries?

It is unrealistic to expect a model for effective thermal conductivity which is a function of relative conductivity, κ, and volume fraction, ϕ, alone to give accurate predictions for all composite media. The ability to identify the continuous and discontinuous phases has already been noted as another important factor, for example (Chapter 2). In addition, the shape and orientation of the discontinuous phase is important.

Figure 5.10 shows numerical results of the enhancement in effective thermal conductivity for various solid geometric dispersions for a range of aspect ratios with $\kappa = 1000$. The need for more detailed information about the microstructure beyond the relative volume concentrations of the two phases is apparent. The effects of aspect ratio and orientation of the particles are investigated. In particular, numerical results for a rectangular prism, a parallel cylinder, a perpendicular cylinder, and an
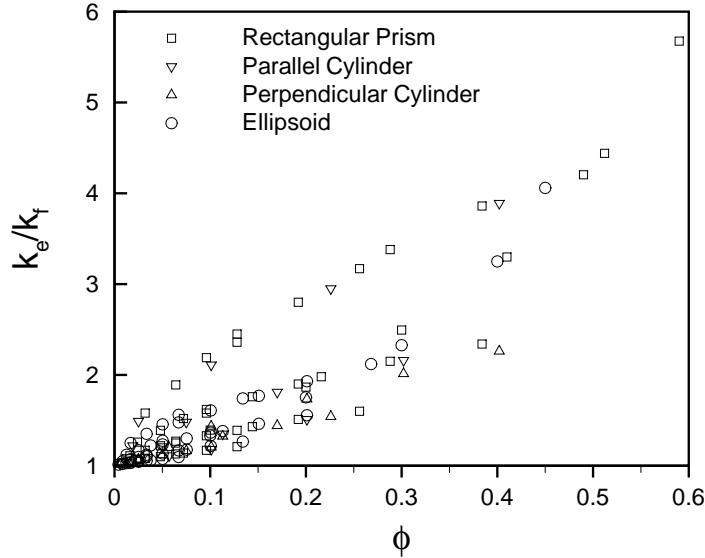
Figure 5.10: Numerical results of effective thermal conductivity for geometric dispersions, $\kappa = 1000$

ellipsoid in a unit cube are considered. Three cases can be identified: these are (1) tall and slender cylinders (high aspect ratio), (2) square cylinders (moderate aspect ratio), and (3) short and latitudinous cylinders (low aspect ratio). It is expected that enhancement in effective thermal conductivity is largest for case (1), where the highly conductive cylindrical particle is well-connected throughout the medium, and smallest for case (3), where the poor connectivity of the highly conductive phase throughout the medium causes an insulating effect dominated by the low conductivity fluid. In addition, numerical simulations were performed for $\kappa = 1000$, 100, and 10, but due to the large number of similar graphs resulting from considering all three conductivity ratios, only the results for $\kappa = 1000$ are presented in the body of the section. Such additional numerical data would not convey any new information to the reader beyond that the agreement between the model and the numerical results improves as κ is reduced. Before the numerical results are presented, definitions of the aspect ratio and identification of characteristic cells for the various geometries are described.

5.4.3 Aspect Ratio

The aspect ratio and volume fraction must be defined for each geometric dispersion. These are summarized at the end of this section in Table 5.1. A convenient definition of the aspect ratio is as follows:

$$\alpha \equiv \frac{L_z}{L_{xy}} \tag{5.21}$$

where L_z is a characteristic length along the $z-$axis, in the direction of heat flow, and $L_{xy} = \sqrt{L_x L_y}$ is a characteristic length scale in the plane perpendicular to heat transfer, the square root of the length scales along the $x-$ and $y-$axes.

Parallel and perpendicular cylinders. A cylinder in a unit cell has in general two characteristic dimensions: these are the ratio, 2ϵ, of its diameter to the lattice spacing in that direction and the ratio, $2h$, of its height to the lattice spacing in this direction. From Equation (5.21), the aspect ratio, which gives a measure of the relative magnitudes of these dimensions, is written as follows:

$$\alpha \equiv \frac{h}{\epsilon} \tag{5.22}$$

The volume fraction of the cylindrical inclusions in terms of its aspect ratio is thus

$$\phi = 2\pi\epsilon^2 h = 2\pi\alpha\epsilon^3 \tag{5.23}$$

Rectangular prisms and ellipsoids. A rectangular prism or an ellipsoid in a unit cell has in general three characteristic dimensions: these are the ratios, $2a$ and $2b$, of its width to the lattice spacing in the lateral directions (along the $x-$ and $y-$axes) and the ratio, $2c$, of its height to the lattice spacing in this direction (along the $z-$axis). In this instance, a characteristic length in the direction perpendicular to heat flow is not immediately obvious since there are two length scales ($2a$, $2b$). From the definition above, however, the geometric mean of these two dimensions as a characteristic length scale in the plane perpendicular to heat flow may arbitrarily be selected so that the aspect ratio can be defined as follows:

$$\alpha \equiv \frac{c}{\sqrt{ab}} \tag{5.24}$$

57

Table 5.1: Aspect ratios and volume fractions of various geometric dispersions in a unit cell

Geometry	Aspect Ratio	ϕ		
Cylinder	h/ϵ	$2\pi\epsilon^2 h$	$=$	$2\pi\alpha\epsilon^3$
Rectangular Prism	$c/\sqrt{ab}$	$8abc$	$=$	$8c^3/\alpha^2$
Ellipsoid	$c/\sqrt{ab}$	$4\pi abc/3$	$=$	$4\pi c^3/3\alpha^2$

The volume fractions of the inclusions in terms of aspect ratio for rectangular prisms and ellipsoids are thus given by

$$\begin{aligned} \phi &= 8abc = \frac{8c^3}{\alpha^2} \qquad \text{(rectangular prisms)} \\ \phi &= \frac{4}{3}\pi abc = \frac{4}{3}\frac{\pi c^3}{\alpha^2} \qquad \text{(ellipsoids)} \end{aligned} \tag{5.25}$$

5.4.4 Characteristic Cells

Characteristic cells for the various geometries are illustrated in Figure 5.11. Symmetry permits only $1/16^{\text{th}}$ (upright circular cylinder, and prolate/oblate spheroids and prismoids) or $1/8^{\text{th}}$ (latitudinous circular cylinder, and general spheroids and rectangular prismoids) of the unit cell to be considered. The problem is still, however, always three dimensional. The top boundary of the cell implemented in FEMLAB is isothermal with $T_H = 1$ and the lower boundary (mid-plane of the unit cell) isothermal with $T_L = 0.5$. The side walls are adiabatic.

When symmetry reduces the computational domain to $1/16^{\text{th}}$ of the unit cell, approximately 20000 Langrangian elements of second order were used. This mesh was found to give convergence of k_e within two-decimal place accuracy ($\leq 0.05\%$) of results from a coarser mesh for the various geometries studied (except in instances where one of the characteristic dimensions of the particle approached the boundaries
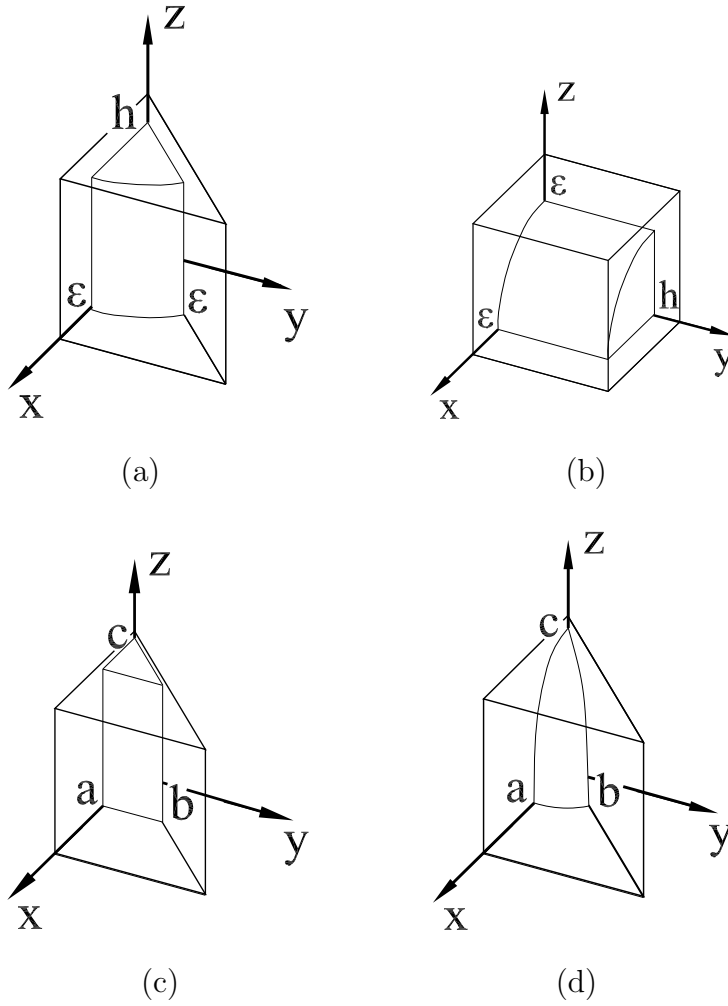
Figure 5.11: Characteristic cells for (a) cylinder with axis parallel to heat flow, (b) cylinder with axis perpendicular to heat flow, (c) rectangular prism, and (d) ellipsoid in a unit cell. Heat flow is along the $z-$axis.

of the cell in which case the mesh was further refined in the vicinity of this point). When the computational domain is $1/16^{\text{th}}$ of the unit cell, relative effective thermal conductivity is given as $k_e/k_f = 8Q$. When symmetry reduces the computational domain to $1/8^{\text{th}}$ of the unit cell, $k_e/k_f = 4Q$, and approximately 40000 Langrangian elements of second order were used. The total heat flow rate, Q, was solved by integrating the heat flux over the upper or lower boundary.

5.4.5 Results

Case 1: $\alpha = 4.5$. The effective thermal conductivities of a tall and slender parallel circular cylinder, a rectangular prism, and an ellipsoid, each inside a unit cell, oriented with their longitudinal axes in the direction of heat flow, were solved numerically for volume fractions from 0.005 to 0.028 (with $\kappa = 1000$). The numerical results for the various geometries are compared with one another in Figure 5.12. The relative enhancment in thermal conductivity, k_e/k_f, is insensitive to the geometry of the particle. The numerical results show that for a given volume fraction, the parallel cylinder gives slightly higher enhancement in thermal conductivity than the ellipsoid and rectangular prism, which gives the lowest enhancement.

Comparisons between the numerical results and the predictions of the models for the various geometries are shown in Figures 5.13 to 5.15. In addition, comparison between the results and predictions of the model for a rectangular prism in a unit cell for $\kappa = 10$ is included in Figure 5.16. This serves to illustrate that the same behaviour is observed as was noted in the dispersion of spheres: that the deviations between the predictions and the numerical results increase with relative conductivity and volume fraction. In addition, the numerical results are closer to the average of the upper and lower bounds for low κ and approach the parallel adiabats model as κ increases. The close agreement between the numerical results and the parallel adiabats model is evident when $\kappa = 1000$. This can be given physical justification by noting that, for
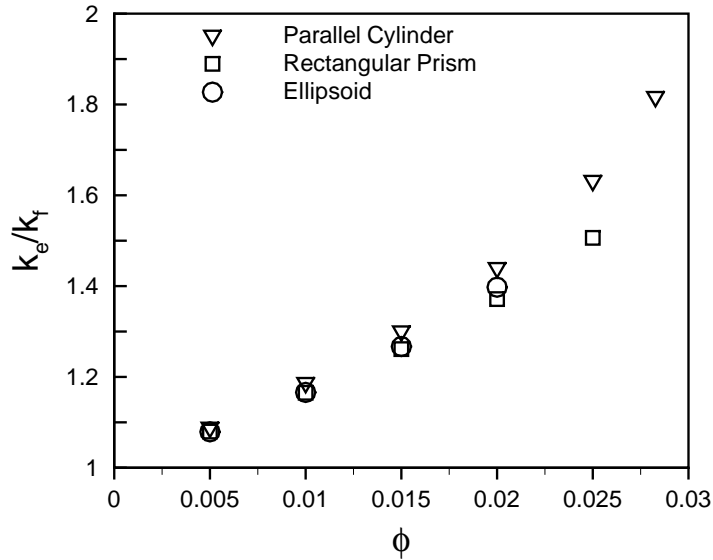
Figure 5.12: Numerical results for parallel cylinder, rectangular prism, and ellipsoid in unit cell, $\alpha = 4.5$ and $\kappa = 1000$

tall and slender dispersions oriented in the direction of heat flow, a highly conductive particle is very effective at confining the total heat flow to a narrow region in the vicinity of the particle. The upper bound greatly overpredicts the results when the conductivity is sufficiently increased. In addition, the upper bound is much more sensitive to the conductivity ratio than is the lower bound.

The models do not give the correct predictions in the sense that the relative enhancement of the ellipsoid is predicted to be larger relative to the parallel and cylinder and rectangular prism of the same aspect ratio, whereas the opposite is observed of the numerical results. The various models, however, are successful in the sense that their predictions for the parallel cylinder, rectangular prism, and ellipsoid are similar to one another; this is in agreement with the numerical results and confirms that the aspect ratio is an important non-dimensional parameter in this problem.
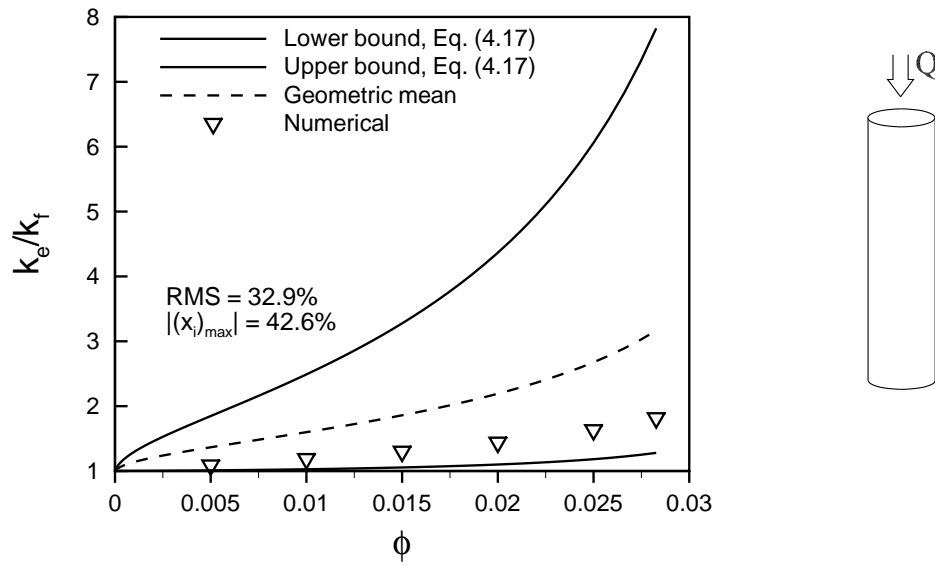
Figure 5.13: Numerical results versus upper and lower bounds for cylinder with axis parallel to heat flow, $\alpha = h/\epsilon = 4.5$ and $\kappa = 1000$
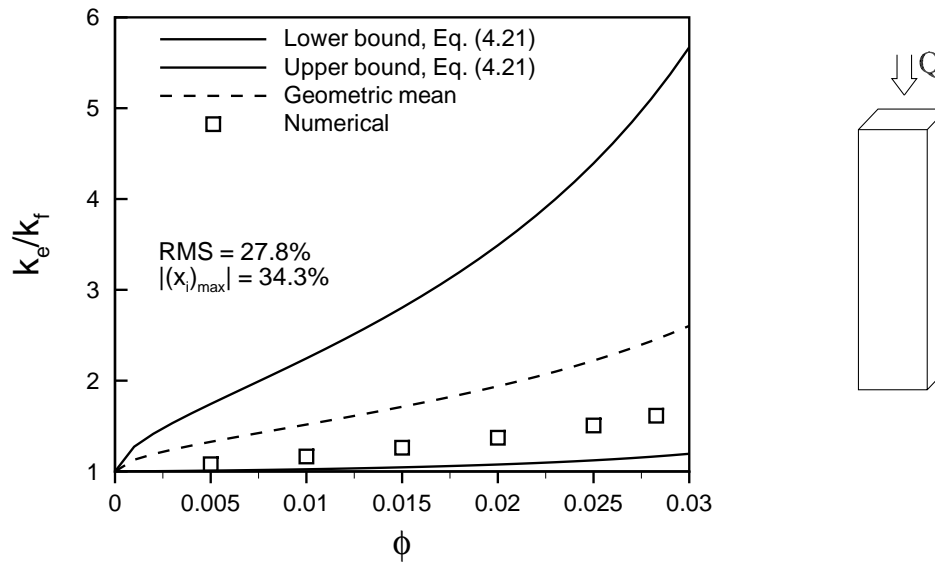
Figure 5.14: Numerical results versus upper and lower bounds for rectangular prism, $\alpha = c/\sqrt{ab} = 4.5$ and $\kappa = 1000$
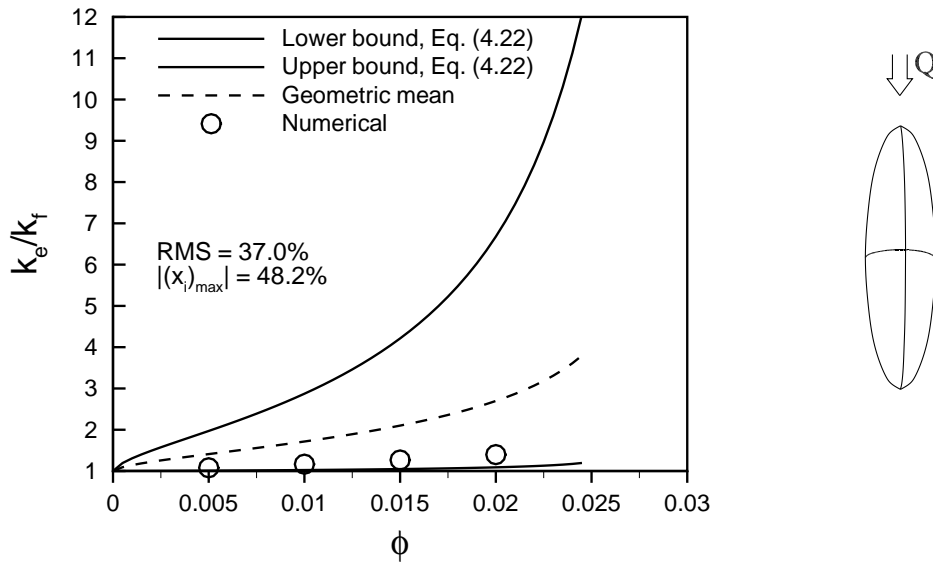
Figure 5.15: Numerical results versus upper and lower bounds for ellipsoid, $\alpha = c/\sqrt{ab} = 4.5$ and $\kappa = 1000$
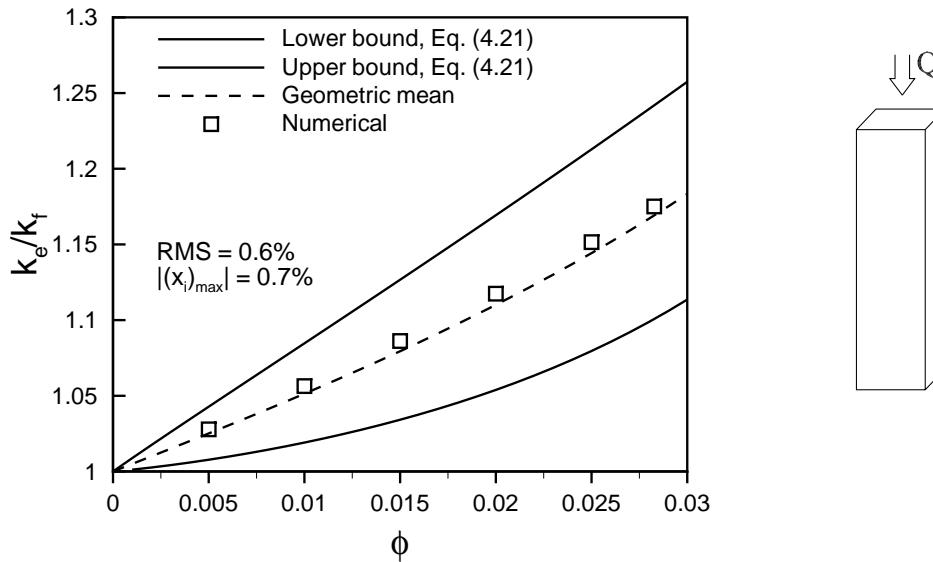
Figure 5.16: Numerical results versus upper and lower bounds for rectangular prism, $\alpha = h/\epsilon = 4.5$ and $\kappa = 10$

63
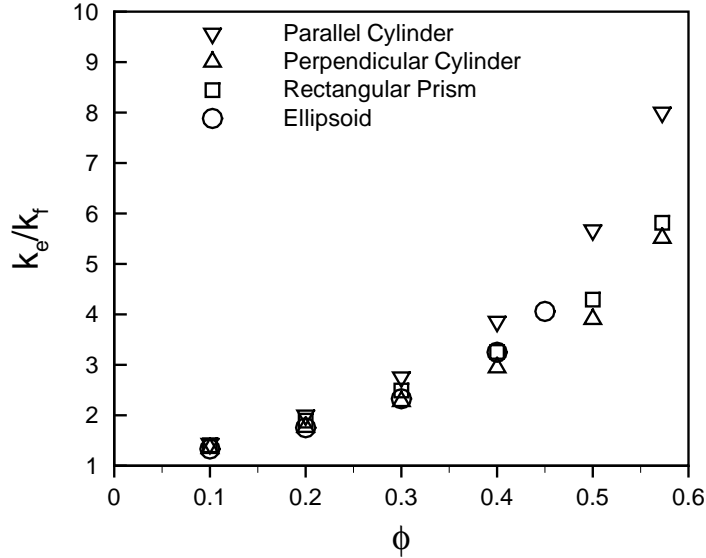
Figure 5.17: Numerical results for parallel square circular cylinder, perpendicular square circular cylinder, cube, and sphere in unit cell, $\alpha = 1$ and $\kappa = 1000$

Case 2: $\alpha = 1$. The effective thermal conductivities of a parallel square circular cylinder, a perpendicular square circular cylinder, a cube, and a sphere, each inside a unit cell, were solved numerically for volume fractions from 0.10 to 0.60 (with $\kappa = 1000$). The numerical results for the various geometries are compared with one another in Figure 5.17. The relative enhancment in thermal conductivity, k_e/k_f, is insensitive to the geometry of the particle up to $\phi \approx 0.30$. At larger volume fractions, the effects of the geometry beyond the aspect ratio become important; however, the results for the various geometries are still in good relative agreement, with a variance of less than 35% even at $\phi = 0.60$ when the particles are close to touching. The numerical results show again that for a given volume fraction, the parallel cylinder gives slightly higher enhancement in thermal conductivity than rectangular prism, the sphere, and the perpendicular cylinder, which gives the lowest enhancement.

Comparisons between the numerical results and the predictions of the models for the various geometries are shown in Figures 5.18 to 5.20. The upper and lower
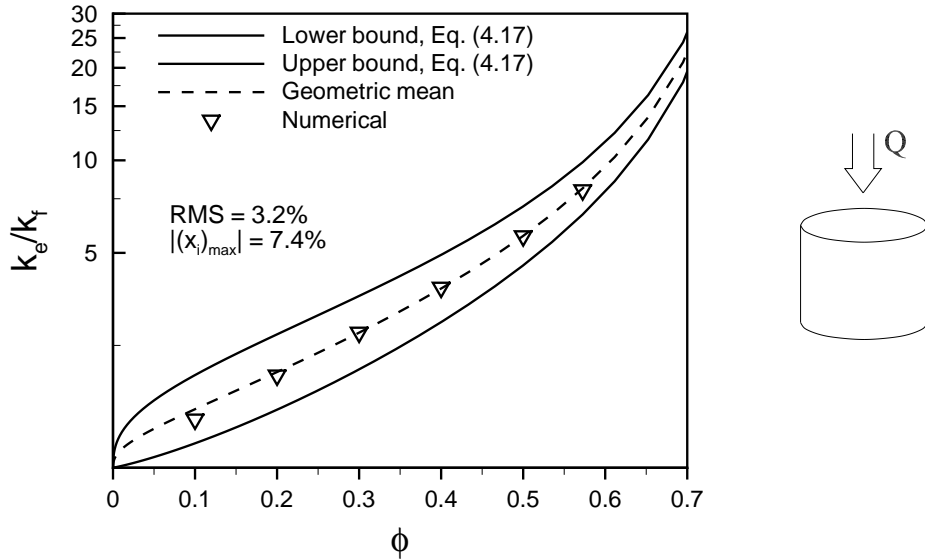
Figure 5.18: Numerical results versus upper and lower bounds for cylinder with axis parallel to heat flow, $\alpha = h/\epsilon = 1$ and $\kappa = 1000$

bounds are much more effective at constraining the range of possible values for $\alpha = 1$ than they are for $\alpha = 4.5$. The agreement with the model (the geometric mean) is excellent, in particular for the parallel square circular cylinder and cube.

Better agreement between the models and results of the parallel cylinder and the cube may be partially related to the lack of curvature these geometries possess in the planes perpendicular to the direction of heat flow. Recall that, in the perpendicular isotherms model formulation, the differential resistance between two planes is the parallel combination of the resistances of the relatively non-conductive fluid and of the highly conductive solid. If the solid is highly conductive, this amounts to essentially neglecting the resistance imposed by the fluid, even if only a small volume within the volume enclosed by two planes perpendicular to the direction of heat flow is highly conductive. This also gives physical grounds for expecting the upper bound to greatly overpredict the numerical results when the aspect ratio of the particle is large.
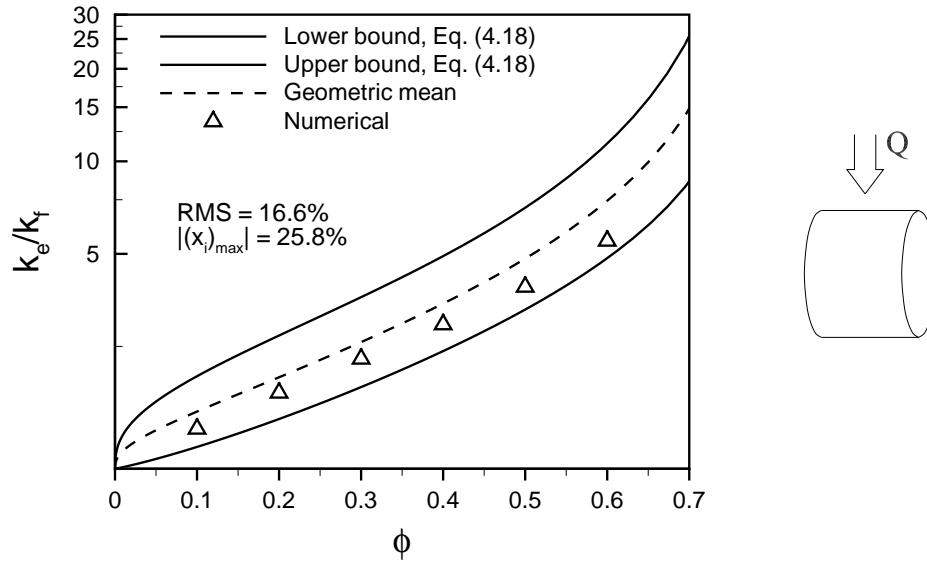
Figure 5.19: Numerical results versus upper and lower bounds for cylinder with axis perpendicular to heat flow, $\alpha = h/\epsilon = 1$ and $\kappa = 1000$
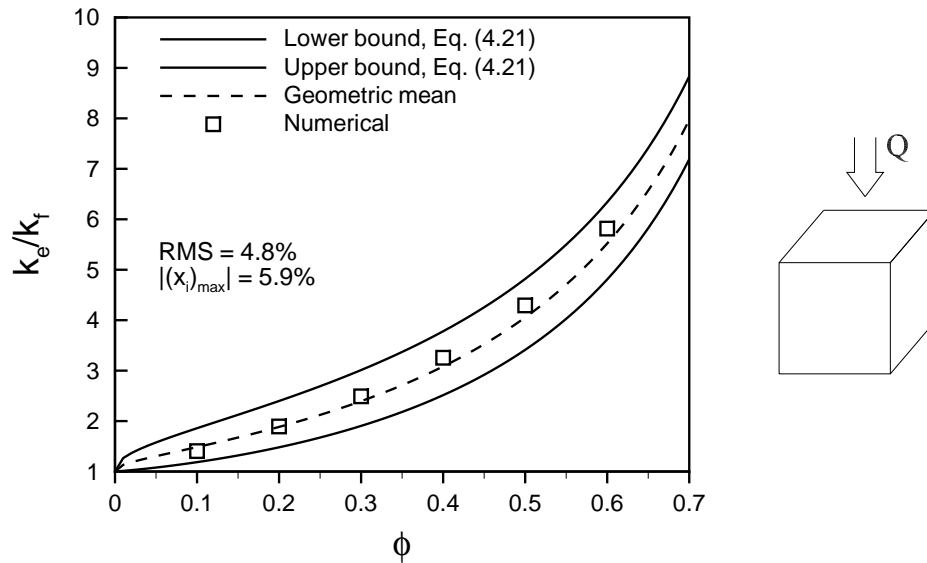
Figure 5.20: Numerical results versus upper and lower bounds for rectangular prism, $\alpha = c/\sqrt{ab} = 1$ and $\kappa = 1000$
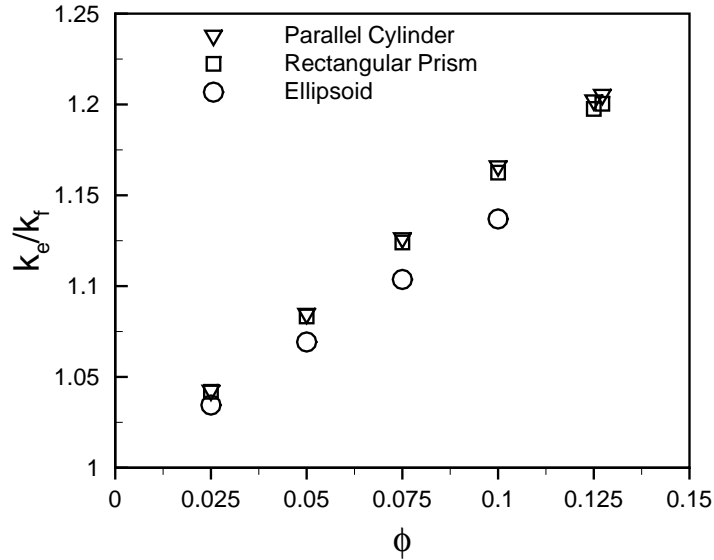
Figure 5.21: Numerical results for parallel cylinder, rectangular prism, and ellipsoid in unit cell, $\alpha = 4.5$ and $\kappa = 1000$

Case 3: $\alpha = 0.22$. The effective thermal conductivities of a short and latitudinous cylinder, a rectangular prism, and an ellipsoid, each inside a unit cell and oriented with their longitudinal axes perpendicular to the direction of heat flow, was solved numerically for volume fractions from 0.025 to 0.125 (with $\kappa = 1000$). The numerical results for the various geometries are compared with one another in Figure 5.21. The relative enhancment in thermal conductivity, k_e/k_f, is relatively insensitive to the geometry of the particle. The numerical results show that for a given volume fraction, the parallel cylinder gives slightly higher enhancement in thermal conductivity than the rectangular prism and ellipsoid, which gives the lowest enhancement.

67
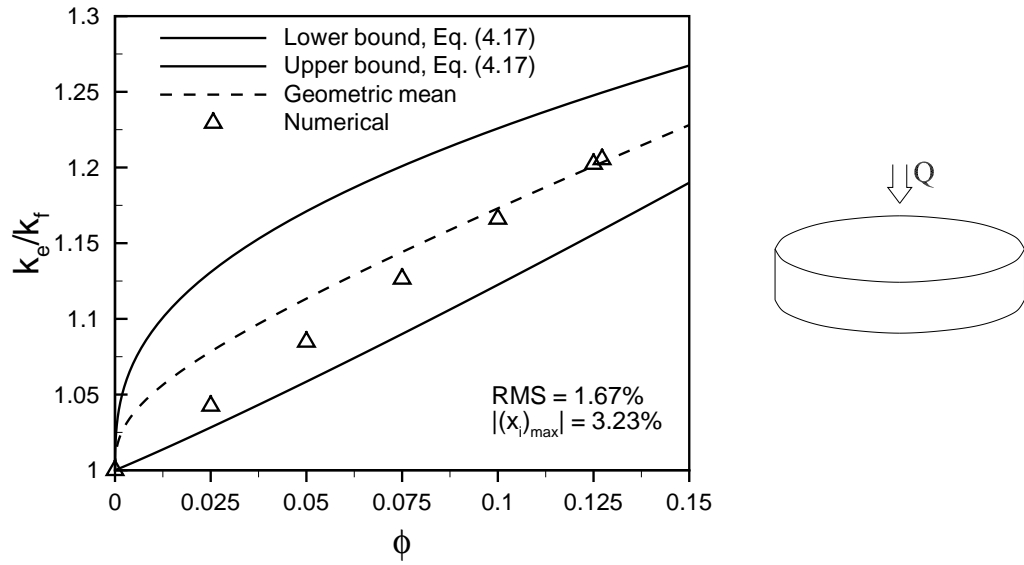
Figure 5.22: Numerical results versus upper and lower bounds for cylinder with axis parallel to heat flow, $\alpha = h/\epsilon = 0.22$ and $\kappa = 1000$
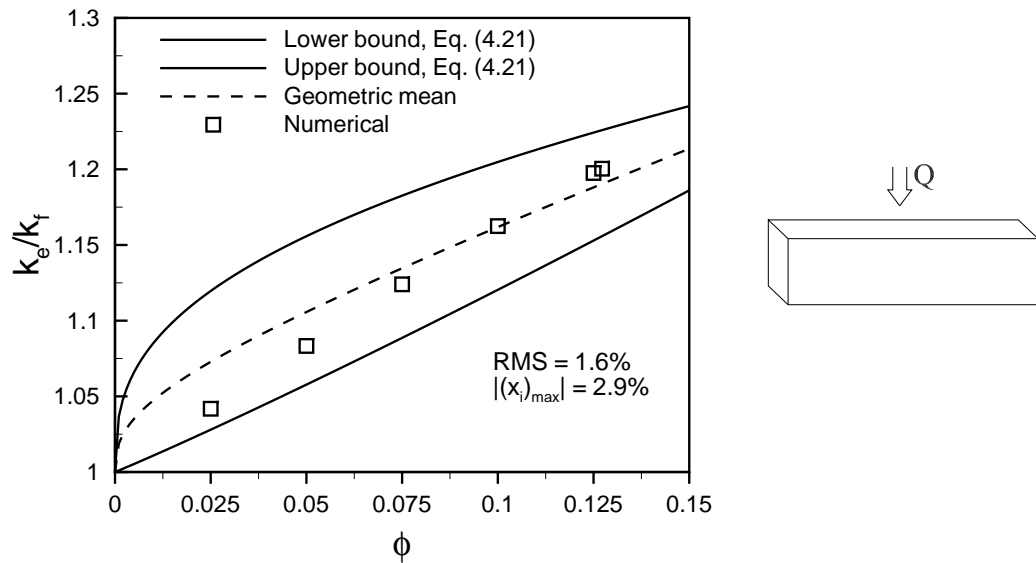
Figure 5.23: Numerical results versus upper and lower bounds for rectangular prism, $\alpha = c/\sqrt{ab} = 0.22$ and $\kappa = 1000$
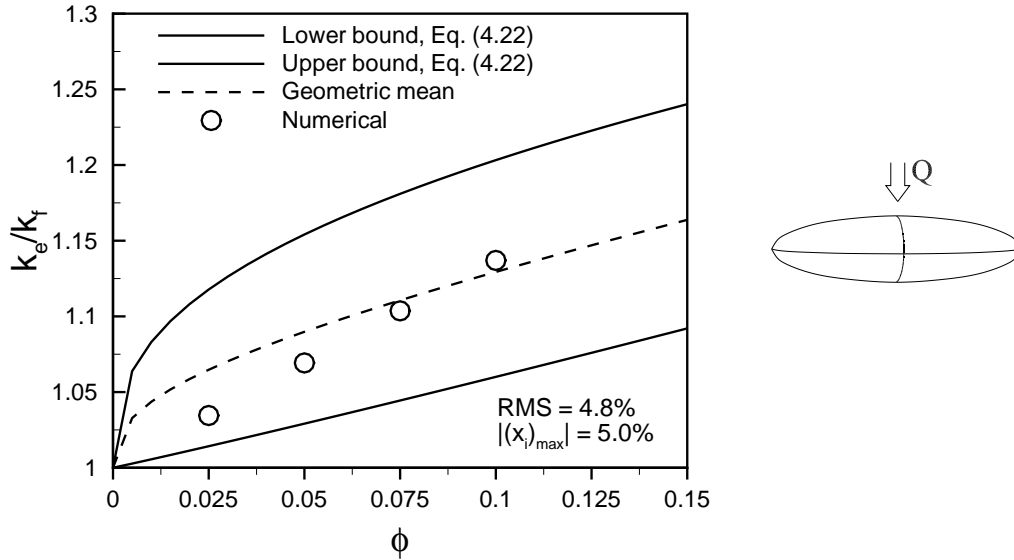
Figure 5.24: Numerical results versus upper and lower bounds for ellipsoid prism with axis, $\alpha = c/\sqrt{ab} = 0.22$ and $\kappa = 1000$

5.4.6   Closing Remarks

The volume fraction is a suitable non-dimensional parameter if all particles can be accurately characterized with the same length scales. More generally, if a relationship is sought between enhancement in thermal conductivity and volume fraction, a defined particle aspect ratio must at least be common for the heterogeneous media for which this relationship is thought to apply. A highly conductive particle is very effective at confining the total heat flow to a narrow region in the vicinity of the particle. As a result, the predictions of the parallel adiabats model are approached as the conductivity ratio of the particle is increased, in particular when the particle is tall and slender (high aspect ratio). The results of assuming parallel adiabats or perpendicular isotherms are similar when the particle has a low aspect ratio (Appendix D). The predictions of the model give the best agreement with numerical results for systems with low aspect ratios, conductivity ratios, and volume fractions.

The aspect ratio is clearly an important parameter beyond the volume fraction and
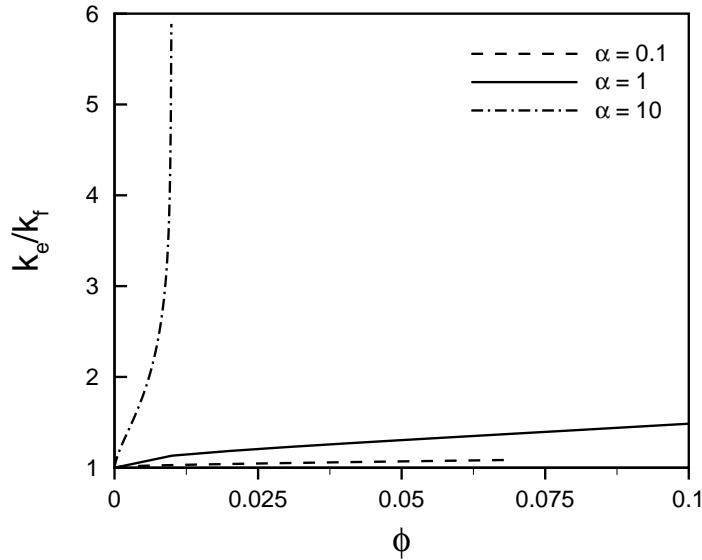
Figure 5.25: Effect of aspect ratio of upright circular cylinder in unit cell - model predictions, $\kappa = 1000$

relative conductivity of the particle, though the specific geometry of the dispersion is not, especially at low volume fractions. This behaviour is well-reflected by the model (Equation (4.17) in Chapter 4). The geometric mean of the upper and lower bounds on effective thermal conductivity for a parallel cylinder in a unit cell are shown, for example, for three conditions with $\kappa = 1000$: these are $\alpha = 0.1$, $\alpha = 1$, and $\alpha = 10$ (Figure 5.25). Note the significant enhancement at very low volume fractions for particles which are very tall and slender.

The upper and lower bounds will, in general, converge as the volume fraction is increased to its maximum if the upper and lower surfaces of the particle are flat and the aspect ratio is greater than or equal to one (for example, a square circular cylinder in a unit cell). Under these circumstances, when the maximum volume fraction is reached, the adiabats are indeed parallel and the isotherms perpendicular, so that the bounds are equivalent and represent the analytical solution.

5.4.7   Clustering

In the literature, the frequent deviations between experimental data and the Maxwell equation at volume fractions less than $\phi = 0.30$ (as low as $\phi = 0.01$ in suspensions of nano-particles) have been attributed in some part to the formation of aggregates or clusters of particles. Keblinski et al. [49], for example, suggest that a cluster of particles behaves like a single large particle and, on these grounds, propose the use of a modified (enhanced) volume fraction. Kumar and Murthy [50] studied this problem numerically and found that clustering has no effect on effective thermal conductivity unless the formation of high-conductivity liquid bridges between the particles is postulated.

The effect of clustering is quantified by solving numerically the effective thermal conductivity of a sphere in a unit cell with the sphere placed at various points within the cell. The points are specified along a line joining the center of the cell to one of the lower vertices of the unit cell. Specifically, effective thermal conductivity of a sphere in a unit cube with $\epsilon = 0.29$ ($\phi = 0.10$) and $\kappa = 1000$ was established (Figure 5.26). Clustering of the particles produces in the most extreme circumstances (i.e. when the spheres are touching and when $\kappa = 1000$) an enhancement of just 4%, calculated by linearly extrapolating effective thermal conductivity to $\chi = 0.29$ using the numerical values at $\chi = 0.30$ and $\chi = 0.31$ in Figure 5.26.

Using the idea discussed by Keblinski et al., we can define an effective volume fraction when the spheres are close to touching as

$$\phi_e \equiv \frac{V_s + V_v}{V_s + V_f} = \frac{7}{6}\pi\epsilon^3 + \chi^3 \tag{5.26}$$

where V_v is one-eighth of the total volume excluded from the sphere in a cube with side length 2χ. Equation (5.26) is valid when $\chi \approx \epsilon$ (Figure 5.26); for $\chi \gg \epsilon$, the assumption that the cluster of particles can be treated as a single larger particle of conductivity k_s is questionable since the resistance of the liquid between particles is
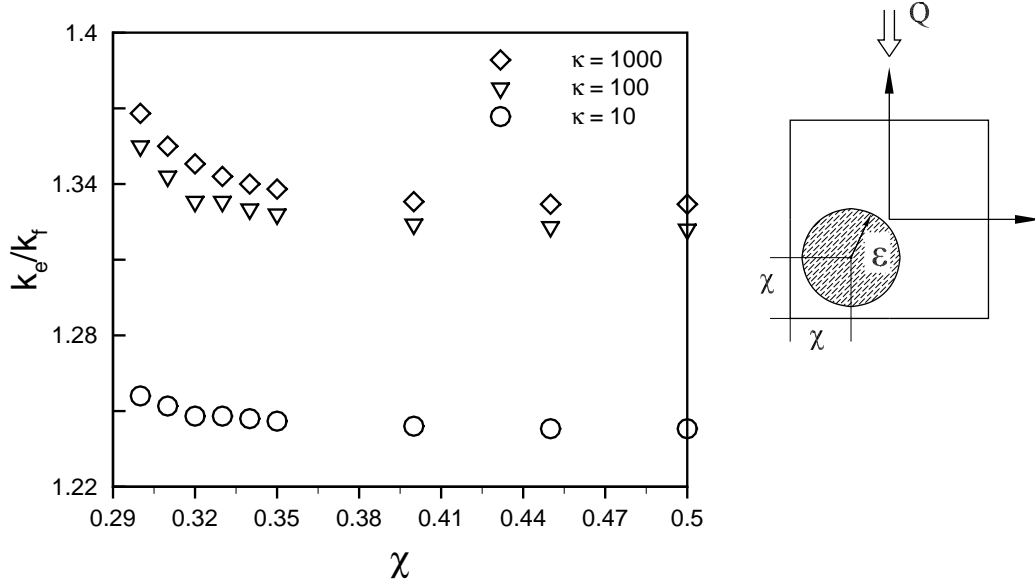
Figure 5.26: Effect of clustering, $\phi = 0.10$ and $\kappa = 1000$

then significant. In addition, it is noted that Equation (5.26) gives a larger enhancement in the volume fraction when the particles are close together but not touching than when the spheres are in fact touching. This behaviour is not in agreement with the numerical data of Figure 5.26, which suggests that the enhancement becomes more significant as the particles are brought closer together. When $\chi = \epsilon$, $\phi_e \approx 0.583$ which is 11% larger than the simple cubic packing fraction.

The comparison with the extrapolated value for k_e/k_f at $\phi = 0.10$ and $\chi = 0.29$ is within 1% of the predictions using the modified volume fraction. This supports the hypothesis of Keblinski et al., but the additional enhancement in effective thermal conductivity that can be attributed to clustering is still very small and cannot explain the anomolous enhancements observed in nanofluids [51]. Although further enhancement is possible if the clusters are larger, in reality, clustering to the extent that solid agglomerates span large distances is unlikely since such clusters would settle out of the fluid. If there is settling, clustering can also have a negative effect on the desired enhancement of the thermal conductivity of the base fluid and the series conduction model would be approached.

5.4.8 Thin Coatings

Two cases in which the particle is surrounded by a thin, homogeneous, and uniform layer of a thermally different material are considered. The first is an investigation of the effect of an oxide layer and the second is one of the effect of ordered liquid layers.

Case 1: Oxides. The diameter of metallic particles used in microelectronics cooling applications is traditionally on the order of microns[4]. The oxides that form are typically on the order of nanometers and have much lower thermal conductivities. For example, aluminum oxide particles typically have bulk thermal conductivities of $\sim 50\ W/mK$ [57] whereas the thermal conductivity of pure aluminum is 237 W/mK [53]. There is often significant uncertainty in the thermal conductivity of the particle. This is one possible reason for the discrepancy between experimental results and model predictions. In such circumstances, it is reasonable to enquire whether the oxide layer is responsible for a significant reduction in the "particle" conductivity.

As a lower limit, the conductivity of the coating is equal to the conductivity of the liquid, $\kappa_c = 1$, and as an upper limit, the conductivity of the coating is equal to the conductivity of the particle, $\kappa_c = \kappa$. When $\kappa_c = 1$, Equation (4.26) recovers Equations (4.8) and (4.16) for a particle of relative radius ϵ; and, when $\kappa_c = \kappa$, the same equations are recovered, but for a particle of relative radius $\epsilon + \tau$. These are thus bounds on the conductivity of the composite particle in the numerical simulations.

Two relative oxide thicknesses were considered, $\tau = 0.02$ and $\tau = 0.05$, for a particle with $\epsilon = 0.30$ and $\kappa = 1000$. For a particle 100 μm in diameter, this corresponds to oxide thicknesses of 7 and 17 μm, respectively. These represent particles with oxide layers much thicker than are ever practically observed; however, given the computational intractability of numerically discretizing domains much smaller than

---

[4]Settling of these micron-sized particles has been a major hurdle to developing suspensions for practical applications. As a result, recent work has turned to nanofluids which are suspensions of particles with diameters on the order of nanometers in typical coolants and polymeric fluids.
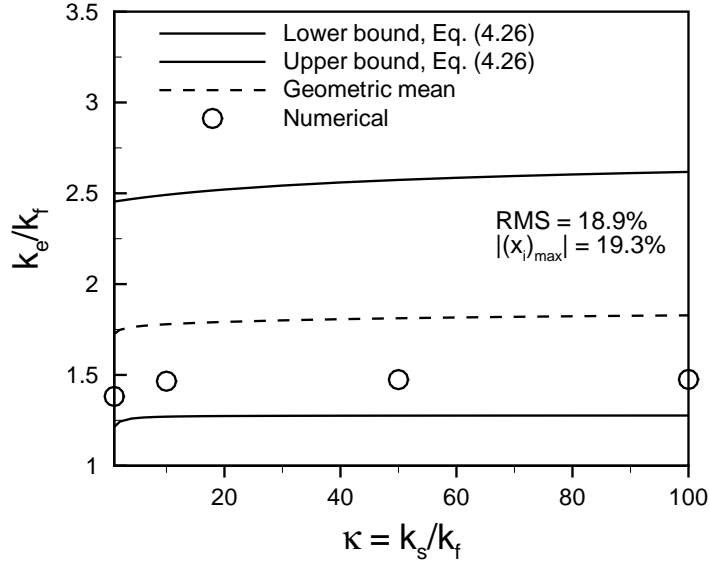
Figure 5.27: Enhancement in thermal conductivity as a function of relative oxide thickness; $\epsilon = 0.30$, $\tau = 0.02$, and $\kappa = 1000$

this, these problems were investigated. The results are shown in Figures 5.27 and 5.28. The numerical results are in good agreement with the predictions of the model; in particular, the results are closer to the lower bound, as expected. In addition, effective thermal conductivity of the medium is within 1% of the enhancement in thermal conductivity of the base fluid for particles of the pure phase for $\kappa = 10$ and $\kappa = 40$ for $\tau = 0.02$ and $\tau = 0.05$, respectively. This suggests that the presence of the oxide is not responsible for a lower particle conductivity unless the thickness of the coating becomes comparable to the diameter of the particle.

Case 2: Ordered liquid layering. Liquid molecules form ordered layers on the surface of a solid. The thicknesses of these layers are typically on the order of nanometers. Yu and Choi [54] have suggested that this ordered liquid layering is responsible for an enhancement in thermal conductivity of the base fluid beyond the predictions of conventional theories such as the Maxwell equation. The authors suggest that this phenomenon prevails at small scales – in applications with nano-particles, for example
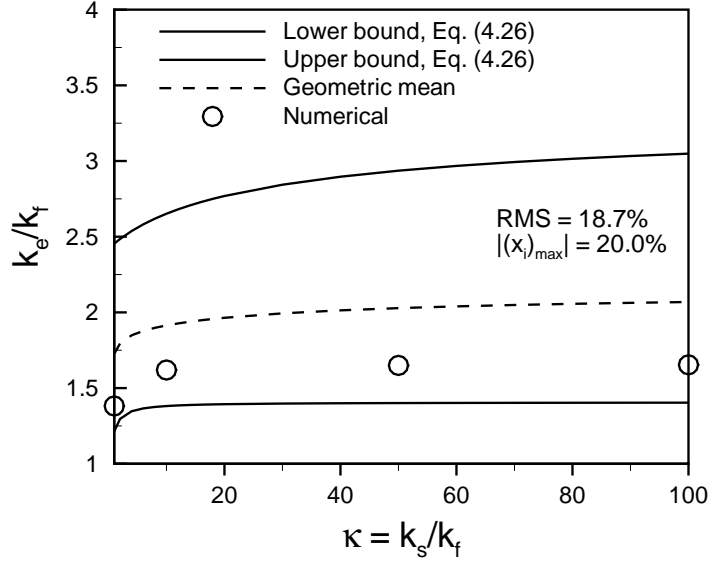
Figure 5.28: Enhancement in thermal conductivity as a function of relative oxide thickness; $\epsilon = 0.30$, $\tau = 0.05$, and $\kappa = 1000$

– and renovate the Maxwell equation to account for a thin coating of a thermally different, uniform, homogeneous, and isotropic material surrounding the particle. The model suggested by Yu and Choi is essentially the Maxwell equation queried at ϕ' where ϕ' is some enhanced volume fraction, and the Maxwell equation has already been established for $\phi \leq 0.30$ (Chapter 2).

Comparisons between the predictions from the model proposed by Yu and Choi and those of the present model are included in Figure 5.29. The authors investigated a range of thicknesses and conductivities of ordered liquid layers. The results are presented specifically for one set of parameters: these are $\kappa = 397$, $\kappa_c = 10$, and $\tau = 2\epsilon/3$ for $\phi \leq 0.05$. The predictions of the present model compare well with those of the renovated Maxwell equation. If the plot were extended to larger volume fractions, however, we would find once again that the Maxwell equation makes predictions of k_e/k_f less than the lower bound; but since typical nanofluids have $\phi \leq 0.05$, this is not problematic.

75
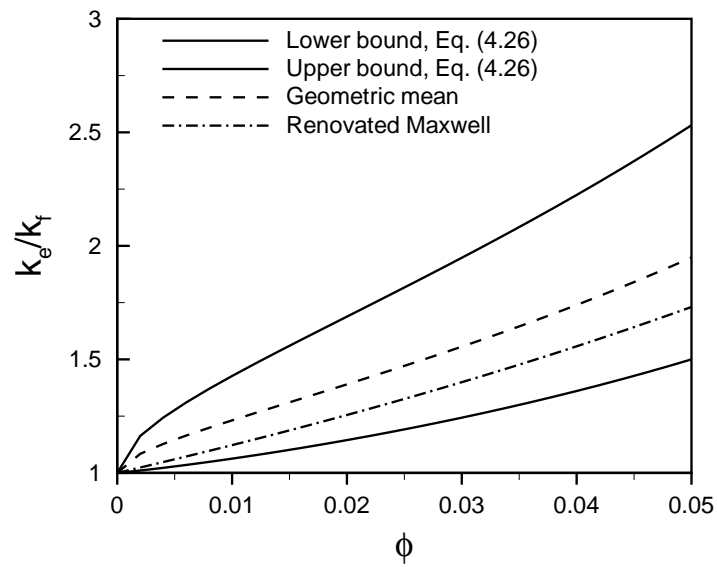
Figure 5.29: Predictions of present model and renovated Maxwell equation (Yu and Choi, [54]); $\kappa = 397$, $\kappa_c = 10$, $\tau = 2\epsilon/3$

Chapter 6

Model Validation

There is a vast body of literature describing experimental works and results for effective thermal conductivity of composite systems. Experimental data of effective thermal conductivity for the class of materials which are of interest in microelectronics cooling applications were selected from the literature. In particular, these materials are suspensions of particles in a continuous phase, typically a polymeric fluid. The experimental data are compared with the model developed for a sphere in a unit cell.

A typical experimental procedure consists of first preparing the samples. By specifying the mass fraction and the density ratio of the two phases, the volume fraction is determined. For example, 3 g of aluminum oxide powder may be combined with 1 g of ethylene glycol (a typical base fluid), to give a volume fraction of approximately $\phi = 0.53$. This involves the assumption that the density of the particle is equal to that of the bulk material, aluminum in this case. The two phases are typically stirred together with a stirring rod and then tested. In some instances, the composite system is hardened prior to the test. In addition, the samples are sometimes prepared a day prior to the tests.

Wong and Bollampaly [55] recently studied the enhancement in the conductivity
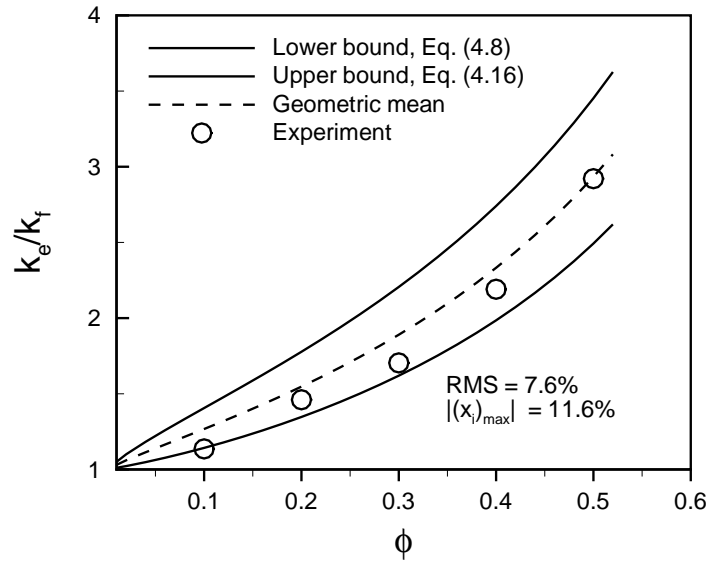
Figure 6.1: Experimental data from Wong and Bollampaly [55] for spherical silica particles in an epoxy resin, $\kappa = 7.7$
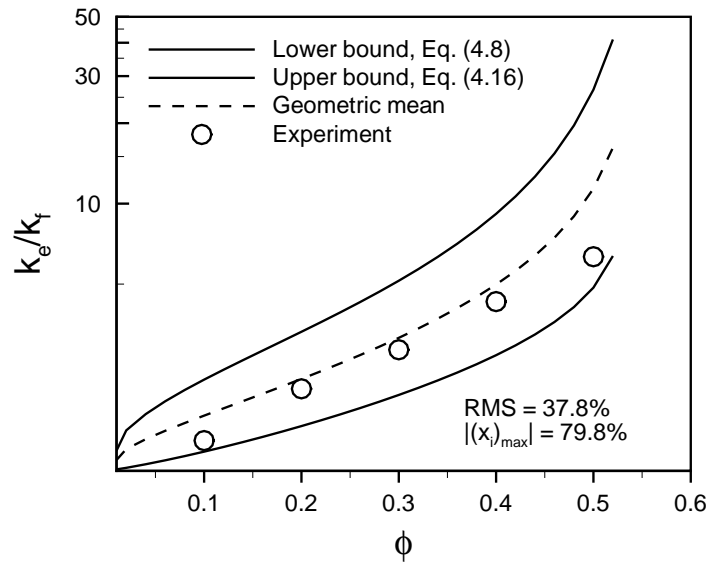
Figure 6.2: Experimental data from Wong and Bollampaly [55] for almost spherical alumina particles in epoxy resin, $\kappa = 184.6$
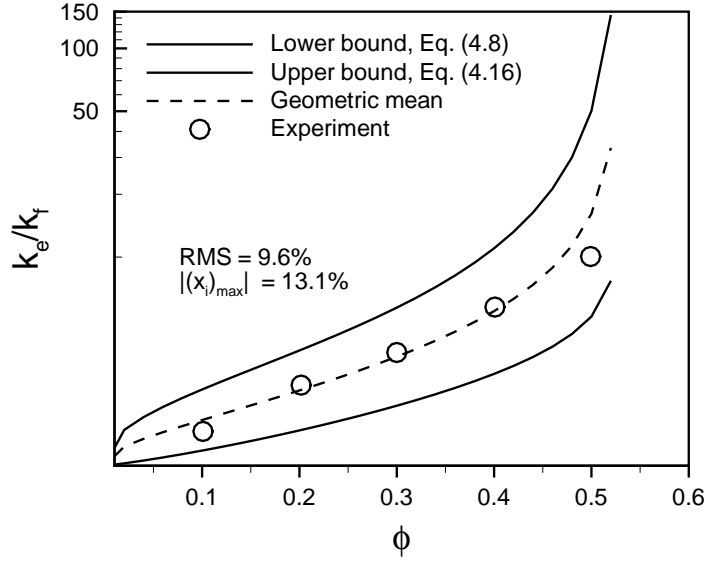
Figure 6.3: Experimental data from Wong and Bollampaly [55] for irregular SCAN particles in epoxy resin, $\kappa = 1128.2$

of an epoxy resin by separately dispersing into it three different types of particles up to volume fractions of $\phi = 0.50$ (Figures 6.1 to 6.3). The particles used were spherical silica ($\kappa = 7.7$), alumina ($\kappa = 184.6$), and silica-coated alumina nitride ($\kappa = 1128.2$). The samples were cured and solidified using a hardener. The agreement with the model for each case is very good - maximum % difference and RMS of 7.6%, 11% for spherical silica particles; 37.8%, 79.8% for alumina particles, and; 9.8% and 13.1% for irregular silica-coated alumina nitride, respectively. In particular, the model shows relatively good agreement for the alumina and silica-coated alumina nitride samples despite the irregular particle geometry.

Sundstrom and Chen [56] studied the effective conductivity of glass dispersions in commercial polystyrene ($\kappa = 7.3$) for three different particle size ranges (62-88 μm, 125-149 μm, and 177-210 μm) up to $\phi = 0.40$. The samples were melted under pressure in a mold and then solidified by cooling. The experimental results (Figure 6.4) show excellent agreement with the model giving an RMS error of 2.1% and maximum difference less than 4%.
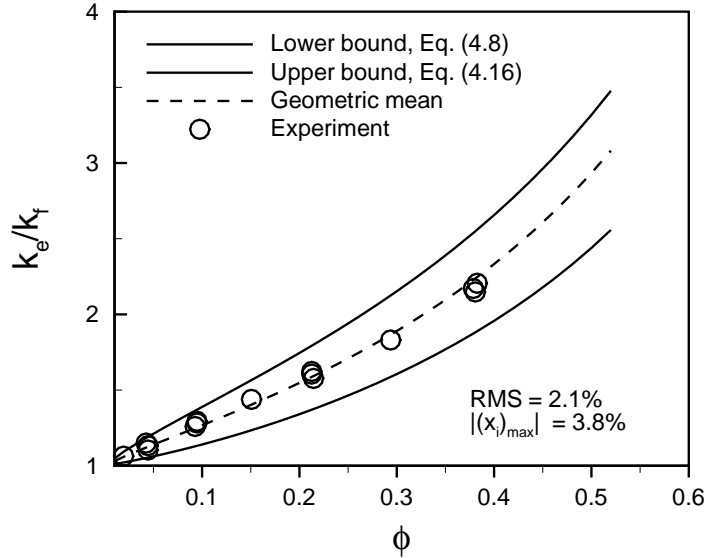
Figure 6.4: Experimental data from Sundstrom and Chen [56] for spherical glass particles in polystyrene, $\kappa = 7.3$

Tavman [57] studied a dispersion of aluminum oxide particles in commerical high density polyethylene ($\kappa = 56.9$). The polyethylene was in powder form and samples were prepared by the mold compression process. The average particle size was 10 to 20 μm. The model shows excellent agreement up to $\phi = 0.10$ beyond which the model begins to underpredict the experimental results (Figure 6.5). The maximum % difference is still 18%, half of the maximum % error obtained from the Maxwell equation.

Lin et al. [58] studied the effective conductivity of cupric oxide ($\kappa = 1067.9$) and aluminum powders ($\kappa = 41.7$) in an epoxy resin. The average particle size of the cupric oxide powder was 3 μm and that of the aluminum powder, 7 μm. A transient method was used to determine the thermal diffusivity of cured spherical samples. The model shows excellent agreement for the composite of the cupric oxide powder (Figure 6.6). The RMS error is reasonable for the aluminum oxide powder composite (15.2%) but it appears that any further loading of the sample will generate experi-
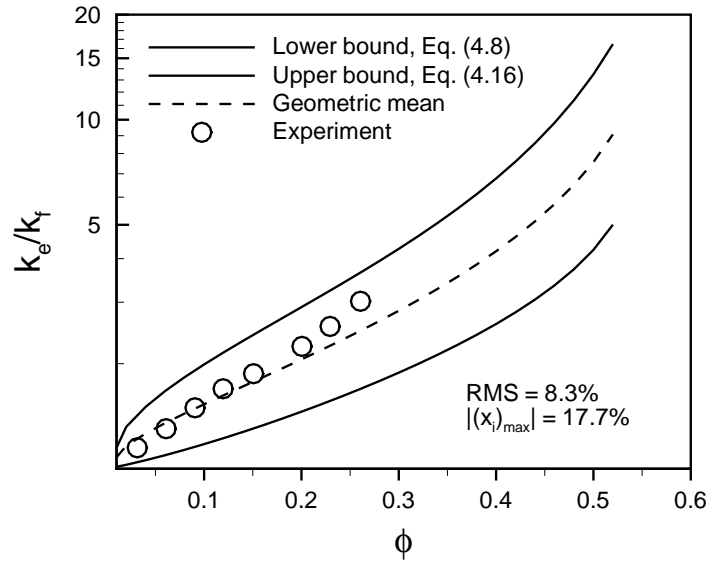
Figure 6.5: Experimental data from Tavman [57] for aluminum oxide particles in HDPE, $\kappa = 56.9$
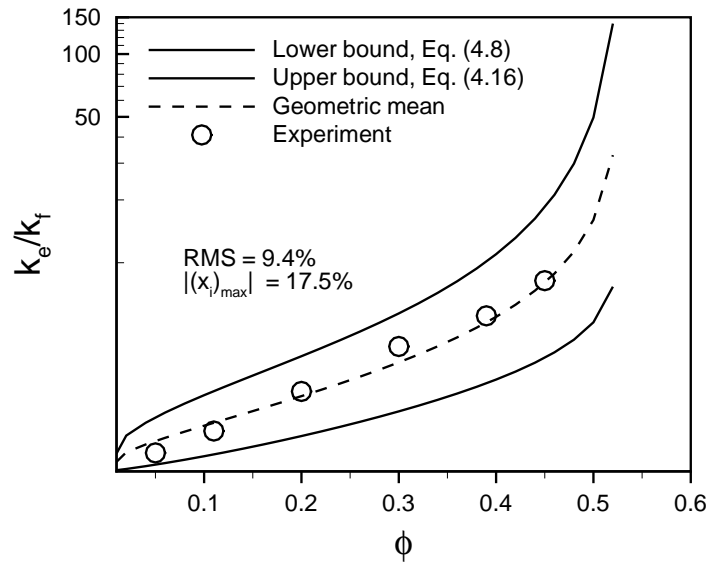
Figure 6.6: Experimental data from Lin et al. [58] for cupric oxide in epoxy resin, $\kappa = 1067.9$
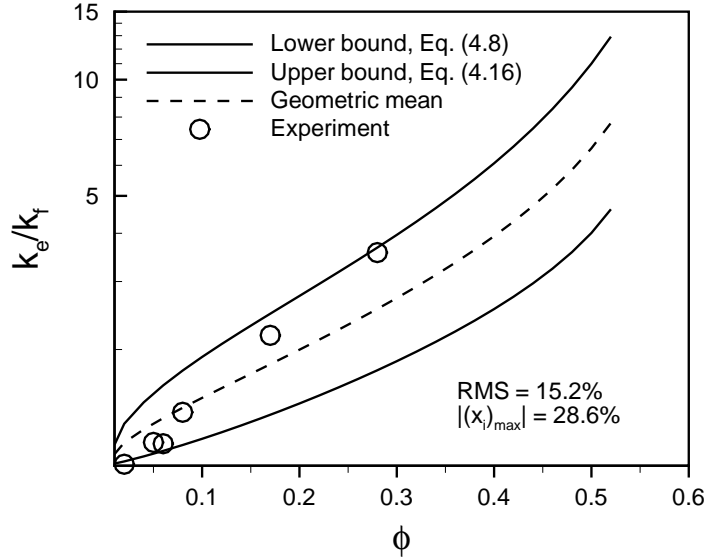
Figure 6.7: Experimental data from Lin et al. [58] for aluminum powders in epoxy resin, $\kappa = 41.7$

mental results higher than the upper bound (Figure 6.7). The model falls roughly 30% below the experimental measurement at $\phi = 28\%$ for this sample.

Woodside and Messmer [44] obtained experimental data for quartz sand packs surrounded by air ($\kappa = 325.8$) for particle volume fractions of 0.41, 0.64, 0.69, and 0.81. The particle conductivity was assumed constant and equal for each sample ($k_s = 8.4\,W/mK$). The measurements were made using the transient hot wire method and agreed well with similar data the authors found in the literature. Recently, Carson et al. [59] showed that the data of Woodside and Messmer lie close to the lower bound of the series conduction model (Figure 6.8). The proposed model of a sphere in a unit cube is not able to capture the behaviour of these samples. A possible explanation of the unusual agreement of the experimental results with the series model is the settling of the quartz sand. Note the relatively large volume fractions for which the data were obtained, alone an indicator of the potential failure of the present model.

Carson et al. [40] studied suspensions of expanded polystyrene (EPS) beads dis-
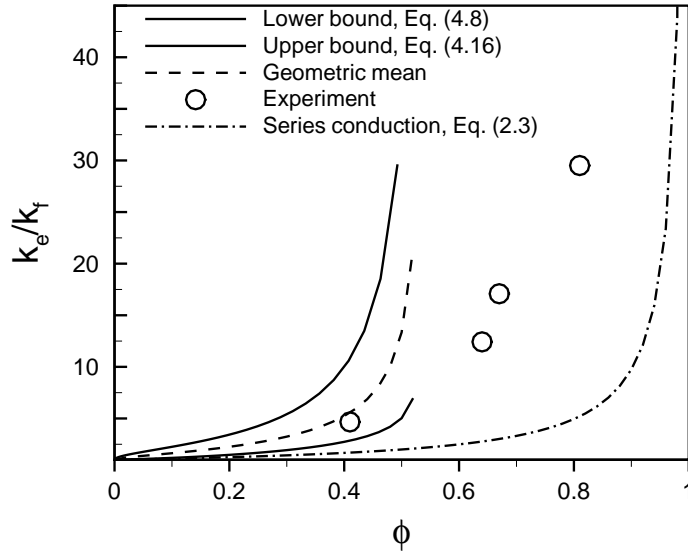
Figure 6.8: Experimental data from Woodside and Messmer [44] for quartz sand in air, $\kappa = 325.8$

persed in a guar gel phase ($\kappa = 19$) for volume fractions from 0.40 to 1.00. A transient method based on the analytical solution for the temperature at the center of a sphere being cooled with convection boundary conditions was used. Experimental data were found to lie on the upper bound of the parallel conduction model (Figure 6.9). The gel was approximately 30 times more dense than the EPS beads. The parallel bound is applicable for systems in which the two phases are well-connected along the axis of heat transfer. This suggests that the EPS beads formed continuous chain structures percolating from the center of the spherical sample to its outer boundary. Since there is no data for volume fractions less than 40%, it is not possible to determine the percolation threshold of this system; however, it is likely that further testing at lower volume fractions would show a significant decrease in effective thermal conductivity with respect to the predictions of the parallel conduction model. Note again the high volume fractions of the dispersed phase achieved by the composite. In such sample, the sphere in a cube model presented in this paper cannot be applied because it is

83
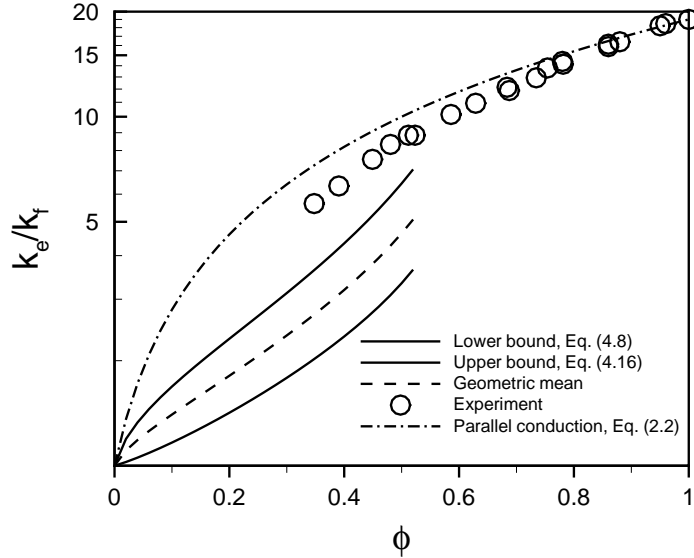
Figure 6.9: Experimental data from Carson et al. [40] for EPS beads in gel, $\kappa = 19$ only valid up to $\phi \approx 52.4\%$.

Although the predictions of the model for a sphere in a unit cell were greater than the numerical results presented in the previous chapter, the experimental results are in good agreement with the model. This suggests that there are certain mechanisms present in the real TIM which act to increase effective thermal conductivity beyond the enhancement for a uniform sphere in a simple cubic lattice arrangement. Possible mechanisms include clustering, particle size distribution, random distributions of particles, and ordered liquid layers. Clustering was shown to enhance effective thermal conductivity, but such systems are unstable. In addition, ordered liquid layering was shown in the previous chapter to have a negligible role in enhancing effective thermal conductivity beyond the predictions of the model. Random distributions were recently investigated by Carson et al. [40] and shown to have negligible effect. It is possible that polydisperse systems possess effective thermal conductivities greater than those of systems for which the dispersed phase is uniform, though the size effect has been shown to be negligible (see Sundstrom and Chen [56], for example).

Chapter 7

Conclusions and Recommendations

7.1 Conclusions

The two simple theorems described by Elrod [39] from which upper and lower bounds for effective thermal conductivity of a sphere, parallel and perpendicular cylinder, rectangular prismoid, and ellipsoid are developed in the present study are extremely powerful. Although these problems have no simple analytical solution, the developed model, which comprises the geometric mean of the upper and lower bounds, are in many instances quite useful at constraining effective thermal conductivity of a regular array of particles suspended in a continuous medium to a narrow range of possible values. The numerical solution of effective thermal conductivity of characteristic cells for various geometries and aspect ratios indicates the following:

1. The model shows good agreement for particles with low to moderate aspect ratios. As the aspect ratio is increased, the upper bound greatly overpredicts the numerical results and the lower bound is a more appropriate approximation for predicting effective thermal conductivity;

2. The numerical results approach the lower bound as the conductivity ratio is in-

creased. Physically, this is because a highly conductive particle is more effective at streamlining the heat flow through its cross-section, thus confining the total heat flow through a narrow cross-section in the vicinity of the particle;

3. Orienting the particles in the direction of heat flow leads to substantial enhancement in thermal conductivity;

4. A limiting enhancement in thermal conductivity, which occurs as the conductivity ratio becomes infinite, is practically achieved (within 2%) even at high volume fractions ($\phi = 0.30$). There is thus very little advantage to further increasing thermal conductivity of the particle. The best method for enhancing thermal conductivity is through the use of particles with high aspect ratios oriented in the direction of heat flow;

5. The enhancement in thermal conductivity for dispersions of particles with similar aspect ratios are similar, and that the specific geometry of the particle is only significant at volume fractions comparable to the maximum packing fraction;

6. A cluster of particles can be accurately treated as a single larger particle whose volume is equal to the sum of the volumes of the clustered particles and the voids within the agglomeration. This leads to an enhancement in effective thermal conductivity beyond that which is predicted for systems composed of regular arrays of particles. Although significant enhancement is possible if the clusters are large, in reality, clustering to the extent that solid agglomerates span large distances is unlikely since such clusters would settle out of the fluid. If there is settling, clustering can also have a negative effect on the desired enhancement of the thermal conductivity of the base fluid [49], and;

7. Ordered liquid layering has very little effect in producing additional enhancement in the thermal conductivity of the base fluid.

In addition, experimental work available in the literature indicates that the agreement between the selected experimental data and the geometric mean of the upper and lower bounds for a sphere in a unit cell are in excellent agreement, even for particles which are irregular in shape. This suggests that the effective thermal conductivity of a TIM is not precisely modeled as a sphere in a unit cell since numerical work indicated that the effective thermal conductivity was closer to the lower bound. Possible mechanisms for this behaviour are size distribution effects, clustering, and random distributions of particles in the medium; although the effects of each one of these on its own have been to shown to produce negligible enhancements beyond those predicted from traditional theories. The developed model is not applicable to systems in which the discontinuous phase is either well-connected throughout or has settled.

7.2 Recommendations

Based on the scope of work addressed in the present study, the following recommendations are made:

1. This work considered the case of a uniform dispersion of particles (spheres, for example) in the continuous phase. In real thermal interface materials, the dispersed particles have a size distribution. It is recommended that the effect of polydisperse particles be investigated.

2. Some thermal interface materials under investigation consist of dispersions of particles with various geometries (platelets and spheres, for example). Models which capture this behaviour are still required.

3. Typical thermal interface materials used in microelectronics cooling applications consist of a fluidic phase into which are dispersed solid particles. In the present

study, effects associated with the wettability of the solid particle by the fluid were neglected. An understanding of the effect of incomplete wetting would be of use in understanding not only effective thermal conductivity, but also the contact resistances at the interfaces between the thermal interface material and the adjoining solids.

4. It would be very beneficial if a non-dimensional parameter were identified such that effective thermal conductivity could be plotted in one-dimension (i.e. k_e as a function of one variable describing the particle geometry, orientation, thermal conductivity, etc.). In the present work, it was suggested that the aspect ratio, conductivity ratio, and the ratio of the volume fraction to the maximum packing fraction likely contain important features of such a non-dimensional parameter.

5. Any model for effective thermal conductivity should in theory work well in both the insulating regime as well as in the conducting regime (e.g. fluids into which are dispersed more conductive particles for thermally conductive materials, and fluids into which are dispersed less conductive particles for insulating materials). The present models could be investigated in the insulating regime[1].

6. In order to bring closure to the study of the thermal resistance of heterogeneous mixtures and fully utilize the present study, more work is required to understand and develop models for the bond-line thickness and contact resistances described in the Introduction.

---

[1]One problem with this is foreseen, and arises in the lack of the so-called critical condition for hollow glass microspheres. The conductivity of the liquid is intermediate to that of the glass and that of the vacuum inside the hollow glass sphere. There thus exists a critical value which the wall thickness must not exceed to produce an insulating effect in the effective medium. The limiting reduction in the thermal conductivity of the base fluid is achieved in taking the limit as the conductivity ratio of the "particle" approaches 0 for a specified thermal conductivity of the "coating." In the present formulation of the problem, however, a vacuum creates a short in the resistance network so that no critical condition is observed.

References

[1] K. W. Garrett and H. M. Rosenberg, 1974, "The thermal conductivity of epoxy-resin/powder composite materials," *J. Phys. D: Appl. Phys.*, **7**, pp. 1247-1258.

[2] A. C. Anderson and R. B. Rauch, 1970, "Low-temperature thermal conductivity of a suspension of copper particles," *J. Phys. D: Appl. Phys.*, **41**, pp. 3648-3651.

[3] G. R. Cunnington, Jr., 1964, "Thermal conductance of filled aluminium and magnesium joints in a vacuum environment," *American Society of Mechanical Engineers*, Paper 64-WA/HT-40, New York, N.Y.

[4] R. S. Prasher, 2003, "Thermal resistance of particle laden polymeric thermal interface materials," *American Society of Mechanical Engineers Int. Mech. Eng. Congress J. Heat Transfer*, **125**, pp. 1170-1177.

[5] G. W. Milton, 2002, *Theory of Composites*, Cambridge University Press, UK.

[6] G. K. Batchelor, 1974, "Transport properties of two-phase materials with random structure," *Annual Rev. Fluid Mech.*, **6**, pp. 227-255.

[7] J. C. Maxwell, 1884, *A Treatise on Electricity and Magnetism (3rd ed.)*, Dover Publications, Inc., USA, pp. 440-441.

[8] A. Eucken, 1932, "Heat transfer in ceramic refractory materials (German)," *Forsch. Geb. Ing. B3*, **353**(16), pp. 1-16.

[9] Lord Rayleigh, 1892, "On the influence of obstacles arranged in rectangular order upon the properties of a medium," *London, Edinburgh, and Dublin Mag. and J. Sci.*, **34**, pp. 481-502.

[10] I. Runge, 1925, *Z. Tech. Physik*, **6**, p. 61.

[11] R. E. Meredith and C. W. Tobias, 1960, "Resistance to potential flow through a cubical array of spheres," *J. Appl. Phys.*, **31**(7), pp. 1270-1273.

[12] R. C. McPhedran and D. R. McKenzie, 1978, "The conductivity of lattices of spheres. I. The simple cubic lattice," *Proc. Royal Soc. London Ser. A*, **359**(1696), pp. 45-63.

[13] D. R. McKenzie and R. C. McPhedran, 1978, "The conductivity of lattices of spheres. II. The body centered and face centered cubic lattices," *Proc. Royal Soc. London Ser. A*, **362**(1709), pp. 211-232.

[14] G. K. Batchelor and R. W. O'Brien, 1977, "Thermal or electical conduction through a granular material," *Proc. Royal Soc. London Ser. A*, **355**(1682), pp. 313-333.

[15] R. L. Hamilton and O. K. Crosser, 1962, "Thermal conductivity of heterogeneous two-component systems," *I & EC Fund.*, **1**(3), pp. 187-191.

[16] L. S. Verma, A. K. Shrotriya, R. Singh, and D. R. Chaudhary, 1991, "Thermal conduction in two-phase materials with spherical and non-spherical inclusions," *J. Phys. D: Appl. Phys*, **24**, pp. 1729-1737.

[17] S. C. Cheng and R. I. Vachon, 1969, "The prediction of thermal conductivity of two and three phase solid heterogeneous mixtures," *Int. J. Heat Mass Transfer*, **12**, pp. 249-264.

[18] Y. Benveniste, 1987, "Effective thermal conductivity of composites with a thermal contact resistance between the constituents: Nondilute case," *J. Appl. Phys.*, **61**, pp. 2840-2843.

[19] J. Felske, 2004, "Effective thermal conductivity of composite spheres in a continuous medium with contact resistance," *Int. J. Heat Mass Transfer*, **47**, pp. 3453-3461.

[20] H.T. Davis, L.R. Valencourt, and C.E. Johnson, 1978, "Transport processes in composite media," *J. Am. Ceram. Soc.*, **58**, pp. 446-452.

[21] D. M. Bigg, 1995, "Thermal conductivity of heterophase polymer compositions, in Y. K. Godovsky and V. P. Privalko (editors), *Advances in Polymer Science 119*, Springer-Verlag, Germany, pp. 1-30.

[22] D. A. G. Bruggeman, 1935, "Calculation of various physical constants in heterogeneous substances. I. Dielectric constants and conductivity of composites from isotropic substances (German)," *Annalen der Physics*, **24**(5), pp. 636-679.

[23] D. Stauffer and A. Aharony, 1992, *Introduction to Percolation Theory*, Taylor and Francis, Washington, DC, USA.

[24] D. M. Bigg, 1984, "The effect of compounding on the conductive properties of EMI shielding compounds," *Adv. Polym. Tech.*, **4**, pp. 255-266.

[25] S. R. Broadbent and J. M. Hammersley, 1957, "Percolation processes I. Crystals and mazes," *Proc. Cambridge Philos. Soc.*, **53**, pp. 629-641.

[26] A. Devpura, P. E. Phelan, and R. S. Prasher, 2000, "Percolation theory applied to the analysis of thermal interface materials in flip-chip technology," *2000 Inter. Soc. Conf. Thermal Ph.*, pp. 21-28.

[27] R. G. Larson, L. E. Scriven, and H. T. Davis, 1977, "Percolation theory of residual phases in porous media," *Nature*, **268**, pp. 409-413.

[28] G. MacKay and N. Jan, 1984, "Forest fires as critical phenomena," *Phys. A: Mathemat. Gen.*, **17**, pp. L757-L760.

[29] M. E. J. Newman, 2002, "Spread of epidemic disease on networks," *Phys. Rev. E*, **66**, pp. (016128-)1-11.

[30] B. Derrida, and J. Vannimenus, 1982, "A transfer-matrix approach to random resistor networks," *J. Phys. A: Math Gen.*, **15**, pp. L557-L564.

[31] S. Torquato, 1985, "Effective electrical conductivity of two-phase disordered composite media," *J. Appl. Phys.*, **58**(10), pp. 3790-3797.

[32] A. K. Sen and S. Torquato, 1989, "Effective conductivity of anisotropic two-phase composite media," *Phys. Rev. B*, **39**(7), pp. 4504-4515.

[33] S. Torquato, 1984, "Bulk properties of two-phase disordered media. I. Cluster expansion for the effective dielectric constant of dispersions of penetrable spheres," *J. Chem. Phys.*, **81**(11), pp. 5079-5088.

[34] Z. Hashin and S. Shtrikman, 1962, "A variational approach to the theory of the effective magnetic permeability of multiphase materials," *J. Appl. Phys.*, **33**, pp. 1514-1517.

[35] J. K. Carson, S. J. Lovatt, D. J. Tanner, and A. C. Cleland, 2005, "Thermal conductivity bounds for isotropic, porous materials," *Int. J. Heat Mass Transfer*, **48**, pp. 2150-2158.

[36] S. Torquato, 1991, "Random heterogeneous media: Microstructure and improved bounds on effective properties," *Appl. Mech. Rev.*, **44**(2), pp. 37-76.

[37] G. E. Schneider and D. Romilly, 1979, "The apparent thermal conductivity of long cylindrical fibers in a matrix," *American Society of Mechanical Engineers*, presented at the Winter Annual Meeting, New York, N.Y., December 2-7, pp. 1-6.

[38] M. M. Yovanovich, G. E. Schneider, and A. B. Strong, 1975, "Transverse apparent thermal conductivity of long rectangular fibers in a matrix," *American Society of Mechanical Engineers*, Paper 75-HT-26, presented at the AIChE-ASME Heat Transfer Conference, San Francisco, CA, August 11-13, pp. 1-6.

[39] H. G. Elrod, 1974, "Two simple theorems for establishing bounds on the total heat flow in steady-state heat-conduction problems with convective boundary conditions," *J. Heat Transfer*, No. 74-HT-C, pp. 65-70.

[40] J. K. Carson, S. J. Lovatt, D. J. Tanner, and A. C. Cleland, 2003, "An analysis of the influence of material structure on the effective thermal conductivity of theoretical porous materials using finite element simulations," *Int. J. Refrig.*, **26**, pp. 873-880.

[41] S. Kumar and J. Y. Murthy, 2005, "A numerical technique for computing effective thermal conductivity of fluid-particle mixtures," *Numerical Heat Transfer, Part B*, **47**, pp. 555-572.

[42] T. B. Lewis and L. E. Nielsen, 1970, "Dynamic mechanical properties of particulate-filled polymers," *J. Appl. Polym. Sci.*, **14**, pp. 1449-1471.

[43] L. E. Nielsen, 1974, "The thermal and electrical conductivity of two-phase systems," *Ind. Eng. Chem., Fundam.*, **13**(1), pp. 17-20.

[44] W. Woodside and J. H. Messmer, 1961, "Thermal conductivity of porous media. I. Unconsolidated sands," *J. Appl. Phys.*, **32**(9), pp. 1688-1699.

[45] J. E. Parrot and A. D. Stuckes, 1975 "Thermal conductivity of solids," *Pion London*, UK, p. 131.

[46] Y. Agari and T. Uno, 1986, "Estimation on thermal conductivities of filled polymers," *J. App. Poly. Comp. Sci.*, **32**, pp. 5705-5712.

[47] O. C. Zienkiewicz and R. L. Taylor, 1989, *The Finite Element Method, 5th ed.*, McGraw-Hill, New York, USA.

[48] M. M. Yovanovich and E. E. Marotta, 2003, "Thermal Spreading and Contact Resistances," Chapter 4 in: A. Bejan and A. D. Kraus, *Heat Transfer Handbook*, John Wiley and Sons, Inc., New Jersey, USA, p. 294.

[49] P. Keblinski, S. R. Phillpot, S. U. S. Choi, and J. A. Eastman, 2001, "Mechanisms of heat flow in suspensions of nano-sized particles (nanofluids)," *Int. J. Heat Mass Transfer*, **45**, pp. 855-863.

[50] S. Kumar and J. Y. Murthy, 2005, "A numerical technique for computing effective thermal conductivity of fluid-particle mixtures," *Numerical Heat Transfer, Part B*, **47**, pp. 555-572.

[51] S. U. S. Choi, Z. G. Zhang, W. Yu, F. E. Lockwood, and E. A. Grulke, 2001, "Anomalous thermal conductivity enhancement in nanotube suspensions," *Appl. Phys. Lett.*, **79**(14), pp. 2252-2254.

[52] I. H. Tavman, 2000, "Thermal conductivity of particle reinforced polymer composites," *Int. Comm. Heat Mass Transfer*, **27**(2), pp. 253-261.

[53] F. P. Incropera and D. P. DeWitt, 2002, *Fundamentals of Heat and Mass Transfer, 5th ed.*, John Wiley & Sons, New York, USA, pg. 905.

[54] W. Yu and S. U. S. Choi, 2003, "The role of interfacial layers in the enhanced thermal conductivity of nanofluids: A renovated Maxwell model," *J. Nanoparticle Research*, **5**, pp. 165-171.

[55] C. P. Wong and R. S. Bollampally, 1999, "Thermal conductivity, elastic modulus, and coefficient of thermal expansion of polymer composites filled with ceramic particles for electronic packaging," *J. Appl. Polym. Sci.*, **74**, pp. 3396-3403.

[56] D. W. Sundstrom and S. Y. Chen, 1970, "Thermal conductivity of reinforced plastics," *J. Comp. Mat.*, **4**, pp. 113-117.

[57] I. H. Tavman, 2000, "Thermal conductivity of particle reinforced polymer composites," *Int. Comm. Heat Mass Transfer*, **27**(2), pp. 253-261.

[58] F. Lin, G. S. Bhatia, and J. D. Ford, 1993, "Thermal conductivities of powder-filled epoxy resins," *J. Appl. Polym. Sci.*, **49**, pp. 1901-1908.

[59] J. K. Carson, S. J. Lovatt, D. J. Tanner, and A. C. Cleland, 2005, "Thermal conductivity bounds for isotropic, porous materials," *Int. J. Heat Mass Transfer*, **48**, pp. 2150-2158.

[60] R. L. Hamilton, 1960, "Thermal conductivity of heterogeneous mixtures," PhD Thesis, University of Oklahoma, pp. 29-36.

Appendix A

Mathematical Formulation of the Maxwell Equation

Maxwell considered the situation where n small spheres of radius r_2 and conductivity k_2 were embedded within a single larger sphere of radius r_1 and conductivity k_1 such that the temperature fields of neighbouring particles are independent of one another. The temperature distribution in each component is defined by the azimuthally independent steady-state diffusion equation,

$$\nabla^2 T_i = \frac{1}{r^2}\frac{\partial}{\partial r}\left(r^2\frac{\partial T_i}{\partial r}\right) + \frac{1}{r^2\sin\theta}\frac{\partial}{\partial \theta}\left(\sin\theta\frac{\partial T_i}{\partial \theta}\right) = 0 \tag{A.1}$$

where $i = 0$ in the effective medium, $i = 1$ in the continuous fluid phase, and $i = 2$ in the solid particle.

Taking the centre of the sphere as the origin, the general solution of Equation (A.1) in each medium is written as

$$T_i = \sum_{m=0}^{\infty}\left(a_{i,m}\,r^m + b_{i,m}\,r^{-(m+1)}\right)P_m(\cos\theta) \tag{A.2}$$

where $P_m(\cos\theta)$ is the mth degree Legendre polynomial. Equation (A.2) can be greatly simplified if we recognize the following: (1) in the effective medium far from the
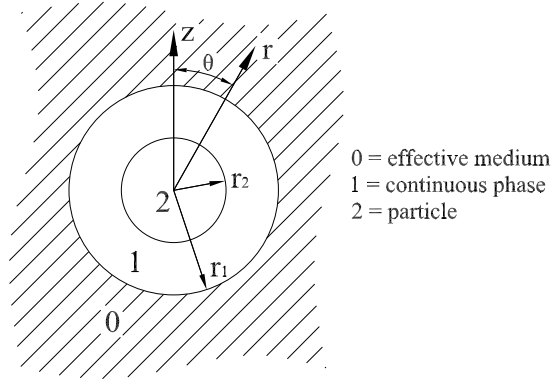
Figure A.1: Cell geometry subject to Maxwell's analysis

particle, the temperature gradient and heat flux are constants, (2) $P_1(\cos\theta) = \cos\theta$, and (3) the boundary conditions connecting each medium impose the same *form* of $T_0(r,\theta)$ on $T_i(r,\theta)$. Making these observations in Equation (A.2) results in a more simple general form,

$$T_i(r,\theta) = \left(A_i + B_i r^{-2}\right)\cos\theta \tag{A.3}$$

A.1 Boundary Conditions

1. ∇T_0 and q_0 are constants far from the particle,

$$\lim_{(r\to\infty,\theta)} T_0(r,\theta) = -\frac{q_0}{k}z = -\frac{q_0}{k}r\cos\theta$$

$$A_0 = -\frac{q_0}{k} \tag{A.4}$$

2. T is bounded at the center of the particle $(r_2 = 0)$,

$$T_2(r_2,\theta) = \left(A_2 r_2 + B_2 r_2^{-2}\right)\cos\theta$$

$$B_2 = 0 \tag{A.5}$$

3. Conduction across the interfaces (energy balance),

$$k_2\left(\frac{\partial T_2}{\partial r}\right)\bigg|_{r=r_2} = k_1\left(\frac{\partial T_1}{\partial r}\right)\bigg|_{r=r_2} \tag{A.6}$$

$$k_1 \left(\frac{\partial T_1}{\partial r}\right)\bigg|_{r=r_1} = k_0 \left(\frac{\partial T_0}{\partial r}\right)\bigg|_{r=r_1} \tag{A.7}$$

4. Continuity of temperature at the interfaces,

$$T_2(r_2, \theta) = T_1(r_2, \theta) \tag{A.8}$$

$$T_1(r_1, \theta) = T_0(r_2, \theta) \tag{A.9}$$

A.2 Solution 1: Neglect Local Distortions in Polarization Field

One method of deriving the Maxwell equation from the above formulation involves solving the temperature field in the surrounding fluid under two conditions: these are (1) when a number of small spheres of conductivity k_2 are embedded in the surrounding fluid and (2) when the composite medium is assumed to be entirely composed of material with conductivity k_e. If it is assumed that the temperature field in the fluid is identical in both cases, then the effective thermal conductivity of the medium can be established by equating the respective polarization fields of cases (1) and (2). Solving Equation (A.1) subject to the boundary conditions yields the temperature field in the discontinuous solid phase,

$$T_s = -\frac{q_0}{k} \left(\frac{3k_f}{k_s + k_f}\right) r \cos\theta \tag{A.10}$$

and the temperature field in the continuous fluid phase,

$$T_f = -\frac{q_0}{k} (r\cos\theta) + \frac{q_0}{k} nr_2^3 \left(\frac{k_s - k_f}{k_s + 2k_f}\right) \left(\frac{\cos\theta}{r^2}\right) \tag{A.11}$$

We define the volume fraction as,

$$\phi = \frac{V_2}{V_1} = \frac{nr_2^3}{r_1^3} \tag{A.12}$$

From Equation (A.11),

$$T_f = -\frac{q_0}{k}\left(r\cos\theta\right) + \frac{q_0}{k}\phi r_1^3 \left(\frac{k_s - k_f}{k_s + 2k_f}\right)\left(\frac{\cos\theta}{r^2}\right) \tag{A.13}$$

However, if the larger sphere had been embedded with a material of thermal conductivity k_e, Equation (A.13) would be written as

$$T_f = -\frac{q_0}{k}\left(r\cos\theta\right) + \frac{q_0}{k}r_1^3 \left(\frac{k_e - k_f}{k_e + 2k_f}\right)\left(\frac{\cos\theta}{r^2}\right) \tag{A.14}$$

In order for Equations (A.13) and (A.14) to produce the same result,

$$\phi\left(\frac{k_s - k_f}{k_s + 2k_f}\right) = \left(\frac{k_e - k_f}{k_e + 2k_f}\right) \tag{A.15}$$

which, when rearranged, is identical to the Maxwell equation.

A.3   Solution 2: Volume-Averaged Fields

Hamilton [60] developed a method of determining effective thermal conductivity from the volume averaged heat flux and temperature gradient in the cell. He defined effective thermal conductivity as the ratio of the average heat flux in the cell to the average temperature gradient in the cell,

$$k_e = \frac{\overline{q}}{\overline{\nabla T}} \tag{A.16}$$

where the overbar indicates a volume average over the cell volume, $V = 4\pi r_1^3/3$:

$$\overline{f} = \frac{1}{V}\int_V f \, dV \tag{A.17}$$

Due to symmetry, only the averaged $z-$components are non-zero. These are given by

$$\overline{q} = \overline{q_1}\left(1 - \phi\right) + \overline{q_2}\,\phi \tag{A.18}$$

in which

$$\overline{q_i} = k_i \, \overline{\nabla T_i} \tag{A.19}$$

and

$$\overline{\nabla T} = \overline{\nabla T_1}\,(1 - \phi) + \overline{\nabla T_2}\,\phi \qquad (A.20)$$

where $\phi = V_2/V_1$ is the particle volume fraction. Consequently, the effective conductivity of the medium becomes

$$k_e = \frac{k_1\,\overline{\nabla T_1}\,(1 - \phi) + k_2\,\overline{\nabla T_2}\,\phi}{\overline{\nabla T_1}\,(1 - \phi) + \overline{\nabla T_2}\,\phi} \qquad (A.21)$$

The solution of the above equations gives the famous result of Maxwell. This analysis has been used to develop similar models where effects such as boundary resistance at the particle/matrix interface or thin coatings are considered [19].

Appendix B

Various Geometric Dispersions With Thin Coatings in a Rectangular Lattice

Upper and lower bounds have also been derived for the various geometries when a uniform shell of a material with different thermal properties surrounds the particle in a rectangular cell. Forcing this thickness, τ, equal to 0, the relative conductivity of the coating, κ_c, equal to 1, and the dimensions of the rectangular cell, A, B, and C, equal to 0.5 recovers the previous relationships (various geometries in a unit cell).

Applying the same procedure described in Chapter 4, upper and lower bounds have been derived for (1) a cylinder oriented with its axis parallel to heat flow, (2) a cylinder oriented with its axis perpendicular to heat flow, (3) a rectangular prism, and (4) an ellipsoid in a rectangular cell for particles with thin coatings of materials with different thermal properties. Figure B.1 is an example of the geometries studied.
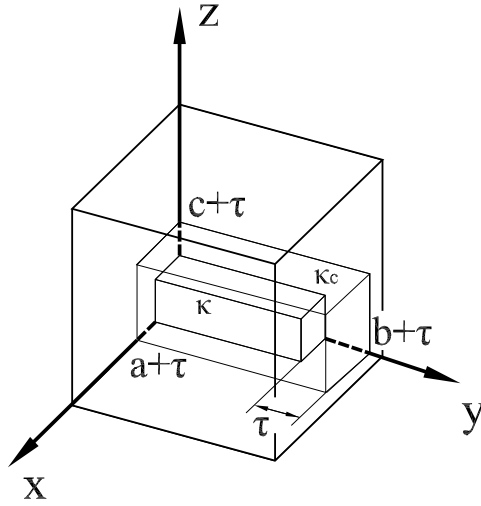
Figure B.1: Rectangular prism with uniform coating inside unit cell – $1/8^{\text{th}}$ unit cell

B.1 Cylinder With Axis Parallel to Heat Flow

A finite circular cylinder oriented with its axis parallel to the direction of heat flow in a rectangular cell has the following lower and upper bounds on effective thermal conductivity when a thin coating of a thermally different material is allowed for:

$$
\left(\frac{k_e}{k_f}\right)_{lb} = 1 - \frac{\pi(\epsilon+\tau)^2}{4AB} + \frac{C}{4AB}\left[\frac{\pi\epsilon^2}{C-Kh-K_c\tau} + \frac{\pi(\epsilon+\tau)^2 - \pi\epsilon^2}{C-K_c(h+\tau)}\right]
$$

$$
\left(\frac{k_e}{k_f}\right)_{ub} = \left\{1 - \frac{(h+\tau)}{C} + \frac{AB}{C}\left[\frac{\kappa\kappa_c\pi\epsilon^2}{\kappa_c h + \kappa\tau}+ \right.\right. \tag{B.1}
$$

$$
\left.\left.\frac{4AB + (\kappa_c-1)\pi(\epsilon+\tau)^2 - \pi\epsilon^2}{h+\tau}\right]\right\}^{-1}
$$

where ϵ is the relative radius of the cylinder, τ is the relative thickness of the coating, $0 \leq \epsilon + \tau \leq 0.5$, and $2h$ is the relative height of the cylinder, $0 \leq 2h + 2\tau \leq 1$; and where κ, κ_c, K, and K_c are defined in Equations (4.6) and (4.29) in Chapter 4 for the particle material and the coating material.

101

B.2 Cylinder With Axis Perpendicular to Heat Flow

A finite circular cylinder oriented with its axis perpendicular to the direction of heat flow in a rectangular cell has the following lower and upper bounds on effective thermal conductivity when a thin coating of a thermally different material is allowed for:

$$\left(\frac{k_e}{k_f}\right)_{lb} = 1 - (\epsilon + \tau)(h + \tau)\frac{C}{AB} + \frac{C}{AB}h\left(I_{lb,1} + I_{lb,2} + I_{lb,3} + \frac{A - (\epsilon + \tau)}{C}\right)$$

(B.2)

$$\left(\frac{k_e}{k_f}\right)_{ub} = \left[1 - \frac{(\epsilon + \tau)}{C} + \frac{AB}{C}(I_{ub,1} + I_{ub,2})\right]^{-1}$$

where

$$I_{lb,1} = \int_0^\epsilon \frac{dx}{C - K_c\sqrt{(\epsilon + \tau)^2 - x^2} - \left(\frac{1}{\kappa_c} - \frac{1}{\kappa}\right)\sqrt{\epsilon^2 - x^2}}$$

$$I_{lb,2} = \int_\epsilon^{\epsilon+\tau} \frac{dx}{C - K_c\sqrt{(\epsilon + \tau)^2 - x^2}}$$

(B.3)

$$I_{lb,3} = \int_0^{\epsilon+\tau} \frac{dx}{C - K_c\sqrt{(\epsilon + \tau)^2 - x^2}}$$

and

$$I_{ub,1} = \int_0^\epsilon \frac{dz}{AB + (\kappa_c - 1)(h + \tau)\sqrt{(\epsilon + \tau)^2 - z^2} + (\kappa - \kappa_c)h\sqrt{\epsilon^2 - z^2}}$$

(B.4)

$$I_{ub,2} = \int_\epsilon^{\epsilon+\tau} \frac{dz}{AB + (\kappa_c - 1)(h + \tau)\sqrt{(\epsilon + \tau)^2 - z^2}}$$

(B.5)

where ϵ is the relative radius of the cylinder, τ is the relative thickness of the coating, $0 \le \epsilon + \tau \le 0.5$, and $2h$ is the relative height of the cylinder, $0 \le 2h + 2\tau \le 1$; and where κ, κ_c, K, and K_c are defined in Equations (4.6) and (4.29) in Chapter 4 for the particle material and the coating material.

B.3   Rectangular Prism

A rectangular prism in a unit cell has the following lower and upper bounds on effective thermal conductivity when a thin coating of a thermally different material is allowed for:

$$
\left(\frac{k_e}{k_f}\right)_{lb} = 1 - \frac{(a+\tau)(b+\tau)}{AB} + \frac{1}{AB}\left[\frac{ab}{C - Kc - K_c\tau}\right.
$$

$$
\left. + \frac{(a+\tau)(b+\tau) - ab}{C - K_c(c+\tau)}\right]
$$

$$
\left(\frac{k_e}{k_f}\right)_{ub} = \left\{1 - \frac{(c+\tau)}{C} + 2\left[\frac{\kappa\kappa_c ab}{\kappa\tau + \kappa_c c}\right.\right.
$$

$$
\left.\left. + \frac{AB + (\kappa_c - 1)(a+\tau)(b+\tau) - ab}{c+\tau}\right]\right\}^{-1}
$$

(B.6)

where $2a$, $2b$, and $2c$ are the dimensions of the prism in the $x-$, $y-$, and $z-$axes, τ is the relative thickness of the coating, and $0 \le a+\tau, b+\tau, c+\tau \le 0.5$. The direction of heat flow is along the $z-$axis. The dimensions $2a$ and $2b$ are interchangeable as expected. The terms κ, κ_c, K, and K_c are defined in Equations (4.6) and (4.29) in Chapter 4 for the particle material and the coating material.

B.4   Ellipsoid

An ellipsoid in a unit cell has the following lower and upper bounds on effective thermal conductivity when a thin coating of a thermally different material is allowed for:

$$
\left(\frac{k_e}{k_f}\right)_{lb} = 1 - \frac{\pi(a+\tau)(b+\tau)}{4AB} + \frac{C}{2AB}(I_{lb,1} + I_{lb,2})
$$

(B.7)

$$
\left(\frac{k_e}{k_f}\right)_{ub} = \left[1 - \frac{(c+\tau)}{C} + 2(I_{ub,1} + I_{ub,2})\right]^{-1}
$$

where

$$I_{lb,1} = \int_0^{b+\tau} \int_0^{a\sqrt{1-\frac{y^2}{b^2}}} \frac{dxdy}{\left\{ C - K_c(c+\tau)\sqrt{1 - \frac{x^2}{(a+\tau)^2} + \frac{y^2}{(b+\tau)^2}} \right.}$$

$$\left. - \left(\frac{1}{\kappa_c} - \frac{1}{\kappa}\right) c\sqrt{1 - \frac{x^2}{a^2} + \frac{y^2}{b^2}} \right\} \tag{B.8}$$

$$I_{lb,2} = \int_0^{b+\tau} \int_{a\sqrt{1-\frac{y^2}{b^2}}}^{(a+\tau)\sqrt{1-\frac{y^2}{(b+\tau)^2}}} \frac{dxdy}{C - K_c(c+\tau)\sqrt{1 - \frac{x^2}{(a+\tau)^2} + \frac{y^2}{(b+\tau)^2}}}$$

and

$$I_{ub,1} = \int_0^c \frac{dz}{\left\{ 2AB - (\kappa - \kappa_c + 1)\pi(a+\tau)(b+\tau)\left[1 - \frac{z^2}{(c+\tau)^2}\right] \right.}$$

$$\left. - \kappa_c \pi ab \left(1 - \frac{z^2}{c^2}\right) \right\} \tag{B.9}$$

$$I_{ub,2} = \int_c^{c+\tau} \frac{dz}{2AB + (\kappa_b - 1)\pi(a+\tau)(b+\tau)\left[1 - \frac{z^2}{(c+\tau)^2}\right]}$$

and where $2a$, $2b$, and $2c$ are the dimensions of the ellipsoid in the $x-$, $y-$, and $z-$axes, τ is the relative thickness of the coating, and $0 \leq a+\tau$, $b+\tau$, $c+\tau \leq 0.5$. The direction of heat flow is along the $z-$axis. The dimensions $2a$ and $2b$ are interchangeable as expected. The terms κ, κ_c, K, and K_c are defined in Equations (4.6) and (4.29) in Chapter 4 for the particle material and the coating material.

Appendix C

Numerical Results

Table C.1: Rectangular prism in a unit cell ($\kappa = 1000$)

a	b	c	ϕ	$\left(\dfrac{k_e}{k_m}\right)_{lb}$	$\left(\dfrac{k_e}{k_m}\right)_{ub}$	$\left(\dfrac{k_e}{k_m}\right)_{geo}$	$\left(\dfrac{k_e}{k_m}\right)_{num}$	% diff.
0.1	0.1	0.1	0.008	1.01	1.24	1.12	1.03	8.09
0.1	0.2	0.1	0.016	1.02	1.25	1.13	1.05	7.04
0.1	0.1	0.2	0.016	1.03	1.64	1.30	1.11	14.58
0.1	0.2	0.2	0.032	1.05	1.65	1.32	1.17	11.62
0.1	0.3	0.1	0.024	1.03	1.25	1.13	1.07	5.95
0.1	0.1	0.3	0.024	1.06	2.41	1.60	1.26	21.10
0.1	0.3	0.2	0.048	1.08	1.66	1.34	1.22	8.72
0.1	0.2	0.3	0.048	1.12	2.45	1.66	1.39	15.89
0.1	0.3	0.3	0.072	1.18	2.47	1.71	1.52	11.03
0.1	0.4	0.1	0.032	1.04	1.25	1.14	1.08	4.97
0.1	0.1	0.4	0.032	1.16	4.56	2.30	1.58	31.26
0.1	0.4	0.2	0.064	1.11	1.66	1.36	1.27	6.45
0.1	0.2	0.4	0.064	1.32	4.76	2.51	1.89	24.53
0.1	0.4	0.3	0.096	1.24	2.48	1.75	1.62	7.50
0.1	0.3	0.4	0.096	1.48	4.84	2.67	2.19	18.08
0.1	0.4	0.4	0.128	1.64	4.88	2.83	2.45	13.40
0.2	0.2	0.1	0.032	1.04	1.25	1.14	1.08	5.50
0.2	0.2	0.2	0.064	1.11	1.66	1.36	1.25	7.79
0.2	0.3	0.1	0.048	1.06	1.25	1.15	1.10	4.01
0.2	0.3	0.2	0.096	1.16	1.66	1.39	1.33	4.34
0.2	0.2	0.3	0.096	1.24	2.48	1.75	1.58	9.72
0.2	0.3	0.3	0.144	1.36	2.48	1.84	1.76	4.36
0.2	0.4	0.1	0.064	1.08	1.25	1.16	1.13	2.77
0.2	0.4	0.2	0.128	1.21	1.66	1.42	1.39	1.98
0.2	0.2	0.4	0.128	1.64	4.88	2.83	2.36	16.62
0.2	0.4	0.3	0.192	1.48	2.49	1.92	1.90	1.10
0.2	0.3	0.4	0.192	1.96	4.92	3.10	2.80	9.73
0.2	0.4	0.4	0.256	2.27	4.94	3.35	3.17	5.27

a	b	c	ϕ	$\left(\dfrac{k_e}{k_m}\right)_{lb}$	$\left(\dfrac{k_e}{k_m}\right)_{ub}$	$\left(\dfrac{k_e}{k_m}\right)_{geo}$	$\left(\dfrac{k_e}{k_m}\right)_{num}$	% diff.
0.3	0.3	0.1	0.072	1.09	1.25	1.17	1.14	2.21
0.3	0.3	0.2	0.144	1.24	1.66	1.44	1.43	0.59
0.3	0.3	0.3	0.216	1.54	2.49	1.96	1.98	-1.08
0.3	0.4	0.1	0.096	1.12	1.25	1.18	1.17	0.77
0.3	0.4	0.2	0.192	1.32	1.66	1.48	1.51	-1.69
0.3	0.4	0.3	0.288	1.72	2.49	2.07	2.15	-3.93
0.3	0.3	0.4	0.288	2.43	4.95	3.47	3.38	2.65
0.3	0.4	0.4	0.384	2.91	4.96	3.80	3.86	-1.68
0.4	0.4	0.1	0.128	1.16	1.25	1.20	1.21	-0.74
0.4	0.4	0.2	0.256	1.43	1.66	1.54	1.60	-3.60
0.4	0.4	0.3	0.384	1.96	2.49	2.21	2.34	-6.09
0.4	0.4	0.4	0.512	3.55	4.97	4.20	4.44	-5.69

Table C.2: Rectangular prism in a unit cell ($\kappa = 100$)

a	b	c	ϕ	$\left(\dfrac{\mathbf{k_e}}{\mathbf{k_m}}\right)_{\mathbf{lb}}$	$\left(\dfrac{\mathbf{k_e}}{\mathbf{k_m}}\right)_{\mathbf{ub}}$	$\left(\dfrac{\mathbf{k_e}}{\mathbf{k_m}}\right)_{\mathbf{geo}}$	$\left(\dfrac{\mathbf{k_e}}{\mathbf{k_m}}\right)_{\mathbf{num}}$	% **diff.**
0.1	0.1	0.1	0.008	1.01	1.19	1.10	1.03	6.19
0.1	0.2	0.1	0.016	1.02	1.22	1.11	1.05	6.02
0.1	0.1	0.2	0.016	1.03	1.47	1.23	1.10	10.29
0.1	0.2	0.2	0.032	1.05	1.55	1.28	1.16	9.37
0.1	0.3	0.1	0.024	1.03	1.23	1.12	1.06	5.29
0.1	0.1	0.3	0.024	1.06	1.92	1.43	1.24	13.28
0.1	0.3	0.2	0.048	1.08	1.58	1.31	1.21	7.35
0.1	0.2	0.3	0.048	1.12	2.14	1.55	1.36	11.74
0.1	0.3	0.3	0.072	1.18	2.24	1.62	1.48	8.54
0.1	0.4	0.1	0.032	1.04	1.23	1.13	1.08	4.51
0.1	0.1	0.4	0.032	1.15	2.77	1.79	1.49	16.40
0.1	0.4	0.2	0.064	1.10	1.60	1.33	1.26	5.55
0.1	0.2	0.4	0.064	1.30	3.45	2.12	1.79	15.86
0.1	0.4	0.3	0.096	1.23	2.30	1.68	1.58	5.90
0.1	0.3	0.4	0.096	1.46	3.82	2.36	2.06	12.49
0.1	0.4	0.4	0.128	1.61	4.04	2.55	2.31	9.57
0.2	0.2	0.1	0.032	1.04	1.23	1.13	1.07	5.03
0.2	0.2	0.2	0.064	1.10	1.60	1.33	1.24	6.84
0.2	0.3	0.1	0.048	1.06	1.24	1.14	1.10	3.76
0.2	0.3	0.2	0.096	1.16	1.62	1.37	1.32	3.92
0.2	0.2	0.3	0.096	1.23	2.30	1.68	1.55	8.00
0.2	0.3	0.3	0.144	1.35	2.36	1.78	1.72	3.65
0.2	0.4	0.1	0.064	1.08	1.24	1.16	1.13	2.63
0.2	0.4	0.2	0.128	1.21	1.63	1.41	1.38	1.81
0.2	0.2	0.4	0.128	1.61	4.04	2.55	2.23	12.55
0.2	0.4	0.3	0.192	1.47	2.39	1.87	1.86	0.85
0.2	0.3	0.4	0.192	1.91	4.30	2.87	2.65	7.69
0.2	0.4	0.4	0.256	2.22	4.45	3.14	3.01	4.24

a	b	c	ϕ	$\left(\dfrac{k_e}{k_m}\right)_{lb}$	$\left(\dfrac{k_e}{k_m}\right)_{ub}$	$\left(\dfrac{k_e}{k_m}\right)_{geo}$	$\left(\dfrac{k_e}{k_m}\right)_{num}$	% diff.
0.3	0.3	0.1	0.072	1.09	1.24	1.16	1.14	2.12
0.3	0.3	0.2	0.144	1.24	1.64	1.42	1.41	0.54
0.3	0.3	0.3	0.216	1.53	2.40	1.91	1.94	−1.09
0.3	0.4	0.1	0.096	1.12	1.24	1.18	1.17	0.76
0.3	0.4	0.2	0.192	1.31	1.64	1.47	1.49	−1.59
0.3	0.4	0.3	0.288	1.70	2.43	2.03	2.11	−3.69
0.3	0.3	0.4	0.288	2.37	4.51	3.27	3.20	2.09
0.3	0.4	0.4	0.384	2.83	4.62	3.61	3.67	−1.59
0.4	0.4	0.1	0.128	1.16	1.25	1.20	1.21	−0.70
0.4	0.4	0.2	0.256	1.42	1.65	1.53	1.58	−3.42
0.4	0.4	0.3	0.384	1.94	2.44	2.18	2.30	−5.74
0.4	0.4	0.4	0.512	3.44	4.71	4.02	4.23	−5.20

Table C.3: Rectangular prism in a unit cell ($\kappa = 10$)

a	b	c	ϕ	$\left(\dfrac{k_e}{k_m}\right)_{lb}$	$\left(\dfrac{k_e}{k_m}\right)_{ub}$	$\left(\dfrac{k_e}{k_m}\right)_{geo}$	$\left(\dfrac{k_e}{k_m}\right)_{num}$	% diff.
0.1	0.1	0.1	0.008	1.01	1.06	1.03	1.02	1.14
0.1	0.2	0.1	0.016	1.02	1.09	1.05	1.03	1.79
0.1	0.1	0.2	0.016	1.02	1.12	1.07	1.06	0.88
0.1	0.2	0.2	0.032	1.05	1.20	1.12	1.10	1.61
0.1	0.3	0.1	0.024	1.03	1.12	1.07	1.05	1.96
0.1	0.1	0.3	0.024	1.05	1.19	1.12	1.11	0.08
0.1	0.3	0.2	0.048	1.07	1.26	1.16	1.14	1.59
0.1	0.2	0.3	0.048	1.09	1.34	1.21	1.20	0.69
0.1	0.3	0.3	0.072	1.14	1.45	1.29	1.28	0.53
0.1	0.4	0.1	0.032	1.04	1.13	1.08	1.06	1.90
0.1	0.1	0.4	0.032	1.10	1.27	1.18	1.19	−0.36
0.1	0.4	0.2	0.064	1.09	1.31	1.19	1.18	1.31
0.1	0.2	0.4	0.064	1.21	1.50	1.35	1.34	0.38
0.1	0.4	0.3	0.096	1.19	1.55	1.36	1.35	0.16
0.1	0.3	0.4	0.096	1.31	1.71	1.50	1.49	0.43
0.1	0.4	0.4	0.128	1.41	1.89	1.64	1.63	0.29
0.2	0.2	0.1	0.032	1.04	1.13	1.08	1.06	2.27
0.2	0.2	0.2	0.064	1.09	1.31	1.19	1.17	2.14
0.2	0.3	0.1	0.048	1.05	1.16	1.10	1.08	2.04
0.2	0.3	0.2	0.096	1.14	1.38	1.25	1.23	1.49
0.2	0.2	0.3	0.096	1.19	1.55	1.36	1.34	1.33
0.2	0.3	0.3	0.144	1.28	1.70	1.47	1.47	0.57
0.2	0.4	0.1	0.064	1.07	1.17	1.12	1.10	1.60
0.2	0.4	0.2	0.128	1.18	1.42	1.30	1.25	3.50
0.2	0.2	0.4	0.128	1.41	1.89	1.64	1.61	1.61
0.2	0.4	0.3	0.192	1.38	1.80	1.57	1.58	−0.24
0.2	0.3	0.4	0.192	1.62	2.21	1.89	1.86	1.35
0.2	0.4	0.4	0.256	1.82	2.46	2.12	2.10	0.83

a	b	c	ϕ	$\left(\dfrac{\mathbf{k_e}}{\mathbf{k_m}}\right)_{\mathbf{lb}}$	$\left(\dfrac{\mathbf{k_e}}{\mathbf{k_m}}\right)_{\mathbf{ub}}$	$\left(\dfrac{\mathbf{k_e}}{\mathbf{k_m}}\right)_{\mathbf{geo}}$	$\left(\dfrac{\mathbf{k_e}}{\mathbf{k_m}}\right)_{\mathbf{num}}$	% diff.
0.3	0.3	0.1	0.072	1.08	1.18	1.13	1.11	1.38
0.3	0.3	0.2	0.144	1.20	1.44	1.32	1.31	0.22
0.3	0.3	0.3	0.216	1.42	1.85	1.62	1.64	−0.90
0.3	0.4	0.1	0.096	1.11	1.19	1.15	1.14	0.61
0.3	0.4	0.2	0.192	1.27	1.48	1.37	1.38	−0.92
0.3	0.4	0.3	0.288	1.56	1.95	1.75	1.78	−2.08
0.3	0.3	0.4	0.288	1.93	2.57	2.23	2.22	0.39
0.3	0.4	0.4	0.384	2.23	2.85	2.53	2.54	−0.74
0.4	0.4	0.1	0.128	1.14	1.21	1.17	1.18	−0.37
0.4	0.4	0.2	0.256	1.36	1.52	1.44	1.47	−2.14
0.4	0.4	0.3	0.384	1.75	2.05	1.89	1.96	−3.34
0.4	0.4	0.4	0.512	2.65	3.14	2.88	2.95	−2.20

Table C.4: Circular cylinder with axis oriented parallel to direction of heat flow, in a unit cell ($\kappa = 1000$)

ϵ	h	ϕ	$\left(\dfrac{k_e}{k_m}\right)_{lb}$	$\left(\dfrac{k_e}{k_m}\right)_{ub}$	$\left(\dfrac{k_e}{k_m}\right)_{geo}$	$\left(\dfrac{k_e}{k_m}\right)_{num}$	% diff.
0.1	0.1	0.006	1.01	1.24	1.12	1.02	8.37
0.1	0.2	0.013	1.02	1.63	1.29	1.09	15.44
0.1	0.3	0.019	1.05	2.39	1.58	1.22	22.65
0.1	0.4	0.025	1.13	4.45	2.24	1.49	33.35
0.2	0.1	0.025	1.03	1.25	1.13	1.06	6.36
0.2	0.2	0.050	1.08	1.66	1.34	1.21	10.00
0.2	0.3	0.075	1.19	2.47	1.71	1.48	13.44
0.2	0.4	0.101	1.50	4.85	2.70	2.11	21.57
0.3	0.1	0.057	1.07	1.25	1.16	1.11	3.65
0.3	0.2	0.113	1.19	1.66	1.41	1.35	3.75
0.3	0.3	0.170	1.42	2.49	1.88	1.81	3.71
0.3	0.4	0.226	2.13	4.93	3.24	2.95	8.99
0.4	0.1	0.101	1.13	1.25	1.19	1.18	0.85
0.4	0.2	0.201	1.33	1.66	1.49	1.51	-1.30
0.4	0.3	0.302	1.75	2.49	2.09	2.16	-3.15
0.4	0.4	0.402	3.00	4.96	3.86	3.89	-0.70

Table C.5: Circular cylinder with axis oriented parallel to direction of heat flow, in a unit cell ($\kappa = 100$)

ϵ	$\mathbf{h}$	ϕ	$\left(\dfrac{\mathbf{k_e}}{\mathbf{k_m}}\right)_{\mathbf{lb}}$	$\left(\dfrac{\mathbf{k_e}}{\mathbf{k_m}}\right)_{\mathbf{ub}}$	$\left(\dfrac{\mathbf{k_e}}{\mathbf{k_m}}\right)_{\mathbf{geo}}$	$\left(\dfrac{\mathbf{k_e}}{\mathbf{k_m}}\right)_{\mathbf{num}}$	% **diff.**
0.1	0.1	0.006	1.01	1.18	1.09	1.02	6.07
0.1	0.2	0.013	1.02	1.43	1.21	1.09	10.25
0.1	0.3	0.019	1.05	1.83	1.38	1.20	13.27
0.1	0.4	0.025	1.12	2.53	1.68	1.41	16.08
0.2	0.1	0.025	1.03	1.23	1.12	1.06	5.71
0.2	0.2	0.050	1.08	1.59	1.31	1.20	8.61
0.2	0.3	0.075	1.18	2.25	1.63	1.45	10.86
0.2	0.4	0.101	1.48	3.85	2.39	2.01	15.89
0.3	0.1	0.057	1.07	1.24	1.15	1.11	3.45
0.3	0.2	0.113	1.19	1.63	1.39	1.34	3.44
0.3	0.3	0.170	1.41	2.38	1.83	1.77	3.18
0.3	0.4	0.226	2.08	4.39	3.02	2.80	7.37
0.4	0.1	0.101	1.12	1.24	1.18	1.17	0.83
0.4	0.2	0.201	1.33	1.65	1.48	1.50	-1.23
0.4	0.3	0.302	1.74	2.43	2.05	2.11	-2.98
0.4	0.4	0.402	2.91	4.63	3.67	3.7	-0.71

Table C.6: Circular cylinder with axis oriented parallel to direction of heat flow, in a unit cell ($\kappa = 10$)

ϵ	$\mathbf{h}$	ϕ	$\left(\dfrac{\mathbf{k_e}}{\mathbf{k_m}}\right)_{\mathbf{lb}}$	$\left(\dfrac{\mathbf{k_e}}{\mathbf{k_m}}\right)_{\mathbf{ub}}$	$\left(\dfrac{\mathbf{k_e}}{\mathbf{k_m}}\right)_{\mathbf{geo}}$	$\left(\dfrac{\mathbf{k_e}}{\mathbf{k_m}}\right)_{\mathbf{num}}$	% **diff.**
0.1	0.1	0.006	1.01	1.05	1.03	1.02	0.94
0.1	0.2	0.013	1.02	1.10	1.06	1.05	0.66
0.1	0.3	0.019	1.04	1.15	1.09	1.09	-0.07
0.1	0.4	0.025	1.08	1.21	1.15	1.15	-0.47
0.2	0.1	0.025	1.03	1.12	1.07	1.05	2.29
0.2	0.2	0.050	1.07	1.27	1.17	1.14	2.36
0.2	0.3	0.075	1.15	1.47	1.30	1.28	1.68
0.2	0.4	0.101	1.32	1.74	1.52	1.49	1.75
0.3	0.1	0.057	1.06	1.17	1.11	1.09	2.01
0.3	0.2	0.113	1.16	1.40	1.28	1.26	1.49
0.3	0.3	0.170	1.33	1.76	1.53	1.52	0.69
0.3	0.4	0.226	1.73	2.35	2.01	1.98	1.7
0.4	0.1	0.101	1.11	1.20	1.15	1.14	0.66
0.4	0.2	0.201	1.28	1.49	1.38	1.39	-0.73
0.4	0.3	0.302	1.59	1.97	1.77	1.80	-1.74
0.4	0.4	0.402	2.29	2.90	2.58	2.59	-0.37

Table C.7: Circular cylinder with axis perpendicular to direction of heat flow, in a unit cell ($\kappa = 1000$)

ϵ	h	ϕ	$\left(\dfrac{k_e}{k_m}\right)_{lb}$	$\left(\dfrac{k_e}{k_m}\right)_{ub}$	$\left(\dfrac{k_e}{k_m}\right)_{geo}$	$\left(\dfrac{k_e}{k_m}\right)_{num}$	% diff.
0.1	0.1	0.006	1.01	1.24	1.12	1.02	8.69
0.1	0.2	0.013	1.02	1.24	1.12	1.03	8.07
0.1	0.3	0.019	1.02	1.25	1.13	1.05	7.35
0.1	0.4	0.025	1.03	1.25	1.13	1.06	6.66
0.2	0.1	0.025	1.04	1.65	1.31	1.11	15.11
0.2	0.2	0.050	1.08	1.66	1.34	1.17	12.59
0.2	0.3	0.075	1.12	1.66	1.36	1.22	10.19
0.2	0.4	0.101	1.15	1.66	1.38	1.27	8.44
0.3	0.1	0.057	1.12	2.45	1.66	1.33	19.70
0.3	0.2	0.113	1.24	2.48	1.75	1.49	15.14
0.3	0.3	0.170	1.36	2.48	1.84	1.63	11.22
0.3	0.4	0.226	1.48	2.49	1.92	1.74	9.01
0.4	0.1	0.101	1.36	4.81	2.56	1.85	27.55
0.4	0.2	0.201	1.71	4.90	2.90	2.26	21.95
0.4	0.3	0.302	2.07	4.94	3.20	2.65	17.16
0.4	0.4	0.402	2.43	4.95	3.47	2.96	14.59

Table C.8: Circular cylinder with axis perpendicular to direction of heat flow, in a unit cell ($\kappa = 100$)

ϵ	$\mathbf{h}$	ϕ	$\left(\dfrac{k_e}{k_m}\right)_{lb}$	$\left(\dfrac{k_e}{k_m}\right)_{ub}$	$\left(\dfrac{k_e}{k_m}\right)_{geo}$	$\left(\dfrac{k_e}{k_m}\right)_{num}$	% **diff.**
0.1	0.1	0.006	1.01	1.17	1.09	1.02	6.23
0.1	0.2	0.013	1.01	1.20	1.11	1.03	6.61
0.1	0.3	0.019	1.02	1.22	1.12	1.04	6.32
0.1	0.4	0.025	1.03	1.22	1.12	1.06	5.88
0.2	0.1	0.025	1.04	1.51	1.25	1.11	11.74
0.2	0.2	0.050	1.08	1.58	1.30	1.16	10.79
0.2	0.3	0.075	1.11	1.60	1.34	1.22	9.03
0.2	0.4	0.101	1.15	1.62	1.36	1.26	7.62
0.3	0.1	0.057	1.12	2.15	1.55	1.31	15.19
0.3	0.2	0.113	1.23	2.30	1.68	1.47	12.86
0.3	0.3	0.170	1.35	2.36	1.78	1.61	9.84
0.3	0.4	0.226	1.47	2.39	1.87	1.72	8.07
0.4	0.1	0.101	1.34	3.73	2.24	1.79	20.10
0.4	0.2	0.201	1.69	4.23	2.67	2.19	18.03
0.4	0.3	0.302	2.03	4.45	3.01	2.57	14.68
0.4	0.4	0.402	2.38	4.57	3.30	2.87	12.81

Table C.9: Circular cylinder with axis perpendicular to direction of heat flow, in a unit cell ($\kappa = 10$)

ϵ	$\mathbf{h}$	ϕ	$\left(\dfrac{\mathbf{k_e}}{\mathbf{k_m}}\right)_{\mathbf{lb}}$	$\left(\dfrac{\mathbf{k_e}}{\mathbf{k_m}}\right)_{\mathbf{ub}}$	$\left(\dfrac{\mathbf{k_e}}{\mathbf{k_m}}\right)_{\mathbf{geo}}$	$\left(\dfrac{\mathbf{k_e}}{\mathbf{k_m}}\right)_{\mathbf{num}}$	$\%$ **diff.**
0.1	0.1	0.006	1.01	1.05	1.03	1.01	1.10
0.1	0.2	0.013	1.01	1.08	1.04	1.03	1.81
0.1	0.3	0.019	1.02	1.10	1.06	1.04	2.14
0.1	0.4	0.025	1.03	1.12	1.07	1.06	1.25
0.2	0.1	0.025	1.03	1.16	1.10	1.07	2.16
0.2	0.2	0.050	1.07	1.26	1.16	1.12	3.33
0.2	0.3	0.075	1.10	1.32	1.21	1.17	3.40
0.2	0.4	0.101	1.13	1.37	1.25	1.21	3.21
0.3	0.1	0.057	1.10	1.37	1.22	1.20	2.12
0.3	0.2	0.113	1.19	1.58	1.37	1.32	3.51
0.3	0.3	0.170	1.29	1.72	1.49	1.44	3.31
0.3	0.4	0.226	1.39	1.83	1.59	1.54	3.09
0.4	0.1	0.101	1.25	1.70	1.46	1.43	1.83
0.4	0.2	0.201	1.50	2.18	1.81	1.73	4.09
0.4	0.3	0.302	1.75	2.52	2.10	2.01	4.28
0.4	0.4	0.402	2.01	2.79	2.37	2.26	4.39

Table C.10: Ellipsoid in a unit cell ($\kappa = 1000$)

a	b	c	ϕ	$\left(\dfrac{k_e}{k_m}\right)_{lb}$	$\left(\dfrac{k_e}{k_m}\right)_{ub}$	$\left(\dfrac{k_e}{k_m}\right)_{geo}$	$\left(\dfrac{k_e}{k_m}\right)_{num}$	% diff.
0.1	0.1	0.1	0.004	1.00	1.23	1.11	1.01	8.80
0.1	0.2	0.1	0.008	1.01	1.24	1.12	1.02	8.69
0.1	0.1	0.2	0.008	1.01	1.59	1.27	1.05	17.22
0.1	0.2	0.2	0.017	1.02	1.62	1.29	1.07	16.73
0.1	0.3	0.1	0.013	1.01	1.24	1.12	1.03	8.34
0.1	0.1	0.3	0.013	1.02	2.24	1.51	1.12	26.07
0.1	0.3	0.2	0.025	1.04	1.63	1.30	1.10	15.69
0.1	0.2	0.3	0.025	1.05	2.35	1.57	1.17	25.29
0.1	0.3	0.3	0.038	1.07	2.39	1.60	1.22	23.51
0.1	0.4	0.1	0.017	1.02	1.24	1.12	1.04	7.91
0.1	0.1	0.4	0.017	1.05	3.83	2.01	1.25	37.61
0.1	0.4	0.2	0.034	1.05	1.64	1.31	1.12	14.50
0.1	0.2	0.4	0.034	1.10	4.26	2.16	1.35	37.41
0.1	0.4	0.3	0.050	1.09	2.41	1.62	1.28	21.51
0.1	0.3	0.4	0.050	1.14	4.44	2.25	1.46	35.40
0.1	0.4	0.4	0.067	1.19	4.55	2.33	1.56	32.97
0.2	0.2	0.1	0.017	1.02	1.24	1.12	1.03	8.31
0.2	0.2	0.2	0.034	1.05	1.64	1.31	1.10	15.82
0.2	0.3	0.1	0.025	1.03	1.24	1.13	1.04	7.77
0.2	0.3	0.2	0.050	1.07	1.65	1.33	1.14	14.53
0.2	0.2	0.3	0.050	1.09	2.41	1.62	1.23	24.00
0.2	0.3	0.3	0.075	1.14	2.44	1.67	1.30	22.02
0.2	0.4	0.1	0.034	1.04	1.25	1.14	1.06	7.19
0.2	0.4	0.2	0.067	1.10	1.65	1.35	1.17	13.17
0.2	0.2	0.4	0.067	1.19	4.55	2.33	1.48	36.56
0.2	0.4	0.3	0.101	1.19	2.45	1.71	1.37	20.04
0.2	0.3	0.4	0.101	1.29	4.67	2.45	1.61	34.39
0.2	0.4	0.4	0.134	1.38	4.74	2.56	1.74	32.00

a	b	c	ϕ	$\left(\dfrac{k_e}{k_m}\right)_{lb}$	$\left(\dfrac{k_e}{k_m}\right)_{ub}$	$\left(\dfrac{k_e}{k_m}\right)_{geo}$	$\left(\dfrac{k_e}{k_m}\right)_{num}$	% diff.
0.3	0.3	0.1	0.038	1.04	1.25	1.14	1.06	7.08
0.3	0.3	0.2	0.075	1.11	1.65	1.35	1.18	13.07
0.3	0.3	0.3	0.113	1.21	2.45	1.72	1.38	19.95
0.3	0.4	0.1	0.050	1.06	1.25	1.15	1.08	6.35
0.3	0.4	0.2	0.101	1.15	1.66	1.38	1.22	11.57
0.3	0.4	0.3	0.151	1.28	2.46	1.77	1.46	17.84
0.3	0.3	0.4	0.151	1.43	4.76	2.61	1.77	32.21
0.3	0.4	0.4	0.201	1.57	4.81	2.75	1.93	29.87
0.4	0.4	0.1	0.067	1.08	1.25	1.16	1.10	5.50
0.4	0.4	0.2	0.134	1.19	1.66	1.41	1.27	9.98
0.4	0.4	0.3	0.201	1.38	2.47	1.85	1.56	15.75
0.4	0.4	0.4	0.268	1.77	4.85	2.93	2.12	27.60

Table C.11: Ellipsoid in a unit cell ($\kappa = 100$)

a	b	c	ϕ	$\left(\dfrac{k_e}{k_m}\right)_{lb}$	$\left(\dfrac{k_e}{k_m}\right)_{ub}$	$\left(\dfrac{k_e}{k_m}\right)_{geo}$	$\left(\dfrac{k_e}{k_m}\right)_{num}$	% diff.
0.1	0.1	0.1	0.004	1.00	1.14	1.07	1.01	5.57
0.1	0.2	0.1	0.008	1.01	1.18	1.09	1.02	6.47
0.1	0.1	0.2	0.008	1.01	1.33	1.16	1.05	9.97
0.1	0.2	0.2	0.017	1.02	1.43	1.21	1.07	11.67
0.1	0.3	0.1	0.013	1.01	1.19	1.10	1.03	6.63
0.1	0.1	0.3	0.013	1.02	1.60	1.28	1.11	13.28
0.1	0.3	0.2	0.025	1.04	1.48	1.24	1.09	11.75
0.1	0.2	0.3	0.025	1.05	1.83	1.39	1.16	16.04
0.1	0.3	0.3	0.038	1.07	1.95	1.44	1.21	16.16
0.1	0.4	0.1	0.017	1.02	1.20	1.11	1.04	6.52
0.1	0.1	0.4	0.017	1.05	2.01	1.45	1.22	15.79
0.1	0.4	0.2	0.034	1.05	1.51	1.26	1.12	11.26
0.1	0.2	0.4	0.034	1.09	2.52	1.66	1.32	20.45
0.1	0.4	0.3	0.050	1.09	2.03	1.49	1.26	15.37
0.1	0.3	0.4	0.050	1.14	2.86	1.81	1.42	21.28
0.1	0.4	0.4	0.067	1.19	3.10	1.92	1.52	20.74
0.2	0.2	0.1	0.017	1.02	1.20	1.11	1.03	6.90
0.2	0.2	0.2	0.034	1.05	1.51	1.26	1.10	12.56
0.2	0.3	0.1	0.025	1.03	1.22	1.12	1.04	6.72
0.2	0.3	0.2	0.050	1.07	1.55	1.29	1.13	12.09
0.2	0.2	0.3	0.050	1.09	2.03	1.49	1.23	17.85
0.2	0.3	0.3	0.075	1.14	2.14	1.56	1.29	17.32
0.2	0.4	0.1	0.034	1.04	1.22	1.13	1.06	6.35
0.2	0.4	0.2	0.067	1.10	1.57	1.31	1.16	11.21
0.2	0.2	0.4	0.067	1.19	3.10	1.92	1.45	24.53
0.2	0.4	0.3	0.101	1.19	2.20	1.62	1.36	16.12
0.2	0.3	0.4	0.101	1.28	3.44	2.10	1.58	24.82
0.2	0.4	0.4	0.134	1.37	3.67	2.24	1.71	23.93

a	b	c	ϕ	$\left(\dfrac{k_e}{k_m}\right)_{lb}$	$\left(\dfrac{k_e}{k_m}\right)_{ub}$	$\left(\dfrac{k_e}{k_m}\right)_{geo}$	$\left(\dfrac{k_e}{k_m}\right)_{num}$	% diff.
0.3	0.3	0.1	0.038	1.04	1.22	1.13	1.06	6.32
0.3	0.3	0.2	0.075	1.11	1.58	1.32	1.17	11.28
0.3	0.3	0.3	0.113	1.21	2.22	1.64	1.37	16.45
0.3	0.4	0.1	0.050	1.06	1.23	1.14	1.08	5.76
0.3	0.4	0.2	0.101	1.14	1.60	1.35	1.21	10.16
0.3	0.4	0.3	0.151	1.28	2.27	1.70	1.45	15.04
0.3	0.3	0.4	0.151	1.42	3.75	2.31	1.74	24.78
0.3	0.4	0.4	0.201	1.56	3.95	2.48	1.89	23.72
0.4	0.4	0.1	0.067	1.08	1.23	1.15	1.10	5.04
0.4	0.4	0.2	0.134	1.19	1.61	1.38	1.26	8.88
0.4	0.4	0.3	0.201	1.37	2.32	1.78	1.54	13.53
0.4	0.4	0.4	0.268	1.74	4.13	2.68	2.08	22.56

Table C.12: Ellipsoid in a unit cell ($\kappa = 10$)

a	b	c	ϕ	$\left(\dfrac{k_e}{k_m}\right)_{lb}$	$\left(\dfrac{k_e}{k_m}\right)_{ub}$	$\left(\dfrac{k_e}{k_m}\right)_{geo}$	$\left(\dfrac{k_e}{k_m}\right)_{num}$	% diff.
0.1	0.1	0.1	0.004	1.00	1.03	1.01	1.01	0.84
0.1	0.2	0.1	0.008	1.01	1.06	1.03	1.02	1.52
0.1	0.1	0.2	0.008	1.01	1.07	1.04	1.03	0.77
0.1	0.2	0.2	0.017	1.02	1.12	1.07	1.05	1.75
0.1	0.3	0.1	0.013	1.01	1.07	1.04	1.02	1.92
0.1	0.1	0.3	0.013	1.02	1.10	1.06	1.06	0.12
0.1	0.3	0.2	0.025	1.03	1.16	1.09	1.07	2.29
0.1	0.2	0.3	0.025	1.04	1.19	1.11	1.10	1.12
0.1	0.3	0.3	0.038	1.06	1.26	1.16	1.14	1.63
0.1	0.4	0.1	0.017	1.02	1.09	1.05	1.03	2.15
0.1	0.1	0.4	0.017	1.04	1.14	1.09	1.09	-0.72
0.1	0.4	0.2	0.034	1.04	1.19	1.11	1.09	2.52
0.1	0.2	0.4	0.034	1.07	1.26	1.16	1.16	0.07
0.1	0.4	0.3	0.050	1.08	1.32	1.19	1.17	1.78
0.1	0.3	0.4	0.050	1.11	1.38	1.24	1.23	0.49
0.1	0.4	0.4	0.067	1.14	1.48	1.30	1.29	0.57
0.2	0.2	0.1	0.017	1.02	1.09	1.05	1.03	2.43
0.2	0.2	0.2	0.034	1.04	1.19	1.11	1.08	3.34
0.2	0.3	0.1	0.025	1.03	1.11	1.07	1.04	2.84
0.2	0.3	0.2	0.050	1.06	1.25	1.15	1.10	4.01
0.2	0.2	0.3	0.050	1.08	1.32	1.19	1.16	3.17
0.2	0.3	0.3	0.075	1.12	1.42	1.26	1.21	4.10
0.2	0.4	0.1	0.034	1.03	1.13	1.08	1.05	2.97
0.2	0.4	0.2	0.067	1.08	1.29	1.18	1.13	4.17
0.2	0.2	0.4	0.067	1.14	1.48	1.30	1.27	2.44
0.2	0.4	0.3	0.101	1.16	1.51	1.32	1.26	4.37
0.2	0.3	0.4	0.101	1.21	1.66	1.42	1.37	3.70
0.2	0.4	0.4	0.134	1.28	1.81	1.52	1.46	4.26

a	b	c	ϕ	$\left(\dfrac{k_e}{k_m}\right)_{lb}$	$\left(\dfrac{k_e}{k_m}\right)_{ub}$	$\left(\dfrac{k_e}{k_m}\right)_{geo}$	$\left(\dfrac{k_e}{k_m}\right)_{num}$	% diff.
0.3	0.3	0.1	0.038	1.04	1.13	1.08	1.05	3.11
0.3	0.3	0.2	0.075	1.09	1.31	1.19	1.14	4.55
0.3	0.3	0.3	0.113	1.18	1.54	1.35	1.28	5.04
0.3	0.4	0.1	0.050	1.05	1.15	1.10	1.07	3.08
0.3	0.4	0.2	0.101	1.13	1.35	1.24	1.18	4.51
0.3	0.4	0.3	0.151	1.23	1.63	1.42	1.35	5.21
0.3	0.3	0.4	0.151	1.32	1.88	1.58	1.49	5.28
0.3	0.4	0.4	0.201	1.43	2.07	1.72	1.62	5.94
0.4	0.4	0.1	0.067	1.07	1.16	1.11	1.08	2.88
0.4	0.4	0.2	0.134	1.17	1.39	1.28	1.22	4.28
0.4	0.4	0.3	0.201	1.31	1.72	1.50	1.43	5.23
0.4	0.4	0.4	0.268	1.57	2.27	1.89	1.76	6.59

Table C.13: Rectangular prism in a unit cell, $\phi = 0.14$ ($\kappa = 1000$)

a	b	c	ϕ	$\left(\dfrac{k_e}{k_m}\right)_{lb}$	$\left(\dfrac{k_e}{k_m}\right)_{ub}$	$\left(\dfrac{k_e}{k_m}\right)_{geo}$	$\left(\dfrac{k_e}{k_m}\right)_{num}$	% diff.
0.2	0.5	0.18	0.14	1.22	1.56	1.38	1.35	2.38
0.2	0.45	0.2	0.14	1.24	1.66	1.44	1.41	1.63
0.2	0.36	0.25	0.14	1.29	1.99	1.6	1.57	2.11
0.2	0.3	0.3	0.14	1.36	2.48	1.84	1.76	4.22
0.2	0.26	0.35	0.14	1.48	3.3	2.21	2.03	8.13
0.2	0.23	0.4	0.14	1.72	4.89	2.9	2.47	14.67
0.2	0.2	0.45	0.14	2.43	9.47	4.79	3.51	26.68

Table C.14: Rectangular prism in a unit cell, $\phi = 0.14$ ($\kappa = 100$)

a	b	c	ϕ	$\left(\dfrac{k_e}{k_m}\right)_{lb}$	$\left(\dfrac{k_e}{k_m}\right)_{ub}$	$\left(\dfrac{k_e}{k_m}\right)_{geo}$	$\left(\dfrac{k_e}{k_m}\right)_{num}$	% diff.
0.2	0.5	0.18	0.14	1.22	1.54	1.37	1.34	2.23
0.2	0.45	0.2	0.14	1.24	1.64	1.42	1.4	1.51
0.2	0.36	0.25	0.14	1.28	1.93	1.57	1.55	1.83
0.2	0.3	0.3	0.14	1.35	2.36	1.78	1.72	3.62
0.2	0.26	0.35	0.14	1.46	3.01	2.1	1.96	6.56
0.2	0.23	0.4	0.14	1.69	4.12	2.64	2.34	11.25
0.2	0.2	0.45	0.14	2.31	6.52	3.88	3.16	18.58

Table C.15: Rectangular prism in a unit cell, $\phi = 0.14$ (constant)($\kappa = 10$)

a	b	c	ϕ	$\left(\dfrac{k_e}{k_m}\right)_{lb}$	$\left(\dfrac{k_e}{k_m}\right)_{ub}$	$\left(\dfrac{k_e}{k_m}\right)_{geo}$	$\left(\dfrac{k_e}{k_m}\right)_{num}$	% diff.
0.2	0.5	0.18	0.14	1.19	1.39	1.29	1.27	1.29
0.2	0.45	0.2	0.14	1.2	1.44	1.32	1.31	0.66
0.2	0.36	0.25	0.14	1.24	1.56	1.39	1.39	0.37
0.2	0.3	0.3	0.14	1.28	1.70	1.47	1.47	0.57
0.2	0.26	0.35	0.14	1.35	1.83	1.57	1.56	0.96
0.2	0.23	0.4	0.14	1.46	1.98	1.7	1.67	1.62
0.2	0.2	0.45	0.14	1.68	2.13	1.89	1.84	2.69

Table C.16: Circular cylinder with axis parallel to direction of heat flow, in a unit cell, $\phi = 0.10$ ($\kappa = 1000$)

ϵ	$\mathbf{h}$	ϕ	$\left(\dfrac{\mathbf{k_e}}{\mathbf{k_m}}\right)_{\mathbf{lb}}$	$\left(\dfrac{\mathbf{k_e}}{\mathbf{k_m}}\right)_{\mathbf{ub}}$	$\left(\dfrac{\mathbf{k_e}}{\mathbf{k_m}}\right)_{\mathbf{geo}}$	$\left(\dfrac{\mathbf{k_e}}{\mathbf{k_m}}\right)_{\mathbf{num}}$	% **diff.**
0.45	0.08	0.10	1.12	1.19	1.15	1.15	0.19
0.35	0.13	0.10	1.13	1.35	1.24	1.21	1.95
0.30	0.18	0.10	1.16	1.55	1.34	1.29	3.94
0.26	0.23	0.10	1.18	1.84	1.47	1.38	6.18
0.25	0.25	0.10	1.20	2.00	1.55	1.44	7.35
0.24	0.28	0.10	1.23	2.24	1.66	1.51	8.94
0.22	0.33	0.10	1.29	2.88	1.93	1.68	12.71
0.21	0.38	0.10	1.41	4.02	2.38	1.95	18.33
0.19	0.43	0.10	1.70	6.66	3.36	2.44	27.45
0.18	0.48	0.10	3.28	19.27	7.95	4.44	44.21

Table C.17: Circular cylinder with axis parallel to direction of heat flow, in a unit cell, $\phi = 0.10$ ($\kappa = 100$)

ϵ	$\mathbf{h}$	ϕ	$\left(\dfrac{\mathbf{k_e}}{\mathbf{k_m}}\right)_{\mathbf{lb}}$	$\left(\dfrac{\mathbf{k_e}}{\mathbf{k_m}}\right)_{\mathbf{ub}}$	$\left(\dfrac{\mathbf{k_e}}{\mathbf{k_m}}\right)_{\mathbf{geo}}$	$\left(\dfrac{\mathbf{k_e}}{\mathbf{k_m}}\right)_{\mathbf{num}}$	% **diff.**
0.45	0.08	0.10	1.12	1.18	1.15	1.15	0.20
0.35	0.13	0.10	1.13	1.33	1.23	1.21	1.86
0.30	0.18	0.10	1.15	1.53	1.33	1.28	3.64
0.26	0.23	0.10	1.18	1.78	1.45	1.37	5.49
0.25	0.25	0.10	1.20	1.92	1.52	1.42	6.41
0.24	0.28	0.10	1.22	2.12	1.61	1.48	7.62
0.22	0.33	0.10	1.28	2.61	1.83	1.64	10.29
0.21	0.38	0.10	1.40	3.37	2.17	1.87	13.95
0.19	0.43	0.10	1.65	4.74	2.80	2.27	19.07
0.18	0.48	0.10	2.89	7.86	4.77	3.61	24.32

Table C.18: Circular cylinder with axis parallel to direction of heat flow, in a unit cell, $\phi = 0.10$ ($\kappa = 10$)

ϵ	$\mathbf{h}$	ϕ	$\left(\dfrac{\mathbf{k_e}}{\mathbf{k_m}}\right)_{\mathbf{lb}}$	$\left(\dfrac{\mathbf{k_e}}{\mathbf{k_m}}\right)_{\mathbf{ub}}$	$\left(\dfrac{\mathbf{k_e}}{\mathbf{k_m}}\right)_{\mathbf{geo}}$	$\left(\dfrac{\mathbf{k_e}}{\mathbf{k_m}}\right)_{\mathbf{num}}$	% **diff.**
0.45	0.08	0.10	1.10	1.15	1.13	1.13	0.23
0.35	0.13	0.10	1.12	1.25	1.18	1.17	1.19
0.30	0.18	0.10	1.13	1.34	1.23	1.21	1.72
0.26	0.23	0.10	1.15	1.44	1.29	1.26	1.85
0.25	0.25	0.10	1.16	1.48	1.31	1.29	1.82
0.24	0.28	0.10	1.18	1.52	1.34	1.32	1.76
0.22	0.33	0.10	1.22	1.61	1.40	1.38	1.62
0.21	0.38	0.10	1.28	1.70	1.48	1.45	1.64
0.19	0.43	0.10	1.39	1.78	1.58	1.54	2.02
0.18	0.48	0.10	1.65	1.87	1.75	1.71	2.49

Table C.19: Ellipsoid in a unit cell, $\phi = 0.04$ ($\kappa = 1000$)

$\mathbf{a}$	$\mathbf{b}$	$\mathbf{c}$	ϕ	$\left(\dfrac{\mathbf{k_e}}{\mathbf{k_m}}\right)_{\mathbf{lb}}$	$\left(\dfrac{\mathbf{k_e}}{\mathbf{k_m}}\right)_{\mathbf{ub}}$	$\left(\dfrac{\mathbf{k_e}}{\mathbf{k_m}}\right)_{\mathbf{geo}}$	$\left(\dfrac{\mathbf{k_e}}{\mathbf{k_m}}\right)_{\mathbf{num}}$	% **diff.**
0.20	0.45	0.10	0.038	1.04	1.25	1.14	1.06	6.90
0.20	0.30	0.15	0.038	1.05	1.42	1.22	1.08	11.20
0.20	0.23	0.20	0.038	1.05	1.64	1.32	1.11	15.51
0.20	0.20	0.23	0.038	1.06	1.78	1.37	1.13	17.71
0.20	0.18	0.25	0.038	1.06	1.95	1.44	1.15	19.97
0.20	0.15	0.30	0.038	1.07	2.39	1.60	1.20	24.81
0.20	0.13	0.35	0.038	1.09	3.08	1.83	1.27	30.41
0.20	0.11	0.40	0.038	1.11	4.31	2.19	1.37	37.47
0.20	0.10	0.45	0.038	1.15	7.18	2.88	1.51	47.37

Table C.20: Ellipsoid in a unit cell, $\phi = 0.04$ ($\kappa = 100$)

a	b	c	ϕ	$\left(\dfrac{k_e}{k_m}\right)_{lb}$	$\left(\dfrac{k_e}{k_m}\right)_{ub}$	$\left(\dfrac{k_e}{k_m}\right)_{geo}$	$\left(\dfrac{k_e}{k_m}\right)_{num}$	% diff.
0.20	0.45	0.10	0.038	1.04	1.22	1.13	1.06	6.14
0.20	0.30	0.15	0.038	1.05	1.36	1.20	1.08	9.52
0.20	0.23	0.20	0.038	1.05	1.52	1.27	1.11	12.51
0.20	0.20	0.23	0.038	1.06	1.62	1.31	1.13	13.86
0.20	0.18	0.25	0.038	1.06	1.72	1.35	1.15	15.14
0.20	0.15	0.30	0.038	1.07	1.95	1.45	1.19	17.45
0.20	0.13	0.35	0.038	1.08	2.24	1.56	1.25	19.53
0.20	0.11	0.40	0.038	1.10	2.62	1.70	1.34	21.34
0.20	0.10	0.45	0.038	1.15	3.12	1.89	1.46	22.90

Table C.21: Ellipsoid in a unit cell, $\phi = 0.04$ ($\kappa = 10$)

a	b	c	ϕ	$\left(\dfrac{k_e}{k_m}\right)_{lb}$	$\left(\dfrac{k_e}{k_m}\right)_{ub}$	$\left(\dfrac{k_e}{k_m}\right)_{geo}$	$\left(\dfrac{k_e}{k_m}\right)_{num}$	% diff.
0.20	0.45	0.10	0.038	1.04	1.13	1.08	1.05	2.98
0.20	0.30	0.15	0.038	1.04	1.17	1.11	1.07	3.60
0.20	0.23	0.20	0.038	1.05	1.21	1.12	1.08	3.58
0.20	0.20	0.23	0.038	1.05	1.22	1.13	1.09	3.38
0.20	0.18	0.25	0.038	1.05	1.24	1.14	1.10	3.09
0.20	0.15	0.30	0.038	1.06	1.26	1.15	1.13	2.31
0.20	0.13	0.35	0.038	1.07	1.28	1.17	1.15	1.38
0.20	0.11	0.40	0.038	1.08	1.29	1.18	1.18	0.42
0.20	0.10	0.45	0.038	1.10	1.31	1.20	1.21	$-0.5xx$

Table C.22: Rectangular prism in a unit cell with conserved volume fraction, $\phi = 0.08$ ($\kappa = 1000$)

a	b	c	ϕ	$\left(\dfrac{k_e}{k_m}\right)_{lb}$	$\left(\dfrac{k_e}{k_m}\right)_{ub}$	$\left(\dfrac{k_e}{k_m}\right)_{geo}$	$\left(\dfrac{k_e}{k_m}\right)_{num}$	% diff.
0.15	0.15	0.45	0.081	1.80	9.10	4.05	2.66	34.27
0.18	0.18	0.33	0.081	1.24	2.91	1.90	1.63	14.17
0.20	0.20	0.25	0.081	1.16	2.01	1.53	1.40	8.63
0.23	0.23	0.20	0.081	1.13	1.66	1.37	1.29	5.93
0.25	0.25	0.16	0.081	1.12	1.48	1.29	1.23	4.24
0.28	0.28	0.13	0.081	1.11	1.36	1.23	1.19	3.03
0.30	0.30	0.11	0.081	1.10	1.29	1.19	1.17	2.12
0.33	0.33	0.10	0.081	1.10	1.24	1.17	1.15	1.42
0.35	0.35	0.08	0.081	1.10	1.20	1.15	1.14	0.86
0.38	0.38	0.07	0.081	1.09	1.17	1.13	1.13	0.42
0.40	0.40	0.06	0.081	1.09	1.14	1.12	1.12	0.08
0.43	0.43	0.06	0.081	1.09	1.13	1.11	1.11	−0.17
0.45	0.45	0.05	0.081	1.09	1.11	1.10	1.10	−0.30

Table C.23: Rectangular prism in a unit cell with conserved volume fraction, $\phi = 0.08$ ($\kappa = 100$)

a	b	c	ϕ	$\left(\dfrac{k_e}{k_m}\right)_{lb}$	$\left(\dfrac{k_e}{k_m}\right)_{ub}$	$\left(\dfrac{k_e}{k_m}\right)_{geo}$	$\left(\dfrac{k_e}{k_m}\right)_{num}$	% diff.
0.15	0.15	0.45	0.081	1.74	5.24	3.02	2.39	20.73
0.18	0.18	0.33	0.081	1.23	2.57	1.78	1.58	11.02
0.20	0.20	0.25	0.081	1.16	1.91	1.49	1.38	7.35
0.23	0.23	0.20	0.081	1.13	1.62	1.35	1.28	5.31
0.25	0.25	0.16	0.081	1.12	1.45	1.27	1.22	3.91
0.28	0.28	0.13	0.081	1.11	1.35	1.22	1.19	2.86
0.30	0.30	0.11	0.081	1.10	1.28	1.19	1.16	2.04
0.33	0.33	0.10	0.081	1.10	1.23	1.16	1.15	1.38
0.35	0.35	0.08	0.081	1.10	1.19	1.14	1.13	0.84
0.38	0.38	0.07	0.081	1.09	1.16	1.13	1.12	0.42
0.40	0.40	0.06	0.081	1.09	1.14	1.12	1.12	0.09
0.43	0.43	0.06	0.081	1.09	1.12	1.11	1.11	−0.15
0.45	0.45	0.05	0.081	1.09	1.11	1.10	1.10	−0.29

Table C.24: Rectangular prism in a unit cell with conserved volume fraction, $\phi = 0.08$ ($\kappa = 10$)

a	b	c	ϕ	$\left(\dfrac{k_e}{k_m}\right)_{lb}$	$\left(\dfrac{k_e}{k_m}\right)_{ub}$	$\left(\dfrac{k_e}{k_m}\right)_{geo}$	$\left(\dfrac{k_e}{k_m}\right)_{num}$	% diff.
0.15	0.15	0.45	0.081	1.38	1.67	1.52	1.50	1.56
0.18	0.18	0.33	0.081	1.18	1.53	1.34	1.33	1.18
0.20	0.20	0.25	0.081	1.13	1.43	1.27	1.25	1.69
0.23	0.23	0.20	0.081	1.11	1.35	1.23	1.20	1.90
0.25	0.25	0.16	0.081	1.10	1.29	1.19	1.17	1.84
0.28	0.28	0.13	0.081	1.10	1.24	1.17	1.15	1.61
0.30	0.30	0.11	0.081	1.09	1.21	1.15	1.13	1.31
0.33	0.33	0.10	0.081	1.09	1.18	1.13	1.12	0.99
0.35	0.35	0.08	0.081	1.09	1.16	1.12	1.11	0.67
0.38	0.38	0.07	0.081	1.08	1.14	1.11	1.11	0.39
0.40	0.40	0.06	0.081	1.08	1.12	1.10	1.10	0.15
0.43	0.43	0.06	0.081	1.08	1.11	1.09	1.09	0.22
0.45	0.45	0.05	0.081	1.08	1.10	1.09	1.09	−0.17

Table C.25: Cube in a unit cell with conserved volume fraction, $\phi = 0.30$

κ	$\left(\dfrac{k_e}{k_m}\right)_{lb}$	$\left(\dfrac{k_e}{k_m}\right)_{ub}$	$\left(\dfrac{k_e}{k_m}\right)_{geo}$	$\left(\dfrac{k_e}{k_m}\right)_{num}$	% diff.
2	1.23	1.26	1.24	1.25	-0.15
4	1.45	1.62	1.54	1.55	-0.76
6	1.57	1.86	1.71	1.73	-1.27
8	1.63	2.03	1.82	1.85	-1.66
10	1.68	2.16	1.90	1.94	-1.96
20	1.78	2.49	2.11	2.17	-2.74
40	1.84	2.73	2.24	2.31	-3.26
60	1.86	2.82	2.29	2.37	-3.46
80	1.87	2.87	2.32	2.40	-3.57
100	1.88	2.90	2.33	2.42	-3.63
200	1.89	2.96	2.37	2.46	-3.77
400	1.90	2.99	2.38	2.48	-3.83
600	1.90	3.00	2.39	2.48	-3.86
800	1.90	3.01	2.39	2.49	-3.87
1000	1.90	3.01	2.40	2.49	-3.88

Table C.26: Rectangular prism ($a = 0.4$, $b = 0.4$, $c = 0.063$) in a unit cell with conserved volume fraction, $\phi = 0.08$

κ	$\left(\dfrac{k_e}{k_m}\right)_{lb}$	$\left(\dfrac{k_e}{k_m}\right)_{ub}$	$\left(\dfrac{k_e}{k_m}\right)_{geo}$	$\left(\dfrac{k_e}{k_m}\right)_{num}$	% diff.
2	1.052	1.043	1.048	1.047	0.06
4	1.091	1.067	1.079	1.077	0.14
6	1.107	1.075	1.091	1.089	0.15
8	1.115	1.080	1.097	1.096	0.15
10	1.121	1.082	1.101	1.100	0.15
20	1.132	1.087	1.110	1.108	0.13
40	1.139	1.090	1.114	1.113	0.11
60	1.141	1.091	1.116	1.114	0.10
80	1.142	1.091	1.116	1.115	0.09
100	1.142	1.092	1.117	1.116	0.09
200	1.144	1.092	1.118	1.117	0.08
400	1.144	1.092	1.118	1.117	0.08
600	1.144	1.093	1.118	1.117	0.08
800	1.145	1.093	1.118	1.117	0.08
1000	1.145	1.093	1.118	1.117	0.08

Table C.27: Sphere with boundary resistance in a unit cell, $\phi = 0.18$, $1 \leq \kappa_c \leq 1000$ ($\kappa = 1000$)

ϵ	t	κ	κ_b	$\left(\dfrac{k_e}{k_m}\right)_{lb}$	$\left(\dfrac{k_e}{k_m}\right)_{ub}$	$\left(\dfrac{k_e}{k_m}\right)_{geo}$	$\left(\dfrac{k_e}{k_m}\right)_{num}$	% diff.
0.3	0.02	1000	1	1.21	2.45	1.73	1.38	19.95
0.3	0.02	1000	10	1.27	2.49	1.78	1.47	17.62
0.3	0.02	1000	50	1.28	2.57	1.81	1.47	18.64
0.3	0.02	1000	100	1.28	2.62	1.83	1.48	19.29
0.3	0.02	1000	500	1.28	2.7	1.86	1.48	20.51
0.3	0.02	1000	1000	1.28	2.72	1.87	1.48	20.84
0.3	0.05	1000	1	1.21	2.45	1.73	1.38	19.95
0.3	0.05	1000	10	1.38	2.65	1.91	1.62	15.39
0.3	0.05	1000	50	1.40	2.94	2.03	1.65	18.67
0.3	0.05	1000	100	1.40	3.05	2.07	1.65	20.06
0.3	0.05	1000	500	1.41	3.22	2.13	1.66	22.11
0.3	0.05	1000	1000	1.41	3.26	2.14	1.66	22.57

Table C.28: Sphere with boundary resistance in a unit cell, $\phi = 0.18$, $1 \leq \kappa_c \leq 1000$ ($\kappa = 100$)

ϵ	$\mathbf{t}$	κ	$\kappa_{\mathbf{b}}$	$\left(\dfrac{\mathbf{k_e}}{\mathbf{k_m}}\right)_{\mathbf{lb}}$	$\left(\dfrac{\mathbf{k_e}}{\mathbf{k_m}}\right)_{\mathbf{ub}}$	$\left(\dfrac{\mathbf{k_e}}{\mathbf{k_m}}\right)_{\mathbf{geo}}$	$\left(\dfrac{\mathbf{k_e}}{\mathbf{k_m}}\right)_{\mathbf{num}}$	% **diff.**
0.3	0.05	100	1	1.21	2.22	1.64	1.37	16.45
0.3	0.05	100	10	1.38	2.42	1.83	1.60	12.42
0.3	0.05	100	50	1.39	2.74	1.96	1.63	16.67
0.3	0.05	100	100	1.40	2.89	2.01	1.64	18.60
0.3	0.05	100	500	1.40	3.16	2.10	1.65	21.61
0.3	0.05	100	1000	1.40	3.23	2.13	1.65	22.26
0.3	0.02	100	1	1.21	2.22	1.64	1.37	16.45
0.3	0.02	100	10	1.27	2.27	1.69	1.45	14.39
0.3	0.02	100	50	1.27	2.38	1.74	1.46	16.08
0.3	0.02	100	100	1.27	2.45	1.77	1.46	17.19
0.3	0.02	100	500	1.27	2.62	1.82	1.47	19.55
0.3	0.02	100	1000	1.27	2.67	1.84	1.47	20.25

Table C.29: Sphere with boundary resistance in a unit cell, $\phi = 0.18$, $1 \leq \kappa_c \leq 1000$ ($\kappa = 10$)

ϵ	t	κ	κ_b	$\left(\dfrac{k_e}{k_m}\right)_{lb}$	$\left(\dfrac{k_e}{k_m}\right)_{ub}$	$\left(\dfrac{k_e}{k_m}\right)_{geo}$	$\left(\dfrac{k_e}{k_m}\right)_{num}$	% diff.
0.3	0.05	10	1	1.18	1.54	1.35	1.28	5.04
0.3	0.05	10	10	1.32	1.83	1.56	1.47	5.65
0.3	0.05	10	50	1.34	2.42	1.8	1.56	13.16
0.3	0.05	10	100	1.34	2.7	1.9	1.6	16.04
0.3	0.05	10	500	1.34	3.14	2.05	1.64	19.9
0.3	0.05	10	1000	1.34	3.22	2.08	1.65	20.61
0.3	0.02	10	1	1.18	1.54	1.35	1.28	5.04
0.3	0.02	10	10	1.23	1.64	1.42	1.34	5.27
0.3	0.02	10	50	1.23	1.94	1.54	1.39	10.23
0.3	0.02	10	100	1.23	2.13	1.62	1.41	12.99
0.3	0.02	10	500	1.23	2.54	1.77	1.46	17.73
0.3	0.02	10	1000	1.23	2.64	1.8	1.47	18.76

Appendix D

Bounds on Long Rectangular Prisms in a Cubic Lattice

Consider an inhomogeneous medium which consists of infinitely long rectangular prisms in a cubic lattice arrangement. A characteristic cell in two dimensions can be identified as follows (Figure D.1):

The upper and lower bounds on the effective conductivity of the inhomogeneous medium are given by examining the total thermal resistance of the cell first in the instance in which isotherms are taken perpendicular to the direction of heat flow (Figure D.2 (a)) and then in the instance in which adiabats are taken parallel to the direction of heat flow (Figure D.2 (b)), respectively, and are given as

$$\left(\frac{k_e}{k_f}\right)_{ub} = \left[1 - 2c + \frac{c}{0.5 + (\kappa - 1)b}\right]^{-1} \tag{D.1}$$

$$\left(\frac{k_e}{k_f}\right)_{lb} = 1 - 2b + \frac{b}{0.5 - Kc} \tag{D.2}$$

where $K = \dfrac{\kappa - 1}{\kappa}$, $\kappa = k_s/k_f$, and k_s, k_f, and k_e are the thermal conductivities of the solid phase, the fluid phase, and the effective medium, respectively; and where b
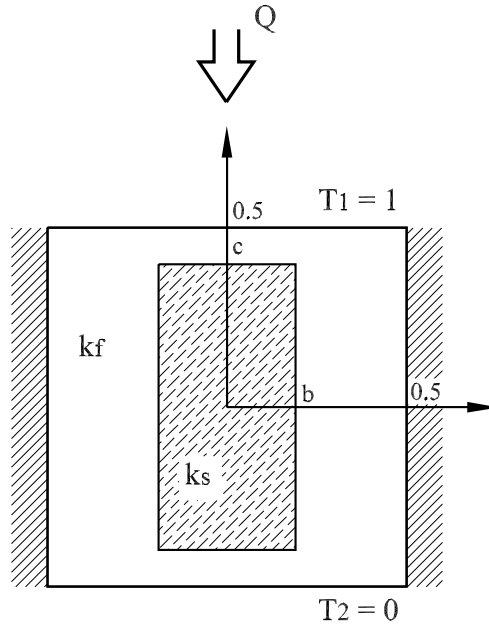
136

Figure D.1: Characteristic cell

is the length of the dispersed prism in the direction perpendicular to heat flow, and c is the length of the prism in the direction parallel to heat flow.

The total heat flow per unit depth through the medium for a particle with aribtrary volume per unit depth is a maximum when $c = 0.5$; conversely, it is a minimum when $b = 0.5$. These cases correspond to parallel and series paths of heat flow, respectively. It thus seems reasonable to expect that the parallel adiabats model is approached for tall and slender particles and that the perpendicular isotherms model is approached for short and latitudinous particles; this statement, however, will be investigated more closely in the following paragraphs.

The upper and lower bounds are shown schematically in Figures D.2 (a) and (b), respectively. The thermal resistance for one-dimensional steady conduction in rectangular co-ordinates is given as

$$R = \frac{L}{kA} \tag{D.3}$$

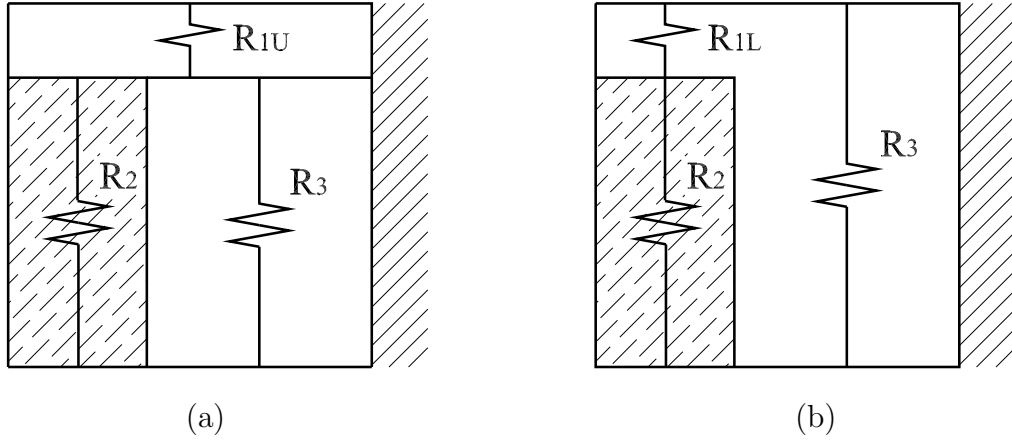where L is the length of the heat flow path, k is the thermal conductivity of the

137

Figure D.2: Resistor networks for (a) upper and (b) lower bounds on k_e

material in this path, and A is the cross-sectional area perpendicular to heat flow (i.e. $A = b \cdot depth$).

We define the aspect ratio as follows:

$$\alpha \equiv \frac{c}{b} \tag{D.4}$$

High α corresponds to tall and slender particles, needle-like in the direction of heat flow; low α correpsonds to short and latitudinous particles, plate-like in the direction perpendicular to heat flow.

For tall and slender particles ($\alpha \gg 1$) of high relative conductivity ($\kappa = k_s/k_f \gg 1$), we expect $R_{1L} + R_2 \simeq R_{1L}$. The parallel adiabats model is physically more appropriate for such geometries and conductivity ratios. This is because the highly conductive particle is very effective at confining the total heat to a narrow region in the vicinity of the particle. The total heat flow per unit depth (Q/d) crossing a plane at $y = c$, for example, is essentially that entering the upper surface of the particle, i.e.

$$\frac{Q}{d} = \frac{2}{d} \int_0^{0.5} q(x, c) \; dx \simeq \frac{2}{d} \int_0^b q(x, c) \; dx.$$

This approximation is even more valid for the total heat flow crossing a plane at $y = 0$.

The following scale analysis reveals that the parallel adiabats and perpendicular isotherms are mutually compatible models for establishing the effective conductivity of systems consisting of short and latitudinous particles ($\alpha \ll 1$):

$$\frac{R_{1L}}{R_{1U}} = \frac{A_U}{A_L} \simeq 1$$

$$\frac{R_{2L}}{R_{2U}} = 1 \qquad\qquad\qquad (\text{D.5})$$
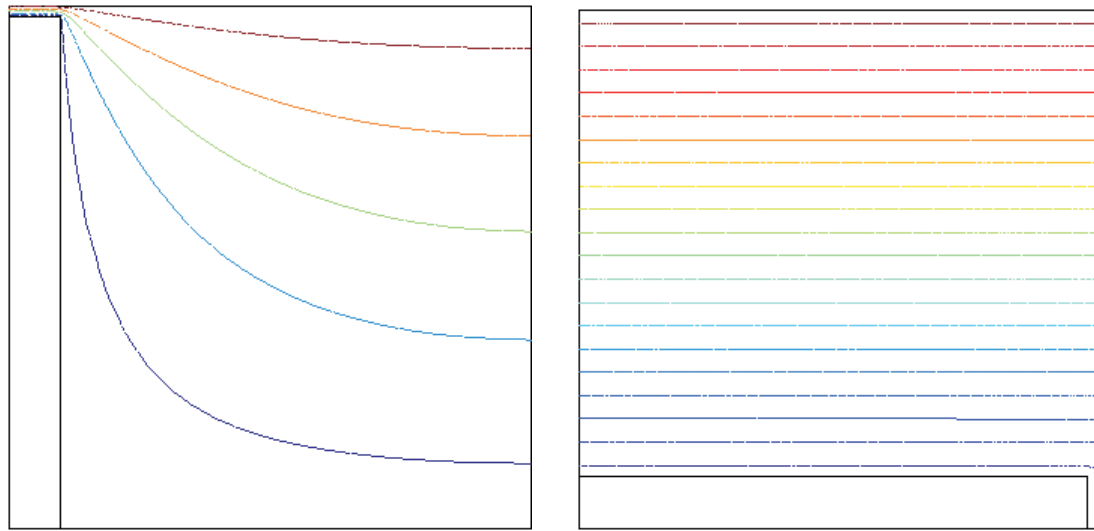
$$\frac{R_{3L}}{R_{3U}} = \frac{0.5}{c} \gg 1$$

but $R_{3L} > R_{1L} + R_2$ which implies that $R_L \simeq R_{1L} + R_2$ and $R_{3U} \gg R_2$ which implies that $R_U \simeq R_{1U} + R_2$. Since $\frac{R_{1L}}{R_{1U}} \simeq 1$ and $\frac{R_{2L}}{R_{2U}} = 1$, $R_L \simeq R_U$ and either configuration of resistors (parallel adiabats or perpendicular isotherms) is expected to give good agreement with the exact value of the effective conductivity for short and latitudinous particles.

D.1   Numerical Results

The comparison between the numerical solution of the effective conductivities with the upper and lower bounds, Equations (D.1) and (D.2), for three cases are shown in Table D.1. For a tall and slender particle ($\alpha = 9.8$), the numerical solution of the effective conductivity is clearly nearer to the value calculated using the parallel adiabats model (as expected). For a thin and latitudinous particle ($\alpha \simeq 0.10$), the numerical solution is somewhat nearer to the value calculated using the perpendicular isotherms model, but in this extreme, the models are mutually compatible: for low α, the solution assuming parallel adiabats approaches that assuming perpendicular isotherms, both of which approach the analytical solution. For a particle with a moderate aspect ratio ($\alpha = 1$), the numerical solution is approximately the average of the solutions given by the bounds. Figure D.3 shows isothermal contours for the three cases studied.
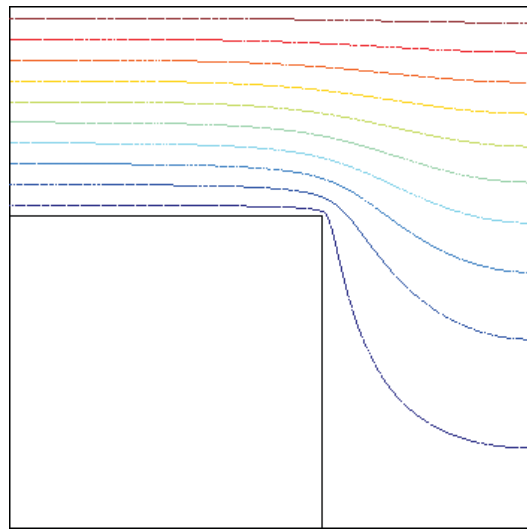
Table D.1: Comparison with numerical results

b	c	α	$\left(\dfrac{k_e}{k_f}\right)_{lb}$	$\left(\dfrac{k_e}{k_f}\right)_{ub}$	$\left(\dfrac{k_e}{k_f}\right)_{num}$	$\dfrac{\displaystyle\int_0^b q(x,c)\,dx}{\displaystyle\int_0^{0.5} q(x,c)\,dx}$
0.05	0.49	9.80	5.67	33.66	7.65	0.633
0.49	0.05	0.10	1.109	1.111	1.110	0.987
0.30	0.30	1.00	1.90	2.49	2.22	0.743

Figure D.3: (a) High, (b) low, and (c) moderate values of the aspect ratio, α. The parallel adiabats model is a good approximation to systems in which the particles have large α and are oriented in the direction of heat flow, (a); the assumptions of parallel adiabats or of perpendicular isotherms are suitable for particles with low α, (b); the average of the two models gives good agreement for particles with moderate aspect ratios ($\alpha \simeq 1$), (c).